Towards a Theory of Discrete and Mesoscopic Wave Turbulence

E. Kartashova*, V. S. L'vov†, S. Nazarenko‡ and I. Procaccia†
* *RISC, J.Kepler University, Linz 4040, Austria*
† *Department of Chemical Physics, The Weizmann Institute of Science, Rehovot 76100, Israel*
‡*Mathematics Institute, University of Warwick, Coventry CV4-7AL, UK*

Discrete wave turbulence in bounded media refers to the regular and chaotic dynamics of independent (that is, discrete in k-space) resonance clusters consisting of finite (often fairly big) number of connected wave triads or quarters, with exact three- or four-wave resonances correspondingly. "Discreteness" means that for small enough amplitudes there is no energy flow among the clusters. Increasing of wave amplitudes and/or of system size opens new channels of wave interactions via quasi-resonant clusters. This changes statistics of energy exchange between waves and results in new, *mesoscopic* regime of *wave turbulence*, where *discrete wave turbulence* and *kinetic wave turbulence* in unbounded media co-exist, the latter well studied in the framework of wave kinetic equations. We overview in systematic manner and from unified viewpoint some preliminary results of studies of regular and stochastic wave behavior in bounded media, aiming to shed light on their relationships and to clarify their role and place in the structure of a future theory of discrete and mesoscopic wave turbulence, elucidated in this paper. We also formulate a set of yet open questions and problems in this new field of nonlinear wave physics, that awaits for comprehensive studies in the framework of the theory. We hope that the resulting theory will offer very interesting issues both from the physical and the methodological viewpoints, with possible important applications in environmental sciences, fluid dynamics, astronomy and plasma physics.

Contents

Introduction

Dispersive waves play a crucial role in a vast range of physical applications, from quantum to classical systems, from microscopic to astrophysical scales. For example, Kelvin waves propagating on quantized vortex lines provide an essential mechanism of turbulent energy cascades in quantum turbulence in cryogenic Helium [70, 86, 114, 115] the momentum and energy transfers from wind to ocean, as well as for navigation conditions

[36]; internal waves on density stratifications and inertial waves due to rotation are important in turbulence behavior and mixing in planetary atmospheres and oceans [16, 30, 75]; planetary Rossby waves are important for the weather and climate evolutions [10]; and Alfven waves are ubiquitous in turbulence of solar wind and interstellar medium [31, 35, 37, 39].

More often than not, nonlinear interaction of different wave modes is important in these and other applications, and there has been a significant amount of work done in the past to describe evolution of such interacting wave systems. There are two major reference points in these studies that describe two different extremes of wave behavior. One of them is a truncated system of three or four waves, which is integrable and exhibits a periodic behavior [117]. In real physical systems, such truncation may correspond to choosing most active modes, e.g. the first few eigen-modes of the corresponding linear problem with a given boundary conditions in a finite domain. The second important reference point is a theory of large sets of modes, which exhibits randomness and which can be described in a statistical way in the continuous (infinite domain) limit: it is presently known as *wave turbulence theory* [122]. This approach was initiated by Peierls in 1929 to describe phonons in anharmonic crystals [96]; and it was reinvigorated in 1960's in plasma physics [29, 111, 125] and in the theory of water waves [119**?**], and by now it has been further applied to description of a great variety of physical phenomena, from synoptic Rossby waves [6, 82, 124**?**] to magnetohydrodynamic turbulence [31, 34, 92], to acoustic waves [71], to waves in stratified [16, 75] and rotating fluids [30], and many other physical wave systems.

The fact that transition from regular to random when the number of degrees of freedom is increased is, of course, typical for physical systems and not surprising. What is surprising, however, that some regularity, characteristic of small number of modes, often persists in much larger and even infinite wave sets, and sometimes such regular motions happily coexist with emerging chaotic behavior. In the other words, regular interactions among a relatively few selected discrete modes remain as important as statistical evolution of the remaining vast majority of the modes. Moreover, it has become increasingly clear that in the majority laboratory experiments and numerical simulations of nonlinear dispersive wave systems the discreteness of the wave-number space due to a finite size remains an important factor which causes the system behave somewhat differently from the predictions of the classical theory of wave turbulence based on the continuous (infinite domain) limit. Moreover, similar behavior often occurs in nature when waves are bounded, e.g. for planetary Rossby waves bounded by the finite planet radius [64]. Description of transition from regular to random regimes and characterization of the intermediate states where both regular and random wave motions are present and mutually inter-connected, is an intriguing and challenging problem. Such intermediate states where the number of waves is big and yet the discreteness of the wavenumber space still remains important are called *discrete* and *mesoscopic wave turbulence*.

The purpose of this review is to summarize an important progress that was done in numerical and experimental studies of stochastic wave behavior in bounded media, aiming to shed light on their relationships and to clarify their role and place in the structure of a future theory of discrete and mesoscopic wave turbulence, elucidated in this paper. The second goal of the review is to identify important yet unresolved problems and to also formulate as yet open questions and problems in this new field of nonlinear wave physics, that awaits for comprehensive studies in the framework of the theory.

The structure of the paper is as follows: **(****)**

I. OVERVIEW OF NONLINEAR WAVE DYNAMICS

A. Normal modes of linearized problem

Dispersive waves are widespread in nature and yet they are quite hard to define mathematically in all generality. Whitham said in his book: "We seem to be left at present with the looser idea that whenever oscillations in space are coupled with oscillation in time through a dispersion relation, we expect the typical effects of dispersive waves" [116]. Indeed, standard mathematical classification of partial differential equations (PDEs) into elliptic, parabolic and hyperbolic is too restrictive for physical applications while it only deals with PDEs of the second order. On the other hand, physical dispersive and nondispersive systems are not restricted by PDEs which are of the second order in time or coordinates, nor do they have to be necessarily even described by PDEs: *e.g.* their equations might involve integral operators as it is indeed the case for the dispersive waves on deep water [72]. Everything becomes clearer if we abandon attempts to classify systems by the types of their evolution equations (such as e.g. elliptic, parabolic and hyperbolic) and instead classify them according to *the form of their typical solutions*. For example, a (possibly nonlinear) evolution equation is called *dispersive* if its linear part has wave-like solutions $\psi(\boldsymbol{r},t)$, that depend on space coordinate $\boldsymbol{r}=\{x,\,y,\,z\}$ and time t as follows:

$$\begin{aligned}\psi(\boldsymbol{r},t) &= A_{\boldsymbol{k}}\exp i(\boldsymbol{k}\cdot\boldsymbol{r}-\omega\,t)+\text{c.c.} \\ &= |A_{\boldsymbol{k}}|\cos(\boldsymbol{k}\cdot\boldsymbol{r}-\omega\,t+\varphi)\,,\end{aligned} \tag{1a}$$

where "c.c." means "complex conjugate". Here $A_{\boldsymbol{k}}=|A_{\boldsymbol{k}}|\exp(i\varphi)\in\mathbb{C}$ is a constant (complex) amplitude, φ is the wave phase, $\boldsymbol{k}\in\mathbb{R}^3$ is a real 3-dimensional wavevector and wave frequency $\omega\equiv\omega(\boldsymbol{k})\in\mathbb{R}$ is such that $\left|\partial^2\omega/\partial k_i\partial k_j\right|\not\equiv 0$, where k_i and k_j are projections of a wavevector $\boldsymbol{k}$. Physically, the latter condition means that wave packets with different wave-numbers propagate at different speeds, so that localized initial data would disperse (spread) in space.

Depending on actual boundary conditions, normal modes of linearized problem may differ from propagating plane waves (1a). For instance, zero boundary conditions in a rectangular box typically (but not always!) lead to standing waves,

$$\psi(\boldsymbol{r},t) = |A_{\boldsymbol{k}}| \sin(\boldsymbol{k}\cdot\boldsymbol{r} + \varphi_{\rm sp}) \sin(\omega t + \varphi_{\rm t})\,, \qquad (1b)$$

where $\varphi_{\rm sp}$ and $\varphi_{\rm t}$ are the space and time phases correspondingly. A more complex form of the normal mode is given by ocean planetary motions in a rectangular domain $[0, L_x] \times [0, L_y]$ with zero boundary conditions, see e.g. [95]:

$$\psi(\boldsymbol{r},t) = |A_{\boldsymbol{k}}| \sin\Big(\pi\frac{mx}{L_x}\Big) \sin\Big(\pi\frac{ny}{L_y}\Big) \sin\Big(\frac{\beta}{2\omega}x + \omega t + \varphi_{\rm t}\Big)\,, \qquad (1c)$$

where $m,\ n \in \mathbb{N}$ are integers and $\omega = \beta/\big[2\pi\sqrt{(m/L_x)^2 + (n/L_y)^2}\,\big]$ with a constant β called Rossby number. Notice, that all normal modes (1) satisfy the Whitham "definition" of waves.

B. Weakly interacting waves

1. Equation of motion

A rather general class of non-dissipative nonlinear waves can be described within the framework of the classical Hamiltonian approach. This means that after a proper change of variables the motion equation in natural variables (fluid velocity, electrical field, density variations, etc.) can be presented in the universal form of canonical Hamiltonian equations for canonical variables $b(\boldsymbol{r},t)$, $b^*(\boldsymbol{r},t)$, which characterize the wave amplitudes. Here " * " denotes complex conjugation. The Hamiltonian equations are most conveniently written in Fourier space, because it is a natural space for describing the wave solutions. Introducing the Fourier transform of $b(\boldsymbol{r},t)$ and calling it $a_{\boldsymbol{k}} \equiv a(\boldsymbol{k},t)$, the Hamiltonian equation can be written as follows [122],

$$i\frac{da_{\boldsymbol{k}}}{dt} = \frac{\partial\mathcal{H}}{\partial a^*_{\boldsymbol{k}}}\ . \qquad (2)$$

Hamiltonian function $\mathcal{H} \equiv \mathcal{H}\{a_{\boldsymbol{k}}, a^*_{\boldsymbol{k}}\}$ (hereafter called for shortness *Hamiltonian*), usually (but not necessarily) is the energy of the wave system, expressed in the terms of the canonical variables $a_{\boldsymbol{k}}$, $a^*_{\boldsymbol{k}}$ for all allowed by the boundary conditions wave vectors $\boldsymbol{k}$. In the simplest case of periodical box $\boldsymbol{k} = 2\pi\boldsymbol{l}/L$, with wavenumber $\boldsymbol{l} \in \mathbb{Z}^d$ and L being the box size and d is space dimension.

For the waves of small amplitudes (for example, when the elevation of the gravity waves on the water surface is smaller then the wavelength) the Hamiltonian can be expanded in powers $a_{\boldsymbol{k}}$ and $a^*_{\boldsymbol{k}}$:

$$\mathcal{H} \ = \ \mathcal{H}_2 + \mathcal{H}_{\rm int}\,, \qquad (3a)$$

$$\mathcal{H}_{\rm int} \ = \ \mathcal{H}_3 + \mathcal{H}_4 + \mathcal{H}_5 + \dots\,, \qquad (3b)$$

where $\mathcal{H}_j$ is a term proportional to product of j amplitudes $a_{\boldsymbol{k}}$ and the interaction Hamiltonian $\mathcal{H}_{\rm int}$ describes the wave coupling, as explained below. We omitted here the independent of $a_{\boldsymbol{k}}$ and $a^*_{\boldsymbol{k}}$ part of the Hamiltonian $\mathcal{H}_0$, because it does not contribute to the motion equation (2). In this paper we consider only waves exited about steady equilibrium states, i.e. if absent initially, the waves must remain absent for all time, $a_{\boldsymbol{k}} = a^*_{\boldsymbol{k}} \equiv 0$. Thus, the linear Hamiltonian is zero, $\mathcal{H}_1 = 0$.

Expansion (3b) utilizes the smallness of the wave amplitudes, therefore, generally speaking,

$$\mathcal{H}_3 > \mathcal{H}_4 > \mathcal{H}_5 > \dots\ . \qquad (4a)$$

In particular cases, due to specific symmetries of a problem, the odd expansion terms vanish (i.e. for spin waves in magnetics with exchange interactions, Kelvin waves on quantum vortex lines). In these cases, instead of (4a) one requires:

$$\mathcal{H}_3 = \mathcal{H}_5 = \mathcal{H}_7 = \dots = 0\,, \qquad (4b)$$

$$\mathcal{H}_4 > \mathcal{H}_6 > \mathcal{H}_8 > \dots\ . \qquad (4c)$$

Three-wave interactions often dominate in wave systems with small nonlinearity, e.g. for Rossby waves in the atmosphere and ocean, capillary waves on the water surface, drift waves in plasmas, etc. On the other hand, if $\mathcal{H}_3 = 0$, or if three-wave resonances are forbidden (in the sense that will be clarified below) the leading nonlinear processes may be four-wave interactions. Further, there are examples of systems where the four-wave interaction is absent and the leading nonlinear process is five-wave, e.g. for one-dimensional gravity water waves [24, 40, 73], or even six-order, e.g. for Kelvin waves on quantum vortex lines [70, 77]. However, such higher-order wave systems are rather rare and, therefore, in this paper we will discuss only three- and four-wave interactions, that describes vast amount of weakly interacting waves. However, mesoscopic turbulence in the higher-order systems can be studied along the same lines as the three- and four-wave interacting systems [40, 43, 48], but this subject lies outside the scope of present paper.

2. Non-interacting waves

The first physically meaningful expansion term, quadratic Hamiltonian

$$\mathcal{H}_2 = \sum_{n=1}^{\infty} \omega_{\boldsymbol{k}} |a_{\boldsymbol{k}}|^2\,, \qquad (5a)$$

according to Eq. (2) produces a linear equation of motion,

$$i\,\frac{da_{\boldsymbol{k}}}{dt} = \omega_{\boldsymbol{k}} a_{\boldsymbol{k}}\,, \qquad (5b)$$

and thus describes noninteracting waves with the dispersion relation $\omega_{\boldsymbol{k}} \equiv \omega(\boldsymbol{k})$. For waves, considered in this

paper, when $\min_{a_{\boldsymbol{k}},a^*_{\boldsymbol{k}}}\{\mathcal{H}\} = \mathcal{H}_0$, $\omega_{\boldsymbol{k}} \geq 0$. Notice, that $\mathcal{H}_2$ in Eq. (5a) does not have $a_{\boldsymbol{k}}a_{-\boldsymbol{k}}$ and $a^*_{\boldsymbol{k}}a^*_{-\boldsymbol{k}}$ terms. They were removed by linear canonical transformation [known as the Bogolubov transformation] after which $a_{\boldsymbol{k}}$, $a^*_{\boldsymbol{k}}$ becomes normal modes of the linearized problem, in which $\mathcal{H}_2$ takes the fully diagonal form (5a).

3. Three-wave interactions

First contribution to the interaction Hamiltonian $\mathcal{H}_{\rm int}$ is

$$\mathcal{H}_3 = \frac{1}{2}\sum_{\boldsymbol{k}_1,\boldsymbol{k}_2,\boldsymbol{k}_3} V^1_{23}a^*_1a_2a_3\delta^1_{23} + \text{c.c.}\,, \tag{6a}$$

describes the processes of decaying of single wave into two waves ($1 \Rightarrow 2$ processes) or confluence of two waves into a single one ($2 \Rightarrow 1$ processes). In Eq. (6) for brevity we introduced notations $a_1 \equiv a_{\boldsymbol{k}_1}$ etc. and δ^1_{23} is the Kronecker symbol, i.e $\delta^1_{23} = 1$ if and only if $\boldsymbol{k}_1 + \boldsymbol{k}_2 = \boldsymbol{k}_3$. Clearly, $V^1_{23} = V^1_{32}$. Generally speaking, $\mathcal{H}_3$ also includes $a_1a_2a_3$ and $a^*_1a^*_2a^*_3$ terms that describe $3 \Leftrightarrow 0$ processes (confluence of three waves or spontaneous appearance of three waves out of vacuum). However they can be eliminated by corresponding nonlinear transformation [122] that leads to the canonical form of $\mathcal{H}_3$, presented in Eq. (6).

Hamiltonian $\mathcal{H}_2 + \mathcal{H}_3$ with Eq. (2) yields the three-wave equation:

$$i\,\frac{da_{\boldsymbol{k}}}{dt} = \omega_{\boldsymbol{k}}a_{\boldsymbol{k}} + \sum_{\boldsymbol{k}_1,\boldsymbol{k}_2}\left[\frac{1}{2}V^{\boldsymbol{k}}_{12}a_1a_2\delta^{\boldsymbol{k}}_{12} + V^{1\,*}_{\boldsymbol{k}2}a_1a^*_2\delta^1_{\boldsymbol{k}2}\right]. \tag{6b}$$

Two sets of terms in the RHS of this equation have time dependence of the form $\exp[-i(\omega_2 + \omega_3)t]$ and $\exp[-i(\omega_2 - \omega_3)t]$ correspondingly [we used shorthand notations, $\omega_j \equiv \omega(\boldsymbol{k}_j)$]. They become important if their frequencies are close to the eigen-frequency of $a_{\boldsymbol{k}}$, $\omega_{\boldsymbol{k}}$: $\omega_2+\omega_3 \approx \omega_{\boldsymbol{k}}$ or $\omega_2-\omega_3 \approx \omega_{\boldsymbol{k}}$. By relabeling the wavevectors, we can write both of these conditions in the same form as follows,

$$\omega(\boldsymbol{k}_1) + \omega(\boldsymbol{k}_2) \;=\; \omega(\boldsymbol{k}_3)\,. \tag{7a}$$

This condition of time synchronization should be complemented by the condition of space synchronization that formally originates from the Kronecker symbols in Eq. (6b),

$$\boldsymbol{k}_1 + \boldsymbol{k}_2 \;=\; \boldsymbol{k}_3\,. \tag{7b}$$

Both relations (7) are named the resonance conditions of the three-wave interactions, or conditions of the *three-wave resonances*.

There exists a simple conditions for the three-wave resonance conditions to be satisfied for the power-law dispersion relations $\omega \sim k^\alpha$ (α=const). A simple sketch Figures 1 and 2 (first suggested in [111]) demonstrates

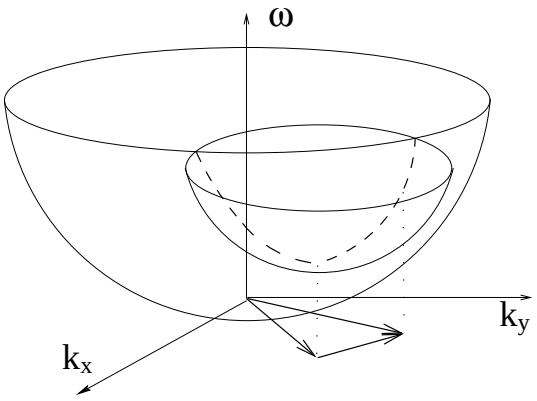

FIG. 1: Graphical solution for the three-wave resonant condition: solutions exist for $\alpha \geq 1$.

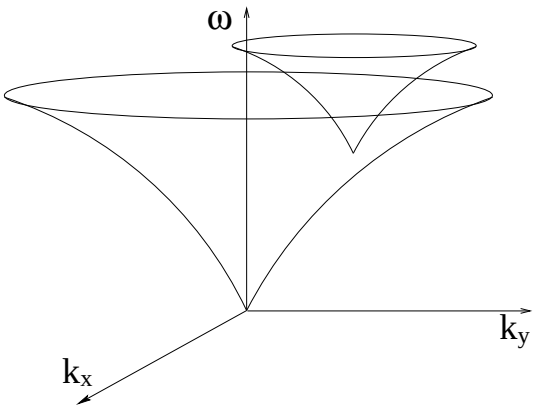

FIG. 2: Graphical solution for the three-wave resonant condition: solutions do not exist for $\alpha < 1$.

that the three-wave resonance is possible if and only if $\alpha \geq 1$ for the continuous case, $\boldsymbol{k} \in \mathbb{R}^2$. For, $\alpha \geq 1$, in Figure 1 the resonant solutions correspond to the intersection of the frequency surfaces marked by a dashed line. For, $\alpha < 1$, in Figure 2 there are no nontrivial resonant solutions because the frequency surfaces do not intersect except for one point (the later corresponds to a trivial solution $\boldsymbol{k}_1 = \boldsymbol{k}_3$, $\boldsymbol{k}_2 = 0$).

Obviously, this condition becomes a necessary condition if $\boldsymbol{k}$ is restricted to discrete values due to boundary conditions. Otherwise, $\alpha < 1$, the set of three-wave resonances is empty and we have to look for higher order resonances [**?**]. The same condition applied for the three-dimensional systems, even though there is no clear graphical demonstration in this case.

4. Four-wave interactions

When the three-wave resonances are forbidden, one has to account for processes with weaker nonlinearity, the four-wave interactions. The canonical part of the four-

wave interaction Hamiltonian,

$$\mathcal{H}_4 = \frac{1}{4} \sum_{\boldsymbol{k}_1,\boldsymbol{k}_2,\boldsymbol{k}_3,\boldsymbol{k}_4} T_{34}^{12} a_1^* a_2^* a_3 a_4 \, \delta_{34}^{12} \,, \tag{8a}$$

describes a 4-wave scattering processes $2 \Leftrightarrow 2$. The rest of the terms in the $\mathcal{H}_4$, $a_1 a_2 a_3 a_4^*$, $a_1 a_2 a_3 a_4$ and its complex conjugates describe $1 \Leftrightarrow 3$ and $4 \Leftrightarrow 0$ processes, can be eliminated by an appropriate nonlinear canonical transformation. After that the four-wave interaction Hamiltonian takes the canonical form (8a). Note that besides trivial symmetries with respect to the indexes permutations, $1 \leftrightarrow 2$ and $3 \leftrightarrow 4$, the interaction coefficient has the symmetry $T_{12}^{34} = \left(T_{34}^{12}\right)^*$, because the Hamiltonian has to be real, $\mathcal{H}_4 = \mathcal{H}_4^*$.

The dynamical equation for the four-wave case follows from (2) with the Hamiltonian $\mathcal{H} = \mathcal{H}_2 + \mathcal{H}_4$:

$$i\frac{da_{\boldsymbol{k}}}{dt} = \omega_{\boldsymbol{k}} a_{\boldsymbol{k}} + \frac{1}{2} \sum_{\boldsymbol{k}_1,\boldsymbol{k}_2,\boldsymbol{k}_3} T_{23}^{\boldsymbol{k}1} a_1^* a_2 a_3 \delta_{23}^{\boldsymbol{k}1} \,. \tag{8b}$$

Considering this equation similarly to (6b), one realizes that the terms in the RHS of Eq. (8b) oscillate with the frequencies $\omega_2 + \omega_3 - \omega_1$ and becomes resonant if this combination is close to $\omega_{\boldsymbol{k}}$. in the other words, the condition of time synchronization (after proper renaming of the variables) takes the form (9a)

$$\omega(\boldsymbol{k}_1) + \omega(\boldsymbol{k}_2) = \omega(\boldsymbol{k}_3) + \omega(\boldsymbol{k}_4) \,, \tag{9a}$$

$$\boldsymbol{k}_1 + \boldsymbol{k}_2 = \boldsymbol{k}_3 + \boldsymbol{k}_4 \,, \tag{9b}$$

while Eq. (9b) represents condition of space synchronization that comes from the Kronecker symbol in Eq. (8b).

For continuous case, if $\omega = k^\alpha$ and $\boldsymbol{d} = 1$ (e.g. Kelvin waves on quantum vortex lines), the four-wave resonance conditions (9) may have solutions only if $\alpha \leq 1$ [120].

Notice that in quantum mechanics language, Eqs. (7) and (9), being multiplied by the Plank constant $\hbar$, can be considered conservation laws for the quasi-particle energy (7a), (9a) and momenta (7b), (9b), involved in the three- and four-quasi-particle interactions correspondingly.

C. Physical examples

In the context of the problem at the hand, a choice of physically important and methodologically illustrative Hamiltonian systems is not an easy task. The corresponding wave systems should preferably be well-studied, both theoretically and experimentally (or numerically). They should be *simple enough* to be understood by the non-experts in the area of wave turbulence and at the same time *not too simple* in order to demonstrate the main characteristics of the resonant wave systems described by different nonlinear dispersive PDEs, with different number of interacting modes and different boundary conditions.

For these purpose, first we have chosen surface water waves, with dispersion relation of the general form:

$$\omega_k = \sqrt{gk + \frac{\sigma\, k^3}{\rho}} \,, \tag{10a}$$

where g is the gravity acceleration, σ is the surface tension and ρ is the fluid density. For small k Eq. (10a) turns into dispersion law for the gravity waves:

$$\omega_k = \sqrt{gk} \,, \tag{10b}$$

while for large k it is simplified to the capillary wave form

$$\omega_k = \sqrt{\frac{\sigma\, k^3}{\rho}} \,. \tag{10c}$$

In both limiting cases the dispersion law have scale-invariant form, $\omega_k \propto k^\alpha$. Notice that for the gravity waves $\alpha = \frac{1}{2} < 1$ and therefore the leading nonlinear processes are four-wave scattering $2 \Leftrightarrow 2$ with the quartets as the primary clusters, while for the capillary waves $\alpha = \frac{3}{2}$ and thus the leading nonlinear processes are three-wave interactions of $2 \Leftrightarrow 1$ type. In this case the primary clusters are triads.

Surface water waves with the general dispersion law (10a) can be described by the Hamiltonian equation of motion in the canonical form (2), that turns into Eq. (6b) for the capillary waves and into Eq. (8b) for the gravity waves. Three-wave interaction coefficient for the capillary waves reads as

$$V_{23}^1 = \frac{i}{8\pi\sqrt{2\sigma}} \sqrt{\omega_1 \omega_2 \omega_3} \times \left[\frac{\mathcal{K}_{k_2,k_3}}{k_1\sqrt{k_2 k_3}} - \frac{\mathcal{K}_{k_1,-k_2}}{k_3\sqrt{k_1 k_2}} - \frac{\mathcal{K}_{k_1,-k_3}}{k_2\sqrt{k_1 k_3}} \right] , \tag{11}$$

where

$$\mathcal{K}_{k_2,k_3} = (\boldsymbol{k}_2 \cdot \boldsymbol{k}_3) + k_2 k_3 \,. \tag{12}$$

The 4-wave interaction coefficient for the gravity waves is given by rather long expressions which can be found in [72].

Probably the simplest known example of the four-wave systems are waves in the nonlinear Shrödinger (NLS) model of nonlinear optical systems and Bose-Einstein condensates [25, 84]. *NLS waves* have dispersion function and interaction coefficient as follows:

$$\omega_k = k^2, \qquad T_{34}^{12} = 1. \tag{13}$$

Another important example of wave system with dominating three-wave interaction, is *Rossby waves*, which are similar to *drift waves* in inhomogeneous plasmas. Their amplitudes can be described by the so-called barotropic vorticity equation which can be presented in the form

similar to the canonical three-wave equation (6b), but all $\boldsymbol{k}$'s taking values only in half of the Fourier space,

$$i\,\frac{da_{\boldsymbol{k}}}{dt} = \omega_{\boldsymbol{k}} a_{\boldsymbol{k}} + \sum_{k_{1x},k_{2x}\geq 0} \Big[\frac{1}{2} V_{12}^{\boldsymbol{k}} a_1 a_2 \delta_{12}^{\boldsymbol{k}} + V_{\boldsymbol{k}2}^{1\,*} a_1 a_2^* \delta_{\boldsymbol{k}2}^1\Big] \qquad (k_x > 0). \tag{14}$$

The phase space in this case is half of the Fourier space is a result is because the original equation in the physical space is for a real variable (barotropic vorticity). The difference in the Hamiltonian structure of the Rossby and capillary waves yields the difference in the form of the conservation laws and therefore in their dynamical behavior. We will discuss this later in greater detail.

Rossby waves on an infinite (or double-periodic) β-plane have dispersion function [6, 123]

$$\omega_{\boldsymbol{k}} = -\frac{\beta\rho^2 k_x}{1+\rho^2 k^2}\,, \tag{15a}$$

where $\rho = \sqrt{gH}/f$ is the Rossby deformation radius H is the fluid layer thickness, $f = 2\Omega\sin\theta$ is the Coriolis parameter, θ is the latitude angle (β-plane approximates a local region on surface of a rotating planet), Ω is the planet rotation frequency and β is the gradient of the Coriolis parameter, $\beta = 2\Omega\cos\theta/R$, and R is the radius of the planet.

In the case of zero boundary conditions in a plane rectangular domain (*oceanic Rossby waves*), the form of the eigen-mode is given by Eq.(1c), corresponding dispersion function has the form

$$\omega_k = \frac{\beta L}{2\pi\sqrt{m^2+n^2}}. \tag{15b}$$

Note that this dispersion relation coincides with relation Eq. (15a) in the limit $\rho \to \infty$ taking into account that $(k_x, k_y) = (\beta/2\omega \pm \pi m/L,\, \pm\pi n/L)$ (which follows from Eq.(1c)). However, the resonant mode sets are different because the resonance in $\mathbf{k}$ is now replaced by the resonance conditions in m an n.

One more example is *atmospheric Rossby waves*, propagated on a rotating sphere. Eigen-modes in this case, $Y_\ell^m(\sin\varphi,\lambda)\exp\Big[\dfrac{2im}{\ell(\ell+1)}t\Big]$, are proportional to the spherical functions Y_ℓ^m, where $\ell \geq 1$ and $|m| \leq \ell$ are integers and φ and λ are latitude and longitude correspondingly. In this case dispersion function is of the form

$$\omega_{\ell,m} = -\frac{2\,m\Omega}{[\ell(\ell+1)]}\,. \tag{15c}$$

Notice that difference in the dispersion relations (15) leads to essential difference in the topology of resonant clusters, and consequently to essential difference in the dynamical and statistical behavior of the systems.

For concreteness we present here the interaction coefficients of the Rossby waves in the (infinite or double-periodic) β-plane [98]:

$$V_{23}^1 = -\frac{i\beta}{4\pi}\sqrt{|k_{1x}k_{2x}k_{3x}|} \times\left(\frac{k_{1y}}{1+\rho^2k_1^2} - \frac{k_{2y}}{1+\rho^2k_2^2} - \frac{k_{3y}}{1+\rho^2k_3^2}\right). \tag{16}$$

The interaction coefficients for the atmospheric Rossby waves can be found in [64, 95, 105] and for oceanic Rossby waves - in [66]. To find an analytical expression for an interaction coefficient is sometimes quite a tedious procedure to be done by hand, although in some cases it can be done by modern symbolical programs, e.g. Mathematica (corresponding algorithm and a couple of examples are given in [65]).

II. DIFFERENT REGIMES OF WAVE TURBULENCE

The notion of *wave turbulence* refers to the chaotic dynamics of nonlinearly coupled wave modes. The phenomenon appears in a variety of physical context from surface water waves, through atmospheric planetary waves, plasma waves, acoustic waves in solids and fluids etc. In the case of very large wave amplitudes the wave-interaction frequency becomes comparable with the wave frequency itself. For instance, for the surface waves this happens when the wave amplitudes are of the order of their wave-length. In this case, the inertial forces acting on the fluid particle near the water surface become comparable and sometimes exceed the gravity, in which case waves break producing droplets and foam. This type of turbulence is called *strong wave turbulence* and will not be considered in the present paper. Instead, we consider *weak wave turbulence* that is characterized by a small parameter ε which is roughly the mean ratio of the nonlinear to the linear term in the equation of motion for the three-wave case, or the square root of this ratio for the four-wave systems. For surface waves ε is about the ratio of the wave amplitude to the wave-length λ, for sound in continues media this is the ratio of the density variations to the mean density, etc.

The theory of weak wave turbulence is particularly well developed in the limit of infinite systems where the ratio of the system size L to the characteristic wave length λ is very large,

$$L/\lambda \to \infty. \tag{17}$$

In that limit the observed energy spectrum (energy distribution between modes) is well described by the so called *wave kinetic equations* that received considerable attention in the last half century, see e.g. [88–91, 122]. Following [78] we will call this regime of weak wave turbulence *kinetic wave turbulence*, though another terminology can be found in literature describing this regime is

statistical wave turbulence, e.g. [20, 118], etc. Our choice of terminology is dictated by novel findings of possible chaotic behavior of resonance clusters [**?** **?**]. This means that though statistical description can be used for narrating their dynamics, chaos is restricted by the distinct domains in k-space, not by the whole inertial interval. LPPR-09 In the case when the parameter

$$L/\lambda \sim 1, \tag{18}$$

the dynamics of waves can be very well described by low-dimensional chaotic models of the type studied intensively in recent decades, see e.g. [60, 61].

In this review we explore the non-linear dynamics of weakly interacting waves when the parameter L/λ is neither of order unity nor very large. This regime of parameters cannot be described either by the wave kinetic equations or as low-dimensional chaos; it calls for new approaches and novel concepts, as partially demonstrated in this review.

For decades statistical regime was regarded as complete description of the weakly nonlinear wave systems, while low-dimensional chaos was supposed to describe so-called finite-size effects *outside* the inertial interval, while power energy spectra were to give complete description of the weakly nonlinear wave system *within* the inertial interval. The theory of finite-size effects in resonators was first presented in [44] where it was established, both theoretically and in numerical simulations, that independent clusters of exact resonant triads (or quartets) might exist in the spectral domain well within the inertial interval. Moreover, it was shown numerically that increasing the wave amplitudes (till some limit magnitude) yields no energy spreading from a cluster to the all modes of the spectral domain but rather goes along some "channels" formed by quasi-resonances, that is, resonances with small enough frequency discrepancy. Further increasing of the amplitudes yields classical statistical wave turbulent regime. This way it was first shown that beside kinetic wave turbulence some new turbulent regime exists called nowadays *discrete wave turbulence* [49, 51–53, 85, 90], etc. In [121] it was first shown in numerical simulations that statistical and discrete regimes of wave turbulence do *coexist* at some systems, and this new regime was called *mesoscopic wave turbulence*. Kinematical explanation of this coexistence has been given in [49] in the frame of the two-layer model of *laminated turbulence*.

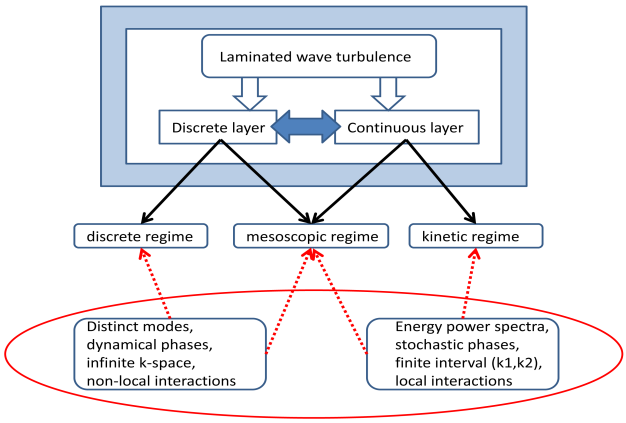

FIG. 3: Different wave turbulent regimes.

A. Laminated wave turbulence

Before elucidating this model, it is instructive first to make a connection between the classical Kolmogorov-Arnold-Moser (KAM) theory [4, 68, 83] and the weakly nonlinear wave systems. For this, we notice that the linearized wave system is obviously integrable, with the wave amplitudes $|a_k|$ and the wave phases $\arg a_k$ being the action and the angle variables respectively. The nonlinear terms should be considered a perturbation to this integrable system. KAM theory says that for sufficiently small perturbation, almost all tori (excluding those involved in frequency resonances) are preserved. On the other hand, near the resonant tori dynamics becomes stochastic. The picture is that for most of the phase space the motion remains periodic with trajectories close to the original unperturbed integrable system, but there will be also sparse stochastic layers around the resonant tori.

Thus, if we consider a set of wave modes (truncated to be finite for clarity), then the surviving tori would correspond to the wave modes which are not in resonance with any other modes. Such modes would move very closely to the oscillatory motion of the linear system, i.e. experience slightly non-sinusoidal periodic oscillations with fixed amplitudes. Thus the energy would be locked in these modes and would not be able to cascade. It is tempting to use this picture to explain the regime of frozen turbulence of capillary waves numerically observed in [100, 101], namely absence of the energy cascade through scales for small forcing levels. Indeed, as it was shown in [48, 52], the exact three-wave resonances are absent for the discrete wavenumbers in the capillary wave case with periodic boundary conditions. On the opposite side, the continuous regime described by the kinetic equation occurs for larger nonlinear disturbances when the stochastic layers expand and cover all of the phase space.

Note that KAM theory should be used with great caution in this case because it excludes resonances of all orders and not only the three-wave ones, and the absence of the higher-order resonances is not yet known. (Note also that KAM mentions only the frequency and not the wavenumber resonances, which broadens the set of excluded resonant modes). Additional uncertainties arise when the system is forced and dissipated because KAM

deals with Hamiltonian systems. However, we will borrow the KAM-style picture that for some intermediate levels of nonlinearity the deterministic and the stochastic motions will coexist. Note that we do not insist anymore that the deterministic motions correspond to non-resonant modes, but instead may involve a *discrete* number of modes in resonance.

This leads to the *model of laminated wave turbulence* [49] which includes two layers of turbulence in a wave system - continuous and discrete layers, each demonstrating specific energetic behavior which is schematically shown in Fig.3). As it was noticed in [53], in various physical systems either statistical or discrete or both layer(s) can be observable. For instance, on-site measurements of tidal currents [32] demonstrate only statistical level while in laboratory experiments [23] only discrete dynamics has been identified. Coexistence of both types of dynamics was shown in [121]. Including additional physical parameters could yield the transition from statistical to discrete layer as it was demonstrated in [22] for capillary water waves, with and without rotation.

Continuous layer can be roughly associated with the kinetic equation, energy cascades, Kolomogorov-Zakharov (KZ) spectra, etc. which were well-studied while the existence of the discrete layer was realized quite recently, in [49]. In order to understand which manifestations of the discrete layer are to be expected in numerical or laboratory experiments, let us regard an example with dispersion function $\omega \sim 1/\sqrt{m^2+n^2}$. First of all, it is important to realize: the fact that the ratio $\alpha_{ij} = \omega_i/\omega_j$ is a rational number *does not imply* that dispersion function ω is a rational function. Indeed, for $\omega \sim 1/\sqrt{m^2+n^2}$ we have

$$\omega : \mathbb{Z} \times \mathbb{Z} \to \mathbb{R} \tag{19}$$

and for wavevectors $\boldsymbol{k}_1 = (2,1)$ and $\boldsymbol{k}_2 = (9,18)$, the ratio $\omega_1/\omega_2 = 1/3$ is rational number though ω is irrational function of integer variables. Decomposition of all waves into disjoint classes for this case and various irrational dispersion can be constructed explicitly (see [48, 50, 53, 55, 56]). These methods based on the profound number-theoretical results will be outlined in Section III (for complete presentation see book [54], Chapter 2). The very important result obtained is the fact that in the nonlinear wave systems resonances form *independent clusters* in k-space.

Physical interpretation of these results is as follows. Resonantly interacting waves change their amplitudes according to Sys.(23) while non-interacting (at the time scale εT) waves have constant amplitudes. This can be clearly seen on the Fig.1 and Fig.3, [44], correspondingly. In schematic presentation of laminated wave turbulence given in [52], Fig.2, non-interacting modes are shown as blue diamonds and resonant modes - as yellow squares. In Fig.5 below non-interacting modes are not shown, for the sake of simplicity.

Natural way to describe transition from resonantly interacting to non-interacting waves is introducing of non-zero resonance broadening into frequency resonance condition (7a) or (9a), thus introducing the notion of *quasi-resonances*. The minimal resonance broadening, necessary for quasi-resonances to appear, has been investigated numerically in [110] both for capillary and gravity water waves. Numerical simulations [3, 108–110] showed that exact and quasi-resonances among the gravity waves are observable not on the time scale $\mathcal{O}(t/\varepsilon^4)$ of kinetic theory but rather on the dynamical time scale. Analytical results on the magnitudes of the resonance broadening necessary for quasi-resonances to occur, were first obtained in [45] while explicit results for various types of water waves have been presented in [51] and will be briefly reviewed in Section III D.

Thus, to differentiate between various wave turbulence regimes let us introduce a number $\mathcal{N}$ of effectively interacting waves and an interaction frequencies Γ. As a rule, a number $\mathcal{N}$ can be estimated as

$$\mathcal{N} \simeq (\Delta_k/\delta_k)^d \,, \tag{20a}$$

where Δ_k is the width of the excited wave spectrum, d is the space dimension of the problem and

$$\delta_k = 2\pi/L \,, \tag{20b}$$

is the k spacing in the box of size L. The later determines the wave eigen-frequency spacing $v_{\boldsymbol{k}}\delta_k$ where $v_{\boldsymbol{k}}$ is the modulus of the the group velocity $\boldsymbol{v}_{\boldsymbol{k}} \equiv d\omega_{\boldsymbol{k}}/d\boldsymbol{k}$.

The interaction frequency Γ characterizes nonlinear frequency broadening, or, in the other words, the inverse correlation time of wave packets. Note that the correlation time is roughly equal to the characteristic time of nonlinear evolution. Various relationships among the interaction frequencies and the frequency spacings, $v_{\boldsymbol{k}}\delta_k$ and Γ, determine different regimes of wave turbulence. (...these estimates should be improved – this is work in progress; some discussion is given in [**?**]).

B. Discrete wave turbulence

In the dynamical regime with strongly correlated phases, the interaction frequencies Γ follow from the dynamical equations of motions (6b) and (8b), see e.g. book [76]:

$$\Gamma_{\text{D}}^{3\text{w}} \;\simeq\; |VA_{\boldsymbol{k}}| \,, \tag{21a}$$

$$\Gamma_{\text{D}}^{4\text{w}} \;\simeq\; |TA_{\boldsymbol{k}}^2| \,, \tag{21b}$$

Here $V = V_{12}^{\boldsymbol{k}}$ and $T = T_{23}^{k1}$ are the interaction coefficients of the Hamiltonians $\mathcal{H}_3$ and $\mathcal{H}_4$ (Eqs. (6a) and (8a)) with all wave vectors taken to be of the same order of magnitude $k_1 \sim k_2 \sim k_3 \sim k$, restricted by conditions $\boldsymbol{k} = \boldsymbol{k}_1 + \boldsymbol{k}_2$ and $\boldsymbol{k} + \boldsymbol{k}_1 = \boldsymbol{k}_2 + \boldsymbol{k}_3$ respectively. The subscript D stands for "dynamical" to distinguish it from the "kinetic" regime, see below, and the superscripts $3W$ and $4W$ stand for the "three-wave" and "four-wave" respectively.

For very small wave amplitudes, when the interaction frequency is less then the finite-box frequency spacing,

$$\Gamma_{\text{D}} \ll v_{\boldsymbol{k}}\delta_k\,, \tag{22}$$

only exact resonances determine wave behavior. This inequality applies for both 3W and 4W systems (i.e. here $\Gamma_{\text{D}} = \Gamma_{\text{D}}^{3W}$ or $\Gamma_{\text{D}} = \Gamma_{\text{D}}^{4W}$). In this case, isolated *the primary clusters*, triads in three-wave systems or quartets in four-wave systems, typically demonstrate periodical behavior. We will review the dynamics of the isolated triads and quartets in the next two subsections, because they contain essential elements and the type of connections important in larger clusters.

1. Dynamics of an isolated triad

Primary resonance cluster in the case of 3-wave resonances, also called *a triad*, Eqs.(7), is described by a truncated system of three modes. Dynamical system corresponding to an isolated triad can easily be deduced from (6b):

$$\begin{aligned} i\,\frac{d}{dt}A_1 &= V_{12}^{3\,*}A_2^*A_3\,,\\ i\,\frac{d}{dt}A_2 &= V_{12}^{3\,*}A_1^*A_3\,,\\ i\,\frac{d}{dt}A_3 &= V_{12}^{3}A_1A_2\,, \end{aligned} \tag{23a}$$

where similarly to (1) we introduce "slow" complex amplitudes A_j of resonantly interacting waves with $\omega_1 + \omega_2 = \omega_3$, $\boldsymbol{k}_1 + \boldsymbol{k}_2 = \boldsymbol{k}_3$, $\omega_j \equiv \omega(\boldsymbol{k}_j)$, $j = 1,2,3$, their modulus C_j and phases φ_j:

$$A_j \equiv a_j\exp(i\omega_j t) \equiv C_j\exp(i\varphi_j)\,,\quad C_j \equiv |A_j|\,. \tag{23b}$$

Notice that the phase ψ of the interaction coefficient

$$V_{12}^{3} \equiv Z\exp(i\psi)\,, \tag{24a}$$

plays no role in the wave dynamics. By proper change of variables

$$A_j \equiv -iB_j\exp(-i\psi)\,, \tag{24b}$$

Eqs. (23) take the Manley-Rowe form [80], free of the phase ψ (and imaginary unite i):

$$\begin{aligned} \frac{d}{dt}B_1 &= ZB_2^*B_3\,,\\ \frac{d}{dt}B_2 &= ZB_1^*B_3\,,\\ \frac{d}{dt}B_3 &= -ZB_1B_2\,. \end{aligned} \tag{24c}$$

Equations (24c) are symmetric with respect to replacing two low-frequency modes $1 \Leftrightarrow 2$. The mode with highest frequency (which in this paper will be always denoted by subscript " $_3$ ") is special.

On the face of it, Eqs. (24c) involves six dynamical variables, i.e. B's and their complex conjugates. In fact, in terms of C_j and φ_j, defined by Eqs. (23b), one gets

$$\frac{d\,C_1^2}{dt} = \frac{d\,C_2^2}{dt} = -\frac{d\,C_3^2}{dt} = 2ZC_1C_2C_3\,\cos\varphi_{12,3}\,, \tag{25}$$

where the *dynamical phase* of a triad

$$\varphi_{12,3} \equiv \varphi_1 + \varphi_2 - \varphi_3\,, \tag{26}$$

is the only combination of phases which affects the triad dynamics.

Eq. (25) immediately show that system (24c) has two independent conservation laws, known as Manley-Rowes integrals,

$$\begin{cases} I_{23} = C_2^2 + C_3^2\,, \quad I_{13} = C_1^2 + C_3^2\\ I_{12} = I_{13} - I_{23} = C_1^2 - C_2^2\,, \end{cases} \tag{27}$$

and this allows to express three amplitudes C_j via one of them only. The phase space of Eqs. (24c) becomes two-dimensional, with unknowns C_1 and $\varphi_{12,3}$, which yields integrability of Eqs. (24c). Solutions of Eqs. (24c) are Jacobian elliptic functions and whether or not its dynamics is periodic is determined by the energy in the ω_3-mode (for details see [60]). New insights into the general dynamics of a triad were recently obtained in [13] where the notion of *dynamical invariant* has been introduced. Simply speaking, dynamical invariant can be regarded as a time-dependent conservation law and is a useful tool for investigating time evolution of primary and small generic clusters of triads. For a triad it reads

$$S_0 = Z\,t - \frac{F\left(\arcsin\left(\left(\frac{R_3-v}{R_3-R_2}\right)^{1/2}\right),\left(\frac{R_3-R_2}{R_3-R_1}\right)^{1/2}\right)}{2^{1/2}(R_3-R_1)^{1/2}(I_{13}^2 - I_{13}I_{23} + I_{23}^2)^{1/4}}, \tag{28}$$

where F is the elliptic integral of the first kind and variables v, R_1, R_2, R_3 are explicit functions of initial conditions. For given initial conditions, intersection of level surfaces of dynamical invariant and of two independent Manley-Rowes integrals gives the solution trajectory of (24c). Explicit expressions for all variables in terms of initial conditions and examples of solution trajectories can be found in [15]. Nevertheless even this simple dynamics offers the first opportunity to discuss the energy flow within generic resonance cluster.

To this aim we discuss the evolution the evolution of the triad of amplitudes with special initial conditions, when only one mode is appreciably excited at zero time. If $C_1(t=0) \gg C_2(t=0)$ and $C_1(t=0) \gg C_3(t=0)$, then $I_{23}(t=0) \ll I_{13}(t=0)$. The integrals of motion are independent of time, therefore $I_{13} \gg I_{23}$ at all later times, and hence $C_1(t)^2 \gg C_2(t)^2$. Moreover, $C_1(t)^2 \gg C_3(t)^2$ at all times. Indeed, the assumption $C_1(t)^2 \lesssim C_3(t)^2$ yields $I_{13} \simeq I_{23}$, which is not tenable. This means that the ω_1-mode, being the only essentially exited one at $t = 0$ cannot redistribute its energy to

the other two modes in the triad. The same is true for the ω_2-mode. For this reason the lower frequency modes with frequencies $\omega_1 < \omega_3$ and $\omega_2 < \omega_3$ are called *passive modes*, or *P-modes* [61].

On the other hand, the conservation laws (27) cannot restrict the growing of P-modes from the initial conditions when only ω_3-mode is appreciably excited: $C_3(t=0) \equiv C_{3,0} \gg C_{1,0}\,, C_{2,0}$. In this case the P-mode amplitudes will grow exponentially:

$$C_1(t)\,, C_2(t) \propto \exp \nu_3\, t\,, \quad \nu_3 = |Z\,|C_{3,0}|\,. \tag{29}$$

This phenomenon is a particular case of the *decay instability* (see e.g. [76]) and is known in various fields under different names: parametric resonance in classical mechanics (with the simplest example: parametric pendulum), Suhl instability of spin waves (1956, [1]), Oraevsky -Sagdeev decay instability of plasma waves (1962, [94]), etc. In its general form it was first obtained in 1967 by Hasselmann [33], both for the case of 3- and 4-wave systems.

For us is important that the energy, initially localized in ω_3-mode, is transferred during time $1/\nu_{\rm d}$ into ω_1 and ω_2 modes until magnitudes of all three modes became comparable. Therefore ω_3-mode is called *active mode* in or *A-mode* [61]. An A-mode, being initially excited, is capable to share its energy with two P-modes within the triad. The notions of *A-* and *P-modes* proved to be very useful for description of energy percolation within generic resonance clusters [13, 14, 52, 53, 78], etc.

In particularly, in [14] effect of the dynamical phase (26) on non-linear amplitudes' evolution has been studied. It was shown that if initially dynamical phase is zero it will remain zero at all times while amplitudes will change sign periodically. On the other hand, if for very small but nonzero initial phase amplitudes become purely positive. Moreover, if initial phase increases from from 0 to $\pi/2$, both the range of amplitude variations and period of motions decrease drastically: for some initial conditions the amplitudes become of an order smaller. The difference in evolution of A- and P-mode is clearly demonstrated in Fig.1, [14]: if initially A-mode has maximal amplitude, all three modes interact effectively. In the case when initially one of P-modes is essentially excited - it keeps its energy while A-mode exchanges energy with another P-mode. Independently of details of initial values, the variation range of the amplitudes is minimized when the initial condition for the dynamical phase φ is equal to $\pi/2$.

Explicit expression for dynamical phase can be found in [53] in the form

$$\cot|\varphi_{12,3}(T)| \sim \frac{q}{Z^3\tau^3} \sum_{i=0}^{\infty} \frac{q^i}{1-q^{2i+1}} \sin(2i+1)\pi\frac{T-t_0}{\tau} \times \sum_{j=0}^{\infty} \frac{(2j+1)\,q^j}{1-q^{2j+1}} \cos(2j+1)\pi\frac{T-t_0}{\tau} \tag{30}$$

where μ, τ, t_0, q are known expression of initial conditions [15].

As it was pointed out in [14], the different choice of initial dynamical phase can be used in real physical systems for controlling energy input, exchange and output in laboratory experiments, e.g. in Tokamaks, *at no energy cost* while the energy of the system which is independent of the phase.

2. Dynamics of an isolated quartet

Primary cluster if 4-wave system is called *a quartet* and is described by truncated system of four modes. Dynamical system corresponding to an isolated quartet can easily be deduced from (8b) by substitution of slow amplitude A_j according to Eq. (23b):

$$\begin{aligned} i\,\frac{d}{dt}A_1 &= SA_2^*A_3A_4 + \Delta_1 A_1\,, \\ i\,\frac{d}{dt}A_2 &= SA_1^*A_3A_4 + \Delta_2 A_2\,, \\ i\,\frac{d}{dt}A_3 &= S^*A_4^*A_1A_2 + \Delta_3 A_3\,, \\ i\,\frac{d}{dt}A_4 &= S^*A_3^*A_1A_2 + \Delta_4 A_4\,, \end{aligned} \tag{31a}$$

$$\Delta_j \equiv \sum_{i=1}^{4} T_{ij}|A_j|^2 - \frac{1}{2}\,T_{jj}|A_1|^2\,, \tag{31b}$$

where real interaction coefficients $T_{\boldsymbol{k},\boldsymbol{k}'} = T_{\boldsymbol{k}',\boldsymbol{k}} \equiv T^{\boldsymbol{k},\boldsymbol{k}'}_{\boldsymbol{k},\boldsymbol{k}'}$ are responsible for the nonlinear shifts of frequency Δ_j and (generally speaking, complex) coefficient $S = T^{12}_{34}$ for the energy exchange within the quarter.

Eqs. (31) for quartet are essentially more cumbersome than Eqs. (23) for the triad. Besides complex interaction coefficient S they involve 10 real coefficients $T_{\boldsymbol{k},\boldsymbol{k}'}$, while Eqs. (23) involve only one coefficient $|Z|$ which can be removed by the renormalization of time scale. Nevertheless, system (31) allows effective analysis [107], similar to what has been done above for a triad Eqs. (23). Similarly to Eqs. (25) one gets

$$\begin{aligned} \frac{d\,C_1^2}{dt} &= \frac{d\,C_2^2}{dt} = -\frac{d\,C_3^2}{dt} = -\frac{d\,C_4^2}{dt} \\ &= 2|S|C_1C_2C_3C_4\,\sin(\arg S - \varphi_{12,34})\,, \end{aligned} \tag{32a}$$

where the *quartet phase*

$$\varphi_{12,34} \equiv \varphi_1 + \varphi_2 - \varphi_3 - \varphi_4\,, \tag{32b}$$

is the only combination of phases which affects the quartet dynamics.

It is clear from Eqs. (32) that besides the Hamiltonian, Eqs. (31) have three independent Manley-Rowe integrals, say:

$$\begin{aligned} I_{13} &= C_1^2 + C_3^2\,, \quad I_{14} = C_1^2 + C_4^2\,, \\ I_{23} &= C_2^2 + C_3^2\,. \end{aligned} \tag{33a}$$

The other motion integrals are linear combinations of these three:

$$\begin{aligned} I_{24} &= C_2^2 + C_4^2\,, \quad I_{1234} = C_1^2 + C_2^2 + C_3^2 + C_4^2\,, \\ I_{1,2} &= C_1^2 - C_2^2\,, \quad I_{3,4} = C_3^2 - C_4^2\,. \end{aligned} \tag{33b}$$

Integrals (33) allow to express four amplitudes C_j in terms of just one of them. Therefore the phase space of Eqs. (31) for quartet become two dimensional, say C_1 and $\varphi_{12,34}$, exactly as it happens for a triad, Eqs. (23). The only technical difference is that analytical expression for the modulus of the resulting elliptic integral is more involved and variety of different dynamical scenarios is substantially richer (see [107] for details). The general answer can be given again, similar to the case of triad, in terms of Jacobean elliptic functions, which allows a universal approach to analytical study of the dynamical behavior of quartet for arbitrary initial conditions.

However, there exist two major differences in triad and quartet dynamics:

• First, the variation range of the amplitudes in a triad is *always* minimized for dynamical phase equal to $\pi/2$; this is not the case for a quartet [107].

• Second, *no criterion of instability* can be formulated for a quartet [33].

Nevertheless, some useful information about the energy transfer within a quartet can be obtained by considering its evolution from a particular initial conditions. Indeed, consider first the case, when at $t = 0$ one mode, say ω_1, is essentially excited:

$$C_{1,0} \gg C_{2,0} \simeq C_{3,0} \simeq C_{4,0} \equiv c_0\,, \tag{34a}$$

where $C_{j,0} \equiv C_j(t=0)$. It follows from the motion integrals I_{23} and I_{24}, Eqs. (33), that the amplitudes $C_2(t)$, $C_3(t)$ and $C_4(t)$, being initially small, remains small forever:

$$\begin{aligned} C_2(t)\,, C_3(t) &\le \sqrt{C_{2,0}^2 + C_{3,0}^2} \simeq c_0\,, \\ C_2(t)\,, C_4(t) &\le \sqrt{C_{2,0}^2 + C_{4,0}^2} \simeq c_0\,, \end{aligned} \tag{34b}$$

Therefore the energy transfer in this case is essentially suppressed.

Considering the case, when at $t = 0$ two modes are essentially excited we have to introduce different types of modes pairs - one-side-pair and two-side-pair, referring to the form resonance conditions (9):

$$\text{1-pairs:} \quad (\omega_1, \omega_2)\,,\ (\omega_3, \omega_4)\,. \tag{35a}$$

$$\text{2-pairs:} \quad (\omega_1, \omega_3)\,,\ (\omega_1, \omega_4)\,,\ (\omega_2, \omega_3)\,,\ (\omega_4, \omega_3)\,, \tag{35b}$$

denoted further as *1-pair* and *2-pair* correspondingly.

If at $t = 0$ one of the 2-pairs, say (ω_1, ω_3), is excited:

$$C_{1,0} \simeq C_{3,0} \gg C_{2,0} \simeq C_{4,0} \equiv c_0\,, \tag{36a}$$

then one of the Manley-Rowe integrals (in this case I_{24}) prevents the rest of two modes from growing:

$$C_2(t)\,, C_4(t) \le \sqrt{C_{2,0}^2 + C_{4,0}^2} \simeq c_0\,. \tag{36b}$$

The situation is different, when at $t = 0$ one of the 1-pairs, say, $(\omega_1\,, \omega_2)$ is excited:

$$C_{1,0} \sim C_{2,0} \gg C_{3,0} \simeq C_{4,0}\,. \tag{37}$$

In this case there are no restrictions originating from the Manley-Rowe integrals and the system evolution requires more detailed analysis directly from the Eqs. (31).

During initial evolution, at which inequalities (38) still hold one can neglect feedback of ω_3 and ω_4 modes on ω_1 and ω_2 modes. Then the first two of Eqs. (31a) yield

$$\begin{aligned} A_1(t) &= C_{1,0} \exp(i\Delta_{1,0} t)\,, \quad \Delta_{1,0} \equiv \frac{T_{11}}{2} C_{1,0}^2 + T_{12} C_{2,0}^2\,; \\ A_2(t) &= C_{2,0} \exp(i\Delta_{2,0} t)\,, \quad \Delta_{2,0} \equiv \frac{T_{22}}{2} C_{2,0}^2 + T_{12} C_{1,0}^2\,. \end{aligned} \tag{38a}$$

The second two of Eqs. (31a) simplifies to

$$\begin{aligned} i\,\frac{d\,A_3}{dt} &= \Delta_{3,0}\, A_3 + \mathcal{P} A_4^*\,, \\ -i\,\frac{d\,A_4^*}{dt} &= \Delta_{4,0}\, A_4^* + \mathcal{P}^* A_3\,; \end{aligned} \tag{38b}$$

where

$$\begin{aligned} \mathcal{P} &\equiv S^* C_{1,0} C_{2,0} \exp[\,i\,(\Delta_{1,0} + \Delta_{2,0})\,t\,]\,, \\ \Delta_{3,0} &\equiv T_{31} C_{1,0}^2 + T_{32} C_{2,0}^2\,, \quad \Delta_{4,0} \equiv T_{41} C_{1,0}^2 + T_{42} C_{2,0}^2\,. \end{aligned} \tag{38c}$$

Solutions of linear Eqs. (38b) has the form:

$$\begin{aligned} A_3(t) &= C_{3,0} \exp\big[(i\,\omega_3 + \nu_{12})t\big]\,, \\ A_4^*(t) &= C_{4,0} \exp\big[(-i\,\omega_4 + \nu_{12})t\big]\,, \end{aligned} \tag{39a}$$

where

$$\begin{aligned} \omega_3 &= (\Delta_{1,0} + \Delta_{2,0} - \Delta_{3,0} + \Delta_{4,0})/2\,, \\ \omega_4 &= (\Delta_{1,0} + \Delta_{2,0} + \Delta_{3,0} - \Delta_{4,0})/2\,, \end{aligned} \tag{39b}$$

$$\begin{aligned} \nu_{12}^2 &= |\mathcal{P}|^2 - \frac{1}{4}\Big(\sum_{j=1}^{4} \Delta_{j,0}\Big)^2 \\ &= |S|^2 C_{1,0}^2 C_{2,0}^2 - \big(\mathcal{T}_1 C_{1,0}^2 + \mathcal{T}_2 C_{2,0}^2\big)^2/4\,, \end{aligned} \tag{39c}$$

$$\begin{aligned} \mathcal{T}_1 &\equiv \frac{1}{2} T_{11} + T_{12} + T_{13} + T_{14}\,, \\ \mathcal{T}_2 &\equiv T_{12} + \frac{1}{2} T_{22} + T_{23} + T_{24}\,. \end{aligned} \tag{39d}$$

When $\nu_{12}^2 > 0$, Eqs. (39a) predict exponential grow of amplitudes A_3 and A_4 with the increment of the *modulation instability* (according to the standard terminology in the field [76]) $\nu_{12} > 0$. In this case the energy goes from initially excited 1-pair $(\omega_1\,, \omega_2)$ to the second 1-pair

$(\omega_3\,,\omega_4)$ with the characteristic time $\simeq 1/\nu_{12}$. Similarly, if one initially excites 1-pair $(\omega_3\,,\omega_4)$, energy effectively can go to the 1-pair $(\omega_1\,,\omega_2)$, if $\nu_{34} > 0$.

Notice, that according to Eq. (29), the increment ν_3 in a triad is always positive, meaning that A-mode in a triad is always unstable with respect to decay into two P-modes. The situation is different for quartets: Eq. (39c) does not guarantee that ν_{12}^2 is positive. For example, if $C_{1,0} \gg C_{2,0}$ or $C_{1,0} \ll C_{2,0}$, ν_{12}^2 is negative with any relationships between interaction coefficients. In case $C_{1,0} = C_{2,0}$ Eq. (39c) turns into

$$\nu_{12}^2 = \left[|S|^2 - \left(\mathcal{T}_1 + \mathcal{T}_2\right)^2/4\right] C_{1,0}^4\,, \tag{39e}$$

and shows that ν_{12}^2 can be either positive or negative, depending on the relations between $|S|$ and $(\mathcal{T}_1+\mathcal{T}_2)/2$. For negative ν_{12}^2 Eqs. (39a) describe pure oscillatory behavior of the amplitude A_3 with the frequencies $\omega_3 \pm |\nu_{12}|$ and A_4 with the frequencies $\omega_4 \pm |\nu_{12}|$. This means that the amplitudes do not grow in time and the energy transfer between the pairs $(\omega_1\,,\omega_2)$ and $(\omega_3\,,\omega_4)$.

As it was pointed out in [33], for a special type of quartets, with one of the 1-pairs formed by two equal wavevectors, say $\mathbf{k}_1 = \mathbf{k}_2$, criterion of instability can be formulated, for in this case we deal with an instability of a single monochromatic wave. In the water wave context, it is known as *Benjamin-Fair* instability [7].

3. Generic clusters

The study of dynamic behavior of the primary clusters, triads and quartets, is important for many reasons. First of all, they are physically relevant in the *discrete and mesoscopic wave turbulent systems* and can be used to interpret not only some laboratory experiments but also real physical phenomena, for instance, intra-seasonal oscillations in the Earth's atmosphere [60].

Interestingly, many generic clusters of connected triads are also integrable, in a sense that corresponding dynamical system is solvable in integrals [13] or at least necessary number of conservation laws is written out explicitly [112, 113]. Examples of integrable dynamical systems describing various clusters of two connected triads will be regarded in details in Section III B where two possible classes of double-triad clusters are discussed - butterflies (connection *via* one mode) and kites (connection *via* two modes). Integrability of double-triad cluster depend on many factors, first of all, on the connection type(s) within a cluster, that is, whether connecting mode or modes is (are) active or passive in one or both triads. Another important factor is the ratio of interaction coefficients of two connected triads.

Obviously, due to the criterion of instability, a special choice of initial conditions, i.e. initial energy distribution within the modes of a cluster, will always yield regular integrable behavior. Nice example is given by a cluster connected by one mode, active in both triads, with the condition that Hamiltonian is equal to zero (notice that it does not mean that the modes' phases are equal to zero).

For a big class of physically relevant initial conditions, dynamics of generic clusters consisting of a few hundred triads can be reduced to the dynamics of many smaller or even primary clusters [61]. Moreover, even big generic clusters are sometimes integrable, for instance, cluster of *arbitrary finite number* N of triads, all connected *via* one joint A-mode, if some conditions on the ratio of interaction coefficients are satisfied in which N-star cluster is integrable for *arbitrary* initial energy distribution within a cluster. Clusters of this form are called N-stars, in Section III B examples of 3-stars will be given appearing in real physical system (atmospheric planetary waves).

Cluster of N triads each connected only with two neighbor triads *via* one mode is called N-chain. N-chains have been studied numerically for $N \leq 8$, for real amplitudes and various initial energy distributions within a cluster [58]. Characteristic modes' behavior in the case $N = 4$ is shown in Fig. 2, [13], for all eight modes forming the cluster. Time evolution of the modes looks quite regular though no exact results on the integrability of N-chains are known.

Thus, for generic clusters of triads one can expect in some cases regular or even integrable motion. However most of them will demonstrate chaotic behavior, even in the smallest possible clusters of two connected triads, not speaking of bigger generic clusters. In Fig.4, example of Poincaré section is shown for butterfly 2-chain with connecting mode being P-mode in both triads and with ratio of interaction coefficients equal to 3/4.

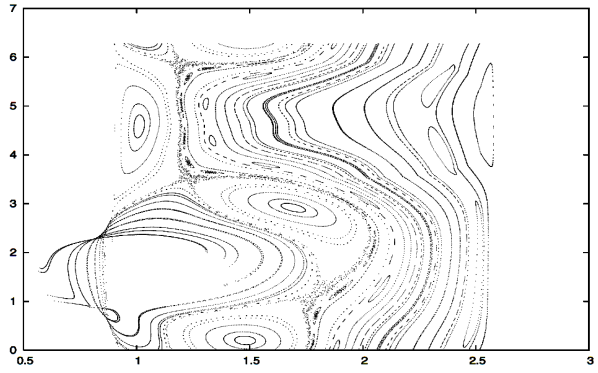

FIG. 4: Example of Poincaré section for a non-integrable butterfly cluster.

One of the most tedious and time-consuming parts of the numerical simulations aiming to establish whether or not dynamics is chaotic, is the choice of initial conditions. A special procedure has been worked out that guarantees a uniform distribution of initial conditions according to

Liouville measure, as well as assures that all conservation laws have the same value on each Poincaré section [59]. On the other hand, just simply choosing initially real amplitudes one gets regular evolution in the same resonance cluster.

Dynamics of bigger generic clusters of triads is practically not studied. One can put a lot of questions, for instance, whether thermodynamic states will be formed in chaotic clusters? Would some regimes exist where energy is concentrated in a special set of modes, similar to the phenomenon of Bose-Einstein condensation? Should we expect a turbulent state similar to the classical Kolmogorov cascade through the scales if including forcing and dissipation? If so, would it be similar or different from the KZ spectra of kinetic wave turbulence? etc. etc. Some preliminary answers will be given in Section IV B.

No dynamical results are presently known about clusters of two and more quartets.

C. Kinetic wave turbulence

Kinetic wave turbulence is characterize by the interaction frequencies, Γ_{K},:

$$\Gamma_{\text{K}}^{3\text{w}} \simeq |VA_{\boldsymbol{k}}|^2/\Delta_k v_{\boldsymbol{k}}\,, \tag{40a}$$

$$\Gamma_{\text{K}}^{4\text{w}} \simeq |TA_{\boldsymbol{k}}^2|^2/\Delta_k v_{\boldsymbol{k}}\,, \tag{40b}$$

for 3- and 4-wave systems correspondingly.

Note that for both (40a) and (40a) - and in fact for processes with any finite number of waves - the following universal relation between the kinetic and the deterministic timescales takes place:

$$\Gamma_{\text{K}} \simeq \frac{\Gamma_{\text{D}}^2}{\Delta_k v_{\boldsymbol{k}}}. \tag{41}$$

The upper bound for applicability of wave kinetic equations follows from the condition $\Gamma_{\text{K}} \ll \Delta_k v_{\boldsymbol{k}}$ which gives:

$$|VA_{\boldsymbol{k}}| \ll \Delta_k v_{\boldsymbol{k}}\,, \quad \text{3-wave systems,} \tag{42a}$$

$$|TA_{\boldsymbol{k}}^2|^2 \ll \Delta_k v_{\boldsymbol{k}}\,, \quad \text{4-wave systems.} \tag{42b}$$

On the other hand, the wave amplitudes should be big enough in order to provide the mean-free path $\ell = v_{\boldsymbol{k}}/\Gamma_{\text{K}}^{\cdots}$ to be less then the system size L:

$$|VA_{\boldsymbol{k}}| \gg v_{\boldsymbol{k}}\sqrt{\Delta_k\delta_k}\,, \quad \text{3-wave systems,} \tag{42c}$$

$$|TA_{\boldsymbol{k}}^2|^2 \gg v_{\boldsymbol{k}}\sqrt{\Delta_k\delta_k}\,, \quad \text{4-wave systems.} \tag{42d}$$

Combining Eqs. (42,a-d) we can easily compute the range of amplitudes in terms of dynamical frequencies Γ_{D}, given by Eqs. (21), corresponding to the region of developed weak wave turbulence described by the kinetic equations:

$$v_{\boldsymbol{k}}\sqrt{\Delta_k\delta_k} \ll \Gamma_{\text{D}} \ll v_{\boldsymbol{k}}\Delta_k\,. \tag{43}$$

D. Mesoscopic wave turbulence

Comparing the region of developed weak wave turbulence, Eq. (43), and the region of low-dimensional chaos, given by Eq. (22): $\Gamma_{\text{D}} \ll v_{\boldsymbol{k}}\delta_k$, one can see that if $\Delta_k \gg \delta_k$ (i.e. for $\mathcal{N} \gg 1$) there exists a gap

$$v_{\boldsymbol{k}}\sqrt{\Delta_k\delta_k} \gtrsim \Gamma_{\text{D}} \gtrsim v_{\boldsymbol{k}}\delta_k\,, \tag{44}$$

in which both equations (43) and (22) are violated. Existence of such a gap was first pointed out in [87] in the context of MHD wave turbulence. Region (44) possess the features of both types of turbulent behavior described above. In other words, in this region both types of turbulence coexist in the system and interact giving birth to a qualitatively new type of weak wave turbulence: *mesoscopic wave turbulence*. It was suggested in [85] (see also [74] and [87]) that in forced wave systems the low-dimensional and the kinetic regimes statistically alternate in time. Namely, the wave energy accumulates during the low-dimensional phase (with almost "frozen" cascade) until when the resonance broadening becomes of order of the k-grid spacing. After that the turbulence cascade is released to higher k's in the form of an "avalanche" characterized by predominantly kinetic interactions. Detailed study and description of such a regime of mesoscopic wave turbulence is one of two main subjects of the present paper.

Strength of wave turbulence typically varies in along the turbulent cascade in the k-space and, therefore, one may expect different wave turbulence regimes present in the different parts of the k-space at the same instant in time. Moreover, on the cross-over regions one can expect nontrivial gradual transition which involves blending and interaction of different dynamical and statistical mechanisms. Examples where the nonlinearity increases along the cascade toward high wavenumbers include the surface gravity waves, Alfven waves in MHD and the planetary Rossby waves. In these cases we expect different regions in the $\boldsymbol{k}$-space with different types of wave behavior: low-dimensional chaos at very low k's with graduate change to discrete wave turbulence and mesoscopic wave turbulence for intermediate k's and kinetic wave turbulence at large k's.

Regime of discrete wave turbulence is sometimes referred to as a finite-dimensional turbulence [78] as opposite to infinite dimensional turbulence [28]. However, in the context of weak wave turbulence this terminology is misleading while KZ spectra and kinetic wave turbulence theory are only valid on the inertial interval which is *always finite*. On the other hand, notion of discrete wave turbulence is introduced to point out the fact that at this regime distinct resonance clusters demonstrate chaotic dynamics which, on the contrary to kinetic regime, is confined into a different (distinct, discrete) isolated sets of modes, and not to all modes of inertial interval simultaneously.

To be specific, we understand these different regimes as follows.

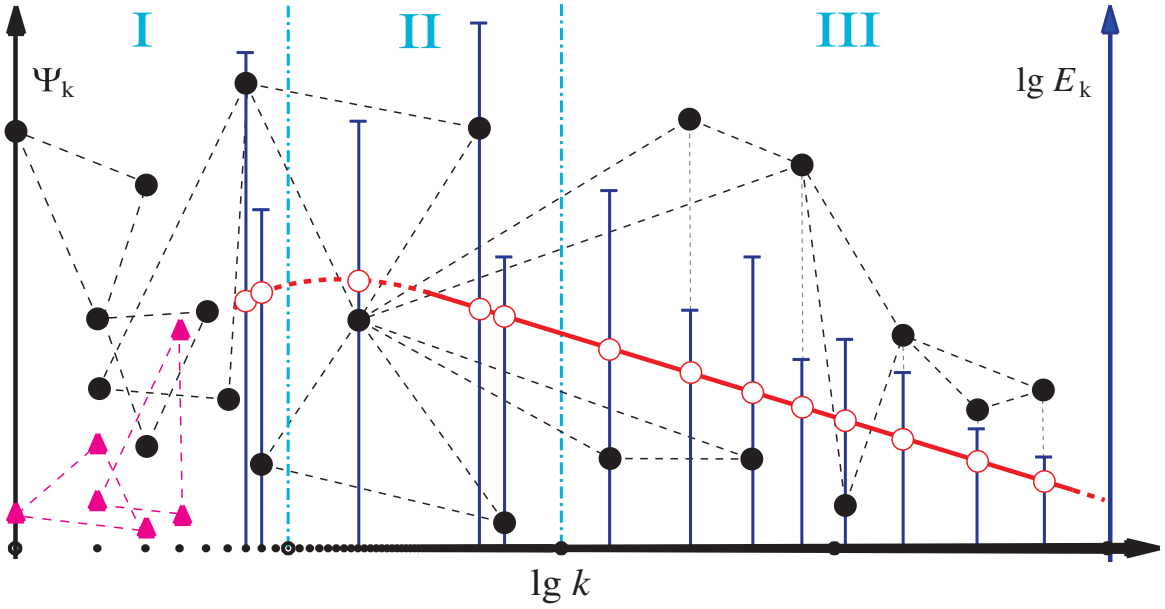

FIG. 5: Color online. Types of turbulent regimes: I – Low-dimensional chaos and discrete wave turbulence, II – Mesoscopic and III – kinetic wave turbulence. Modes of primary clusters, i.e. isolated triads, are denoted by (pink) triangles (connected by dashed lines) in modified polar coordinates, $\log k$ (horizontal axis, formed by small black dots, denoting allowed wavevector lengthes $k_n = 2\pi n/L$) and Ψ_k (left vertical axis). Modes of generic clusters are shown by black full circles. Energy spectrum E_k is depicted as (red) inclined solid line in Log-Log coordinates: $\log E_k$ (right vertical axis) vs. $\log k$. Energy of resonant modes, participating in generic clusters are shown by (blue) vertical solid T-shape lines. Empty circles in corresponding places of the continuous energy spectrum represent "gaps", indicating that for these wavevectors energy is given not by the incline solid line, but by the T-shape lines.

a. Low-dimensional chaos and discrete wave turbulence, as explained above, are regarded as chaotic and/or regular behavior of isolated resonant clusters with exact wave resonances. *Mathematically*, as we will show further, isolated clusters, including primary ones, can be found everywhere in the $\boldsymbol{k}$-space. However, *physically* clusters behave as isolated when the interaction frequency is smaller then the frequency spacing, see inequality (22). Depending on functions $\omega_{\boldsymbol{k}}$, V (or T) and solution $|A_k|$ of the equations of motion, clusters can be physically isolated either in the region of relatively small or relatively high k's in the cases when, respectively, the nonlinearity is increasing along the cascade (surface gravity waves, Rossby waves) or decreasing (capillary waves). To be specific, we will stick to the case when the nonlinearity is increasing toward higher k's. Correspondingly, in Fig. 5 low-dimensional region is shown at low k's. For our purposes it is convenient to display plane wavevectors in modified polar coordinates, $\log k$ (horizontal axis) and Ψ_k (left vertical axis). Right vertical axis, $\log E_k$, will be used later to display energy spectra E_k of developed and mesoscopic turbulence.

All modes in the isolated triads (i.e. primary clusters) are shown in Fig. 5 as (red) triangles, connected by dash lines. They demonstrate periodical behavior. The modes participating in the more complicated clusters with (possible) chaotic behavior are shown as full (green) circles.

b. Mesoscopic turbulence is shown in Fig. 5 as intermediate region II, where both turbulent regimes coexist: i) isolated clusters with energy of resonant modes, denoted as (blue) vertical T-shape solid lines, and ii) "continuous" energy spectrum E_k of developed turbulence characterized by statistical kinetic behavior, shown as (red) solid line with gaps. As we already mentioned, the low-dimensional and the kinetic regimes may sporadically alternate in time in a "sandpile" scenario. We showed energy spectrum in this interval by (red) dashed line to indicate that it is likely to be unsteadily pulsating. The scaling behavior in this range is somewhat upset by the pulsations and interactions with the "privileged" modes belonging to isolated resonant clusters. However, the mean slope is typically steeper in this range than KZ spectra at higher k's (see below). In particular, the slope ω^{-6} was predicted [85] and experimentally confirmed [23] for the gravity water waves (c.f. ω^{-4} for KZ spectrum in this case). Study of this region characterized by interaction between low-dimensional and developed turbulent subsystems is one of the most interesting problems, and it will be considered in the present paper.

c. Kinetic wave turbulence is the most well-studied type of turbulence. For the scale-invariant dispersion laws $\omega_k \propto k^\alpha$, numerous exact stationary solutions of corresponding kinetic equation were found. These solutions can be presented as one-dimensional energy density in the

$\boldsymbol{k}$-space, E_k, defined in such a way that $\int E_k dk/2\pi = E$ is the total energy (*per* unit volume) of the wave system. These spectra have also scale-invariant form $E_k \propto k^{-\beta}$, where energy scaling index β is typically positive (see [122] and references therein). Now it is clear why logarithmic coordinates, $\log E_k$ *vs.* $\log k$, were chosen. In these coordinates the power-law energy spectra E_k are linear. The most important among the power-law solutions is the one that corresponds to the energy cascade through the k-space, i.e. KZ spectra. This is shown schematically in Fig. 5 (on the right). Note that some of the clusters originating in the mesoscopic and even low-dimensional ranges can extend to the range of the developed turbulence. Thus, the wavenumbers belonging to these clusters can behave differently than (more numerous) wavenumbers forming the KZ spectrum. Such a selected wavenumber set would exhibit more coherent behavior at deterministic timescales; the amplitudes of these modes can significantly exceed the KZ spectrum and, therefore, they can cause turbulence intermittency in the k-space. For instance, energy of each mode E_{mode} in primary cluster

$$E_{mode}(t) \sim \mathbf{sn}^2(k\,t, \mu), \tag{45}$$

is defined by initial energy of a triad and initial energy distribution among the modes of a triad, hidden in the coefficient of proportionality and parameters k and μ, and can be pretty big (for explicit formulas see [52]).

III. KINEMATICS OF THE NONLINEAR RESONANCES

Regime of discrete wave turbulence occurs when

$$\frac{\Gamma_{\text{D}}}{\Omega_k} < \frac{1}{kL}. \tag{46}$$

In this case, nonlinear interaction takes place only among the modes which satisfy conditions of exact frequency and wavenumber resonance (7), (9). In this case the equations of motion become,

$$\begin{aligned} i\frac{d}{dt}B_k = & \sum_{\boldsymbol{k}_1,\boldsymbol{k}_2} V^k_{12} B_1 B_2 \delta^k_{12} \delta(\omega_k - \omega_1 - \omega_2) \\ & + 2V^{1\,*}_{k2} B_1 B^*_2 \delta^1_{k2} (\omega_1 - \omega_k - \omega_2). \end{aligned} \tag{47}$$

for the three-wave case and

$$i\frac{d}{dt}B_k = \sum_{\boldsymbol{k}_1,\boldsymbol{k}_2,\boldsymbol{k}_3} T^{k1}_{23} B^*_1 B_2 B_3 \delta^{k1}_{23} (\omega_k + \omega_1 - \omega_2 - \omega_3) \tag{48}$$

for the four-wave. Here, $B_k = a_k e^{i\omega_k t}$ is the interaction representation variable and δ's denote Kronecker symbols (i.e. they are equal to 1 when the corresponding resonances in k and ω are satisfied exactly and equal to 0 otherwise).

Thus, integer solutions of the resonance conditions (7), (9), etc. are defined by the geometry of a nonlinear wave system, that is, by *kinematics*. As soon as these solutions are found, one can study the corresponding dynamical systems (6b) and (8b). Below we begin with analysis of the the integer solutions of the resonant conditions.

A. Number theory and exact resonances

1. Preliminaries

Resonance conditions for three- and four-wave interactions are given by Eqs. (7) and (9). They can be presented in the general form

$$\omega(\boldsymbol{k}_1) \pm \omega(\boldsymbol{k}_2) \pm ... \pm \omega(\boldsymbol{k}_s) = 0\,, \tag{49a}$$

$$\boldsymbol{k}_1 \pm \boldsymbol{k}_2 \pm ... \pm \boldsymbol{k}_s = 0\,, \tag{49b}$$

with $s = 3$ and 4. There exist physical examples of the five- and six-wave systems, $s = 5$ and 6, but we will restrict ourselves in this paper to the three- and four-wave systems, which are more common. In infinite (unbounded) media wavevector $\boldsymbol{k}$ takes values in $\mathbb{R}^d$, where d is the dimension of the space. Let us for simplicity consider the 2D case, $\boldsymbol{k} = (k_x, k_y)$. One can easily find solution of Eqs. (49), if it exists, analytically or numerically. In bounded media the wavenumbers can be regarded as integers; for example in a 2D double-periodic box of size L

$$\boldsymbol{k} = \frac{2\pi}{L}(m, n)\,, \quad m, n \in \mathbb{Z} \tag{50a}$$

with integer m and n being the indexes of Fourier modes. Because of the linear dependence, the resonant conditions on the components of $\boldsymbol{k}$ is equivalent in this case to the respective resonance conditions on indices m and n. Now Eqs. (49) in a 2D double-periodic box take the form:

$$\omega(\boldsymbol{k}_1) \pm \omega(\boldsymbol{k}_2) \pm ... \pm \omega(\boldsymbol{k}_s) = 0\,, \tag{51a}$$

$$m_1 \pm m_2 \pm ... \pm m_s = 0\,, \tag{51b}$$

$$n_1 \pm n_2 \pm ... \pm n_s = 0\,. \tag{51c}$$

For other types of boundary conditions, we also have conditions on indices, but somewhat different from the periodic case. For example, for the Rossby wave system in a square basin with zero boundary condition, there will be a condition on the north-south wavenumber (quantized by index n) but there will be no resonance condition on the east-west wavenumber (quantized by m). For the Rossby waves on a sphere, the resonance condition must be satisfied by the azimuthal index m but not by the polar index ℓ. Instead of the resonance condition, index ℓ satisfies inequalities $\ell_i \geq |m_i|$, $(i = 1, 2, 3)$ and $|\ell_1 - \ell_2| < \ell_3 < \ell_1 + \ell_2$ and the sum of all the three ℓ's must be an odd number [105].

Respectively, the frequency conditions can also be expressed in terms of the indices. Because these conditions are linear in ω's, we can drop numerical (dimensional) pre-factors. For example, for the dispersion laws (10) for

the gravity and capillary waves in the double-periodic box and for the Rossby waves in a 2D box with zero boundary conditions, Eqs. (15b) (ocean), and for the Rossby waves on a sphere,(15c) (atmosphere), we can simply write:

$$\omega(\boldsymbol{k}) \;\propto\; (m^2+n^2)^{1/4}\,, \quad \text{gravity waves,} \tag{52a}$$

$$\omega(\boldsymbol{k}) \;\propto\; (m^2+n^2)^{3/4}\,, \quad \text{capillary waves,} \tag{52b}$$

$$\omega(\boldsymbol{k}) \;\propto\; \frac{1}{\sqrt{m^2+n^2}}\,, \text{ oceanic Rossby waves,} \tag{52c}$$

$$\omega(\boldsymbol{k}) \;\propto\; \frac{m}{\ell(\ell+1)}\,, \text{ atmosph. Rossby waves.} \tag{52d}$$

In these examples, the frequencies $\omega(\boldsymbol{k})$ are *irrational or rational numbers*. Generally speaking, the dispersion laws can be even more complicated objects, transcendental numbers, like $\omega(\boldsymbol{k})$ for gravity waves on water with finite depth h:

$$\omega(\boldsymbol{k}) \propto \left[\sqrt{m^2+n^2}\tanh\left(\frac{2\pi h}{L}\sqrt{m^2+n^2}\right)\right]^{1/2}. \tag{52e}$$

Notice that finding integer solutions of Eqs. (51) is a highly nontrivial problem. There are no general methods to do it analytically. Moreover, in its most general form the problem is equivalent to the Hilbert's 10th problem which is proven to be algorithmically unsolvable. Numerically, the problem amounts in necessity to perform extensive computations with integers, 10^{12} and 10^{48} operations (in physically significant k-domains) for the 3- and the 4-wave systems respectively.

Probably the most often encountered context in which a physicist uses big natural numbers is generation of random numbers. However, finding numerical properties of big integer numbers is not as simple as random number generation. For example, generation of a random number of order 10^{19} is much faster than to establish that a number of order 10^8 can be decomposed into the sum of two integer squares. Computational problems in integers present some specific challenges. First of all, the solution must be *precise* and not approximate as with "reals" (i.e. floating-point numbers). Consider, for instance, a circle of some astronomic radius, say $R = 10^{100}$. Its area can be computed in microseconds with any reasonable precision. However, calculating the precise number of integer points within that same circle by computer is an unrealistic task for modern means - "full search" for multivariate problems in integers consumes exponentially more time with each variable and size of the domain to be explored.

Another important point is that it is not a problem of a "good approximation" - solution in integers either exists or not. Everybody knows that equation $x^2 + y^2 = z^2$ has infinitely many integer solutions named Pythagorean triples, for instance $3^2 + 4^2 = 5^2$. On the other hand, equation

$$x^3 + y^3 = z^3 \tag{53}$$

has no integer solutions which was proven by Euler. Remarkable fact is that we did not choose this equation by chance - it is used in [48] for proving that no resonant triads exist among capillary waves in a rectangular domains with periodic boundary conditions.

In fact, Eq. (53) is a particular case of the famous Last Fermat Theorem stating that equation

$$x^n + y^n = z^n \tag{54}$$

has no solutions for $n > 2$ and all x, y, z, n being integers. It took more than four hundred years of efforts of many famous mathematicians to finally prove this theorem.

Problem to find solutions of Eqs. (51) for different dispersion laws generates various *Diophantine equations* that have to be analyzed and solved in integers. Of course, numerical computations in a small computational domain might help to find some. However this cannot help *to prove* that for some dispersion functions no solutions exist in any domain. The mathematical problems of this kind are the main subject of the analytical number theory and the theory of Diophantine equations.

First theoretical study of general properties of different resonant systems was undertaken in [41, 42] while their physical implications have been briefly presented in [44], together with some numerical simulations to demonstrate that the theoretical findings keep true for quasi-resonances with some small though non-zero resonance width.

General approach to analyze resonance conditions (51) based on a few pure existence theorems is given in [48]. This approach has been further developed in [50] where constructive computational method called *q-class decomposition* have been presented. This method was implemented numerically [55, 56] for a few important irrational dispersion laws in the three- and four-wave interaction systems. Computational scheme for rational dispersion function (52d) can be found in [57] (it uses specific form of the function for fast computing). Below we present a few simple ideas underlying *q-class decomposition*.

2. *q-class decomposition*

a. Simplest version. The main mathematical idea providing a basis for q-class decomposition is very transparent and follows from the properties of rational and irrational numbers. Let us begin with a very simple example: as a reader can easily see, equation

$$a\sqrt{5} + b\sqrt{11} = 0 \tag{55}$$

has no solutions for arbitrary rational a and b. Now let us take for concreteness the dispersion law (52b) for the capillary waves, $\omega(n,m) = (m^2+n^2)^{3/2}$, and put a question: when equation

$$\omega_1 + \omega_2 = \omega_3\,, \quad \omega_j \equiv \omega(n_j, m_j)\,, \tag{56}$$

has solutions with integer n_j, m_j? To answer the question, let re-write each ω_j in the way:

$$\omega_j = p_j\sqrt{q_j}, \quad p_j, q_j \in \mathbb{N} \quad \text{and} \quad q_j \quad \text{is square-free}\,, \tag{57}$$

(here notation $p_j, q_j \in \mathbb{N}$ means that p_j and q_j are natural numbers). Due to the main theorem of arithmetics this presentation is unique and it is an easy exercise to prove that (56) has solutions only if all three vectors have the same irrationalities, that is, if $q_1 = q_2 = q_3$. Obviously, this is only the necessary condition for a solution to exist, not sufficient, but it allows to diminish computational time drastically while highly nonlinear equation (56) on 6 variables is now substituted by *linear* equation $p_1+p_2 = p_3$ on 3 variables only.

This simple example shows that all wavevectors with integer coordinates can be decomposed into non-intersecting classes due to q. This implies that a search for solutions can be performed in each set of wavevectors with the same q separately!

b. Irrational dispersion laws. The situation becomes immediately more involved if degree of irrationality is bigger, even in the case of 3-wave systems. In 4-wave systems already *gluing of classes* does occur [43], that is, the wavevectors from different classes can interact resonantly. However, the gluing is not arbitrary but rather well-structured; for instance, in an arbitrary 4-wave system with irrational dispersion function (e.g. surface gravity waves, Eqs. (58)) only two types of solutions exist:

Type 1: 2 wavevectors belong to q_1-class, while 2 other wavevectors belong to q_2-class with $q_1 \neq q_2$;

Type 2: all 4 wavevectors belong to the same q-class;

The general structure of possible gluing, for arbitrary s-wave system (with finite s) and arbitrary irrational dispersion laws is described by Besikovich theorem [9, 55]. The theorem can also be applied for the systems where waves with different dispersion laws do interact.

This means that for general dispersion law $\omega(n, m) = (m^2 + n^2)^{\pm\alpha}$ with any non-zero rational α which is not an integer, corresponding construction of q-classes can be performed similarly, for instance with $\alpha = 1/2$ (ocean planetary waves), $\alpha = 3/2$ (capillary waves), $\alpha = 1/4$ (gravity water waves), etc. The method can also be applied to any combination of different wave types, for instance, while looking for resonances constructed by two capillary and three gravity waves, etc.

In this paper only 3- and 4-wave systems will be regarded, i.e. the general message we get from these theoretical considerations is as follows. All resonances are formed by the wavevectors belonging to one q-class in a 3-wave system, while in 4-wave systems they can also belong to two different q-classes.

c. Rational dispersion laws. Strikingly enough, one of the most complicated situations is accounted if dispersion function is a rational function, for instance, Eq. (52d): $\omega(\boldsymbol{k}) = m/\ell(\ell + 1)$ (for atmospheric planetary waves), because obviously rational numbers are *linearly dependent* over the field of rational numbers $\mathbb{Q}$ in which case the general methodology of the q-class decomposition cannot be applied. Nevertheless, some computational short-cuts are possible [57] and the resonance solutions of corresponding Eqs. (51) can also be computed in a matter of minutes in computational domain of order of 10^3.

d. Transcendental dispersion laws. Moreover, dispersion functions like Eq. (52e) can be treated similarly with the general methodology based on the *Theorem on the partition* ([48], p. 98). As soon as dispersion function is a function whose values are algebraically independent in some sense, a partition in **k**-space exists. Construction of this partition for the transcendental dispersion law (52e) has been briefly sketched in [43]. In general, if dispersion law can be written as a linear combination of exponents with rational coefficients, Eq. (51a) can also be re-written this way and *Lindemann-Weierstrass theorem* [5] supplies a decomposition.

Method of the q-class decomposition allows to compute and study complete resonance solution sets for many 3- and 4-wave systems and this was how one of the most important characteristics of the wave systems possessing resonances - resonance clustering - has been first discovered [44, 48]. The next important step was to construct a suitable graphical representation for the resonant clusters. The sketch of a possible representation has been given more than ten years ago ([48], Fig.3). This idea has been worked out in more details quite recently in [53, 61] and results are reviewed in the next section.

3. NR-diagram

The classical way to represent nonlinear resonances is constructing *resonance curves*. Resonance curve is the locus of pairs of wavevectors interacting resonantly with a given wavevector. This construction, very popular in 1960th, gives some useful, though partial, information about possible resonances in wave system. For instance, in [79] and [97] resonance curves are studied for three- and four-wave resonance systems correspondingly. The form of resonant curve changes drastically, even for the same dispersion function, according to the magnitudes of a fixed wavevector for which a curve is constructed: it might be an ellipse, be shaped like an hour-glass or even degenerate into a couple of lines.

Resonance curve representation has two drawbacks: 1) it allows to visualize only a part, if any, of resonance set; and 2) there is no constructive way to find integer points on a curve of general form [81]. This means, in particularly, that we can construct a locus on the plane (for 3-wave system) where all the wavevectors should lie that interact resonantly with a fixed one, but we never know whether or not there are any. In the case of 4-wave resonance system we must fixed not one but two wavevectors for constructing corresponding resonance curve.

On the other other hand, having the complete resonance solution set computed, one would definitely like to have have informative graphical representation for all resonance clusters in a given computational domain.

a. 3-wave system. Such a representation has been constructed for 3-wave systems and called topological

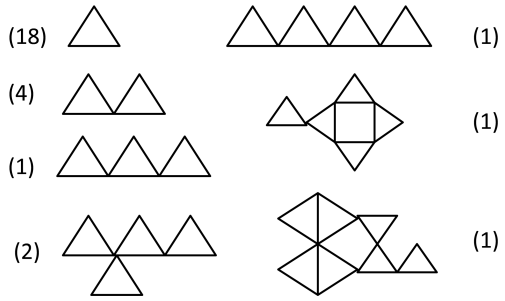

FIG. 6: Resonance of Topological structure of the cluster set for the oceanic planetary waves, $\omega \sim 1/\sqrt{m^2+n^2}$, in the domain $m, n \leq 50$. The number of the clusters of each type is shown in parenthesis.

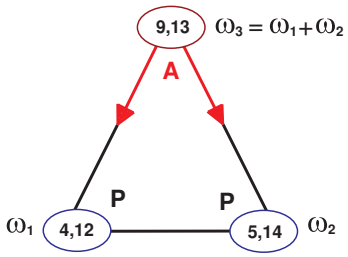

FIG. 7: Example of isolated triad, wave numbers are given for atmospheric planetary waves.

representation of the resonance solution set [62]. In this representation, each mode of a triad is shown as a vertex of a plane graph and those vertexes which belong to one triad are connected by the lines. This way each isolated triad is shown as a triangle, while clusters consisting of a few connected triads, form a graph of special structure. Some examples are shown in the Fig.6. The algorithm of constructing topological presentation has been implemented as on-line service [93], its detailed description is given in [65]. This service can be used for extracting topological structure from given resonance solution set for *arbitrary* 3-wave resonance system. Together with

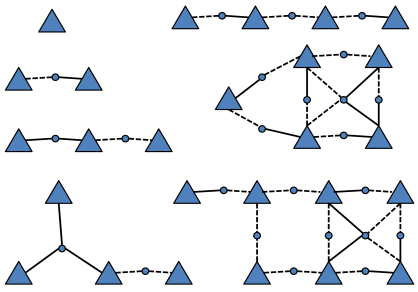

FIG. 8: NR-diagrams for some resonance clusters shown in Fig.6.

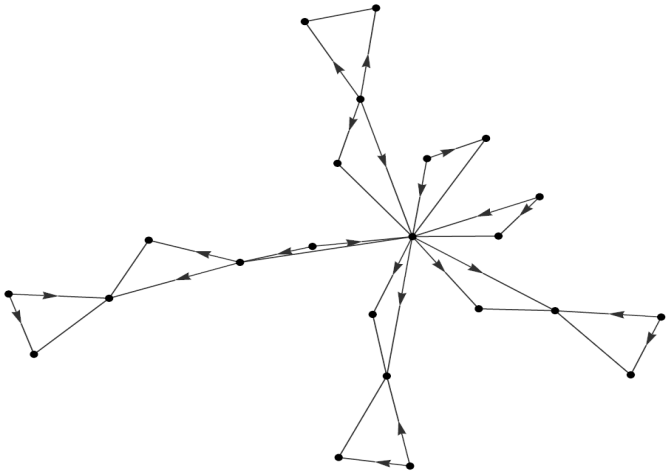

FIG. 9: Topological representation of a 11-triads cluster.

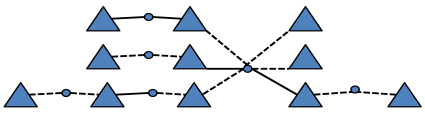

FIG. 10: NR-diagram of a 11-triads cluster shown in Fig.9.

complete resonance solution set, topological structure allows to restore uniquely corresponding dynamical system [62].

On the other hand, including some markers for A- and P-modes into the topological structure, we will get all most important information about cluster dynamics just looking at the picture. This was first proposed in [61] where A-mode has been marked by two out-coming arrows directed to P-modes. Another way use for including dynamic information into the topological structure is just to mark corresponding vertexes with letters A and P, or to combine marked vertexes with marked arrows [52], example of the later is given in Fig.7. This representation, though quite helpful for elucidating small resonance clusters, yields quite big and not easily understandable pictures for a bigger clusters (see Fig.9, cluster appearing in the resonance set for atmospheric planetary waves).

A novel representation of a resonance resonance cluster in form of a *NR-diagram* has been proposed quite recently [53] which combines the clarity and transparency of presentation, both for 3- and 4-wave systems. In a NR-diagram each (hyper-)vertex denotes not a mode but a *primary cluster* - triad in 3-wave system and quartet in 4-wave system. Dynamical information is shown by the form of edges connecting (hyper-)vertexes.

In 3-wave system vertexes are denoted as triangle and

two types of half-arcs are introduced: *bold* for **A**-mode and *dotted* - for **P**-mode. Examples of NR-diagrams for *some* clusters shown in Fig.6 are presented in the Fig.8. Namely, all primary clusters (triads) and generic clusters appearing only once are shown, but for 4 clusters of two triads and for 2 clusters 4 triads only one diagram is included. NR-diagram for 11-triad cluster is shown in Fig.10.

b. 4-wave system. In 4-wave systems even clusters consisting of a small number of connected quartets have already quite non-transparent topological structure [63]. Example of topological structure is given in Fig.11 for 4-quartet cluster appearing among surface wave waves [63]. Moreover, as it was demonstrated in [51], there are exist two types of resonant quartets called *angle*- and *scale*-resonances, with qualitatively different dynamics. Scale-resonances provide effective energy percolation over the wavelengths while angle-resonances distribute energy over phases. Accordingly, resonance clusters can be formed by each type of resonances separately, and also *mixed cascade* is possible, that is, a resonance cluster might be formed by the quartets of both types [51, 63]. We will discuss this intrinsic dynamics below in more details.

In order to keep this dynamical information in a NR-diagram, two types of vertices are introduced - *squares* for scale-resonances and *circles* for angle-resonances. Connections within a cluster of quartets are possible *via* a vertex (a single bold line), edge (double bold) and diagonal (dashed). They are referred to as **V**-, **E**- and **D**-connection types correspondingly, some examples are shown in Fig.12. These connection types help us to

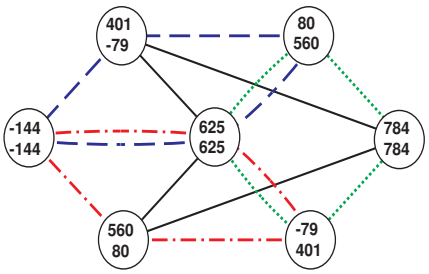

FIG. 11: Topological presentation of a resonance cluster of quartets, wave numbers are given for surface gravity waves. Solid black, dashed blue, dotted-dashed red and dotted green lines connect the wavevectors forming first, second, third and fourth quartets of the cluster correspondingly.

keep the information about 1-pairs (edges) and 2-pairs (diagonals) introduced above. Again, dynamical system for each cluster can be written out explicitly (examples are to be found in [54], Chapter 3).

Various diagram techniques for describing statistical systems are known beginning with the Feynman diagrams. Their main distinction from NR-diagrams is as follows. Only a *sum of statistical diagrams* represent a possible interactions of waves or particles, while each NR-

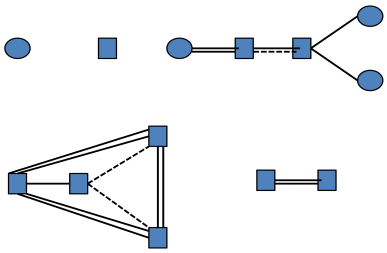

FIG. 12: NR-diagrams of clusters in appearing in four-wave systems (left to right and up to down): primary angle-resonance, primary scale-resonance, mixed cascade consisting of 5 quartets with one **E**-angle-scale, one **ED**-scale-scale and two **V**-scale-angle connections; pure scale-resonance cluster consisting of 4 quartets shown in Fig.11; **E**-scale-scale cluster.

diagram *completely represents* a cluster. Thus, any statistical diagram only gives a term in the perturbation equation and does not allow computing of the amplitudes of scattering process. On the contrary, NR-diagram allows to reconstruct uniquely dynamical systems on the wave amplitudes which can be solved either analytically or numerically.

B. Generic clusters of triads

1. NR-diagrams for 2- and 3-triad clusters

It is very important that primary clusters, triads and quartets, can share wave vectors and thereby form clusters of more complicated structure, similarly to Lego pieces used by a child to build a house. Examples of these structures for different types of waves can be found in [51–53, 57, 62, 63, 78], etc. Below we present all possible types clusters formed by two and three triads and referred to as 2- and 3-triad clusters correspondingly and some of their NR-diagrams.

a. 2-triad clusters 2-triad clusters consist of two triads connected *via* one common mode, referred to as *butterflies*, or two common modes, referred to as *kites*. Dynamics of a cluster depends on the type of the connecting mode which is allows us to distinguish three types of butterflies: PP-, PA- and AA-butterflies, their NR-diagrams are shown in Fig.13. Similarly we will distinguish PP-PP-, PP-AP-, PP-AA- and PA-AP-kites, shown in Fig.14.

b. 3-triad clusters Structure of 3-triad clusters is substantially richer that can be seen from the Fig.15. Some of corresponding NR-diagrams are presented in Fig.16, not all all of them, for the complete set of them contains a few dozens of diagrams.

As was already mentioned, this NR-diagram presentation of a cluster allows to write out explicitly corre-

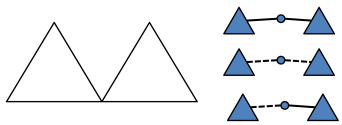

FIG. 13: Topological representation of a butterfly (on the left) and all possible NR-diagrams (on the right).

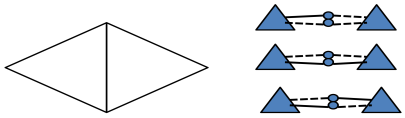

FIG. 14: Topological representation of a kite (on the left) and all possible NR-diagrams (on the right).

sponding dynamical systems. One can also use them as an additional check that resonance solution set was constructed correctly. Indeed, cluster shown in Fig.17, on the left, might be forbidden due to kinematic considerations: if two couples of P-modes coincide, than for some dispersion functions and/or some spectral domains this means that A-modes also coincide, i.e. the cluster is just a triad. The clusters in the middle and on the right are always forbidden, due to dynamical reasoning: no triad can have two A-modes.

One have to understand clearly that *not all* these clusters do appear in each 3-wave system. For instance, kites do appear among oceanic Rossby waves (in the spectral domain $m, n \leq 200$) though have not been found among atmospheric Rossby waves in substantially larger domains. To be more specific, below we describe the clusters formed by atmospheric Rossby waves in the spectral domain $|m|, \ell \leq 1000$. In this domain there exist altogether 1965 isolated triads and 424 clusters consisting of 2 to 3691 connected triads, among them 235 butterflies, 95 triple-triad clusters, etc. Three largest clusters consist

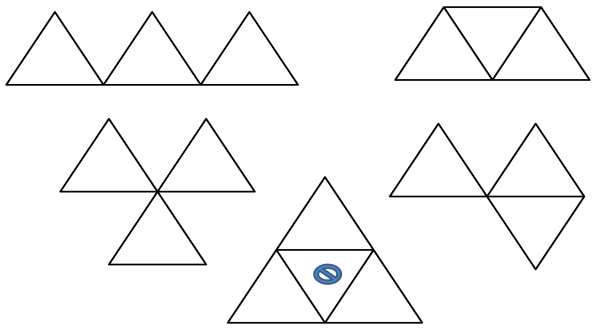

FIG. 15: Topological representation of all 3-triad clusters (the sign $\varnothing$ in the inner triangle shows that this triangle is fictional and does not correspond to a solution).

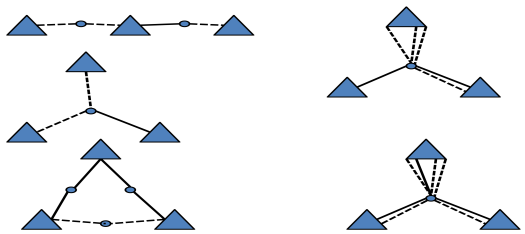

FIG. 16: NR-diagrams for some 3-triad clusters shown in Fig.15.

FIG. 17: Examples of "wrong" NR-diagrams.

of 14, 16 and 3691 connected triads (for overall data see histogram in Fig. 20$\mathcal{A}$). Examples of butterflies and 3-star clusters appearing among atmospheric Rossby waves are given in Fig.18 and Fig.19. Explicit form of the bigger clusters, with wavenumbers shown, can be found in Wolfram Demonstration Project [104] (spectral domain ≤ 200; complete list of clusters in the domain ≤ 1000 is available from authors).

Below we give examples of butterflies and 3-stars appearing in the resonance clustering of atmospheric Rossby waves. We have chosen topological representation in this case for it is convenient for showing specific wavenumbers of the modes forming the cluster. Moreover, some of these clusters will used further for describing numerical simulations, therefore also notations "a", "b" and "c" for distinct triads are added.

2. *PP-reduction of generic clusters*

It is clear from the analysis of the dynamics of isolated triad in II B 1 that any triad, connected to the rest of the cluster via PP-connection cannot accept energy from the cluster. Thus connections in a cluster, involving only P-modes are not penetrative for energy in any directions. Therefore from the dynamical viewpoint it is useful to divide large clusters into "almost separated" subclusters connected by PP-connections. For example, PP-butterfly in Fig. 18$\mathcal{B}$ can be *PP-reduced* into two triads, PPP-star in Fig. 19$\mathcal{D}$ is *PP-reducible* into three triads. *PP-reductions* of triple chains are shown in Fig. 21$\mathcal{B}$, $\mathcal{E}$, $\mathcal{F}$ and $\mathcal{G}$ by dashed lines. Notice that the PP-reduction *does not necessary diminishes* the size of a cluster. Indeed, though it is a case for any N-chain, this is not true anymore for an arbitrary 3-triad cluster (see Fig.19$\mathcal{H}$).

Whether or not a cluster is PP-reducible can be seen immediately from the form of its NR-diagram. Each time a connection formed by two dashed half-arcs occur, we can "cut" it off in the middle (shown as a small circle).

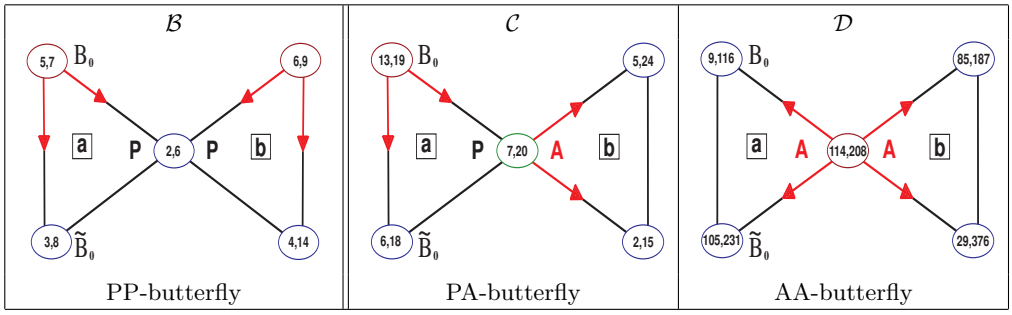

FIG. 18: Color online. Examples of butterflies (Panels $\mathcal{B}$, $\mathcal{C}$ and $\mathcal{D}$) for atmospheric planetary waves. Wave numbers of modes m , ℓ are shown inside ovals. The letters "a" and "b" in square boxes of butterflies denote triads and will be used as subscripts in the corresponding evolution equations for amplitudes and for integrals of motion. In studies of free evolution in Sec. **??** the initial energy is concentrated in the "leading" a-triad in "individual" modes with amplitudes B_0 and $\widetilde{B}_0$ and then goes to the "driven" b-triad.

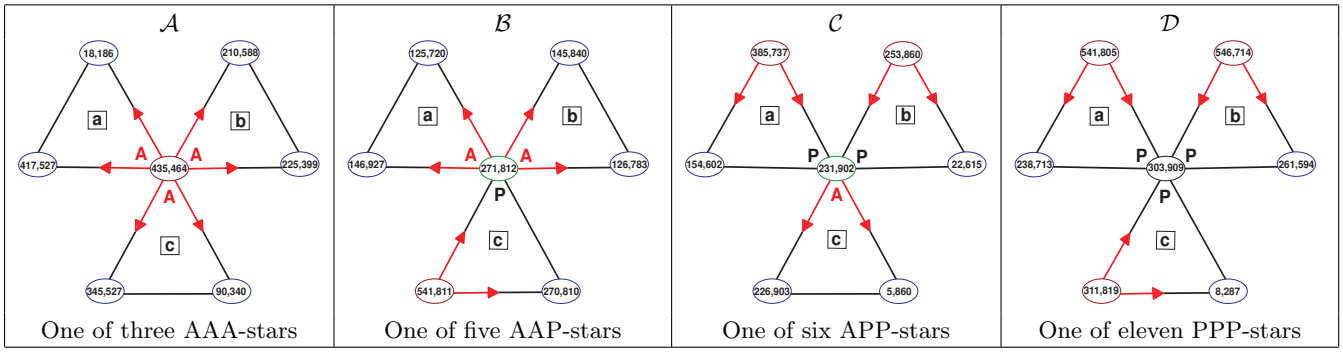

FIG. 19: Color online. Examples of isolated 3-stars for the atmospheric planetary waves. The letters "a", "b" and "c" in square boxes denote triads and will be used as subscripts in the corresponding evolution equations for amplitudes and for integrals of motion. All other notations as in Fig.18.

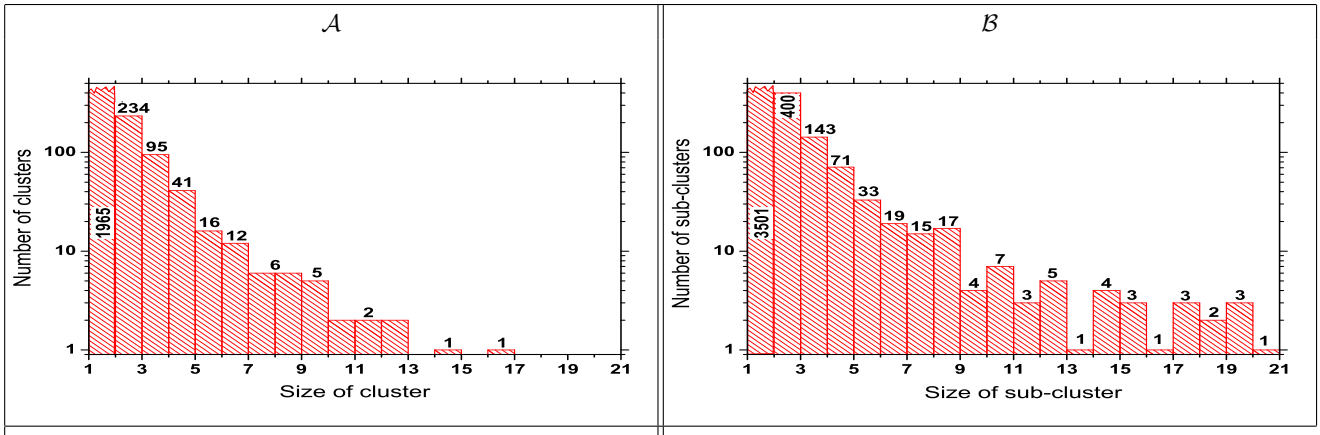

The 3691-triad cluster (monster) is not shown

Sub-cl. size	21	24	28	30	32	33	35	37	38	44	121	127	130
Amount	2	3	1	1	1	2	1	1	1	1	1	1	2

Amount of sub-cluster of size ≥ 21

FIG. 20: Color online. Horizontal axes denote the number of triads in the cluster while vertical axes show the number of corresponding clusters (panel $\mathcal{A}$) and PP-irreducible subclusters (panel $\mathcal{B}$).

.

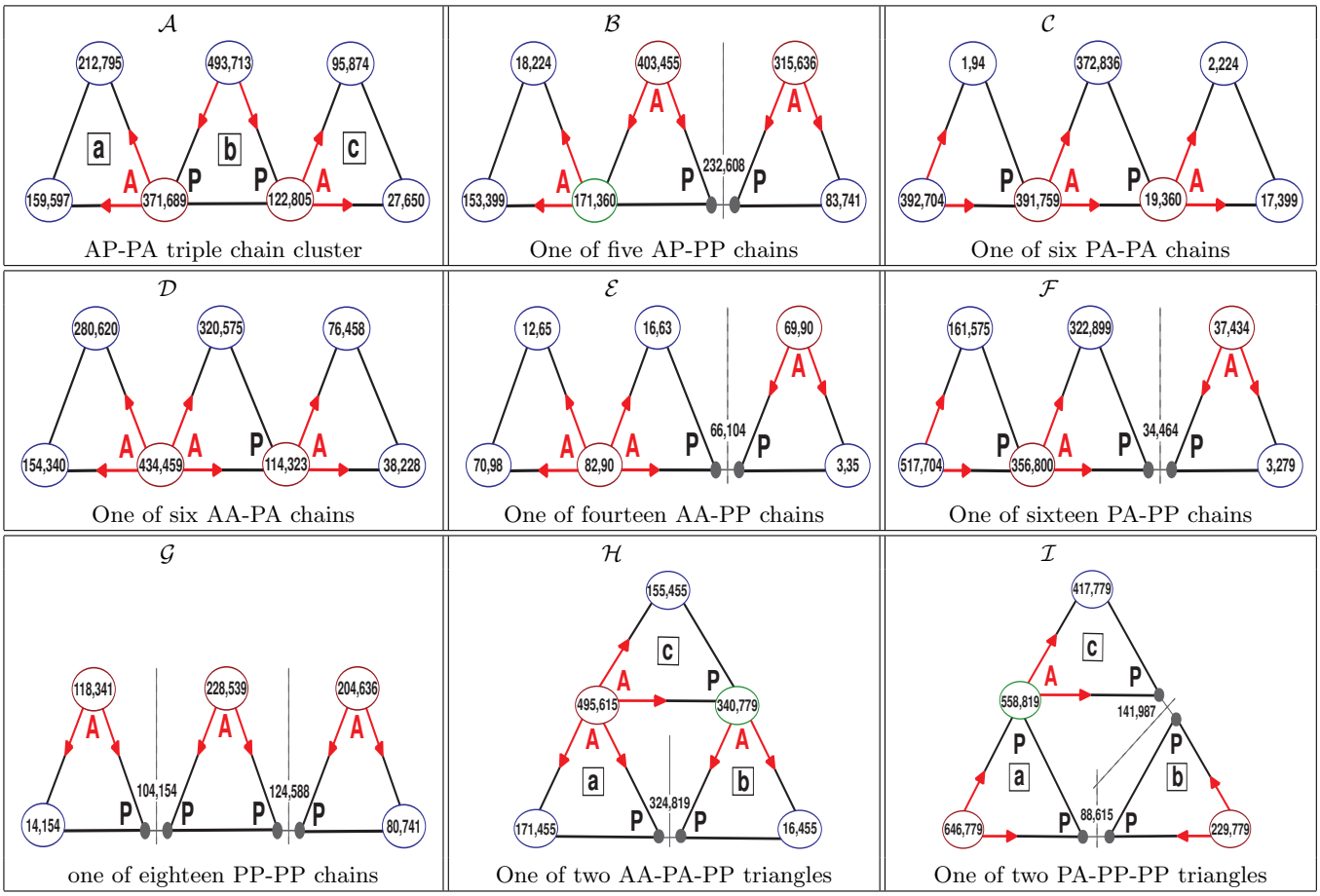

FIG. 21: Color online. In the spectral domain $m \le \ell \le 1000$ of the atmospheric planetary waves there are 66 isolated triple-chain clusters of seven types (examples are shown in panels $\mathcal{A}-\mathcal{F}$) and four triangle clusters with (AA-PA-PP)- and (PA-PP-PP)-connections (examples are shown in panels $\mathcal{H}, \mathcal{I}$)). Common PP-modes are split, denoting difficulty in the energy exchange between corresponding triads. Dashed lines separate PP-irreducible sub-clusters, discussed in Sec. III B 2.

For instance, 11-triad cluster with NR-diagram shown in Fig.10 is PP-reducible into 3 primary clusters (triads) and one 8-triad cluster. After cutting off all completely dashed connections, we will get a set of clusters without any PP-connections. Each of them is called *PP-irreducible cluster*.

For example, triangle cluster in Fig. 21 $\mathcal{I}$ consists of PP-irreducible triad and a PA-butterfly. Statistics of the PP-irreducible clusters of the atmospheric planetary waves is show in histogram in Fig. 20$\mathcal{B}$. We can see that the two largest PP-irreducible clusters (both belonging to the monster) consist of 130 triads.

We remark here again that clusters cannot carry energy flux through PP connections; therefore their dynamics is naturally reduced to the dynamics of PP-irreducible sub-clusters. Thus, for a wide class of initial conditions, relevant both for laboratory experiments and in real phenomena, it is sufficient to study carefully the dynamics of these PP-irreducible clusters to understand the properties of discrete wave turbulence in any cluster.

C. Generic clusters of quartets

The main difference between 3- and 4-wave resonance systems is as follows. In a 3-wave system *arbitrary* resonance generates new wave scales, for resonance condition $\omega_1 + \omega_2 = \omega_3$ forbids three equal wavevectors to form a resonance. The situation is different if resonance condition has the form $\omega_1 + \omega_2 = \omega_3 + \omega_4$. In this case, a resonance can be formed by a two couple of wavevectors with correspondingly equal lengths ($k_1 = k_3$ and $k_2 = k_4$ or $k_1 = k_2$ and $k_3 = k_4$) and therefore no new wavelengths are generated by the solution of this type. This fact though obvious for every physicist have not been in use till recently [51, 63] where complete resonance sets have been computed and investigated.

Thus, from *dynamical* point of view all resonant quartets can be divided into two classes (providing of course that corresponding interaction coefficients do not vanish): *scale-resonances* (providing effective energy percolation over the wavelengths) and *angle-resonances* (distributing energy over phases). It is important to under-

stand that though q-class decomposition yields two types of solutions, with wavevectors belonging to one or two q-classes, these classes *do not correspond* to the scale- and angle-resonances! Indeed, all resonances formed by wavevectors of two $q-classes$ are angle-resonances. But among one q-class solutions we meet both angle- and scale-resonances.

Besides these *dynamical* reasonings which were taken into account while constructing NR-diagrams for a 4-wave system (two forms of vertexes, see Section III A 3) some *kinematic* considerations are also quite helpful for discussing 4-wave system evolution. Indeed, basing on the relations between the wavelengths and directions of wavevectors within a quartet, important types of quartets can be singled out.

To be more precise, all our examples below are given for resonances among surface water waves. Resonance conditions (51) in this case read

$$\sqrt{k_1}+\sqrt{k_2} \;=\; \sqrt{k_3}+\sqrt{k_4}\,, \tag{58a}$$

$$\boldsymbol{k}_1+\boldsymbol{k}_2 \;=\; \boldsymbol{k}_3+\boldsymbol{k}_4\,, \tag{58b}$$

where, as usual $k \equiv |\boldsymbol{k}|$ and $\boldsymbol{k}_i = (m_i, n_i)$ and $k = \sqrt{m^2+n^2}$. Below all data about amount and form of resonant quartets, and resonance clustering are given for spectral domain $|m|, |n| \le \mathcal{N} = 10^3$. (We consider eight quartets, that differ only in permutations

$$\boldsymbol{k}_1 \Leftrightarrow \boldsymbol{k}_2\,,\ \boldsymbol{k}_3 \Leftrightarrow \boldsymbol{k}_4\,,\ (\boldsymbol{k}_1\,,\ \boldsymbol{k}_2) \Leftrightarrow (\boldsymbol{k}_3\,,\ \boldsymbol{k}_4)\,, \tag{59}$$

as the same quartet).

Below we distinguish following kinematic types of resonances:

- *Trivial quartet* which is always an angle-resonance is defined as follows:

$$\begin{aligned} \boldsymbol{k}_1 = \boldsymbol{k}_3 = \boldsymbol{k}\,, \quad \boldsymbol{k}_2 = \boldsymbol{k}_4 = \boldsymbol{k}' \\ \text{and } \boldsymbol{k}_1 = \boldsymbol{k}_4 = \boldsymbol{k}\,, \quad \boldsymbol{k}_2 = \boldsymbol{k}_3 = \boldsymbol{k}'\,, \end{aligned} \tag{60}$$

with any $\boldsymbol{k}$ and $\boldsymbol{k}'$.

- *Collinear quartet* can be either angle- or scale-resonance, and is formed by all 4 collinear wavevectors.
- *Trident* is always a scale-resonance and is formed as follows. One of its 1-pairs (recall Section II B 2) consists of two anti-parallel wavevectors with equal lengths (say $\boldsymbol{k}_1 \uparrow\downarrow \boldsymbol{k}_2$), the second 1-pair is formed by two wavevectors with different lengths.
- *Common quartet* is always a scale-resonance formed by three or four different wavevectors.

1. Trivial quartets

Equation of motion for trivial quartets (60) follows from Eqs. (31) with $S = 0$. This means that $d|A_j|^2/d\,t = 0$ for all $j = 1\,,\ 2\,,\ 3\,,4$, i.e. the energy exchange is absent. But this does not mean that the trivial quartets do not affect on the wave dynamics at all: terms $\Delta_j A_j$ in the RHS of Eqs. (31) describe the nonlinear shift of frequencies, that influences the phase dynamics and consequently the energy exchange in other quartets involving the same modes. This results, for instance, in the dependence of the instability increment (39c) of a quartet on the interaction coefficients $T_{\boldsymbol{k},\boldsymbol{k}'}$, responsible for the frequency shifts Δ_j, according to Eqs. (39d).

2. Collinear quartets

The majority of scale quartets (213760 among 230464 in our spectral domain) are collinear, i.e. are formed by four wavevectors belonging one line. The collinear quartets can, in principle, transfer energy between modes with different scales (lengthes of the wavevector). However, for the gravity waves the interaction coefficients S, responsible for such a transfer in collinear quartets, is equal to zero[24]. Therefore in this particular case collinear quartets have no dynamical significance. On the other hand, coefficients S for other wave systems do not necessarily vanish. Therefore in this review we make some useful remark about general collinear quartets.

Obviously, in a collinear quartet all the ratios $|m_i|/|n_i|$ are the same for all four wavevectors, say $|m_i|/|n_i| = c$. The use of this fact allows to construct series of corresponding solutions (see [63]). For instance, case $c = 0$ corresponds to the solutions lying on the axes X ($n_i = cm_i$) and Y ($m_i = cn_i$), i.e. with all $m_i = 0$ or $n_i = 0$ correspondingly, *e.g.* 4-tuple $\{\{4,0\},\{-49,0\},\{-36,0\},\{-9,0\}\}$. Parametrization of the resonances in this case was first given in [24].

3. Tridents and common quartets

a. Axial tridents. As we mentioned in Sec. **??** tridents are special type of scale quartets in which one of the 1-pairs (say ω_1 and ω_2) has antiparallel wave vectors $\boldsymbol{k}_1 \uparrow\downarrow \boldsymbol{k}_2$ [and thus $(\boldsymbol{k}_1 \cdot \boldsymbol{k}_2) = -k_1 k_2$], while two other wave-vectors have the same length: $k_3 = k_4$ and are equally inclined to $\boldsymbol{k}_1$, i.e. $(\boldsymbol{k}_1 \cdot \boldsymbol{k}_3) = (\boldsymbol{k}_1 \cdot \boldsymbol{k}_4)$.

The parametrization of the tridents, suggested and studied in [74, 85] yields

$$\boldsymbol{k}_1 \;=\; (a,0),\ \boldsymbol{k}_2 = (-b,0),\ \boldsymbol{k}_3 = (c,d),\ \boldsymbol{k}_4 = (c,-d), \tag{61}$$

$$\begin{aligned} a \;&=\; (s^2+t^2+st)^2\,, \quad b = (s^2+t^2-st)^2\,, \\ c \;&=\; 2st(s^2+t^2)\,, \qquad d = s^4-t^4\,, \end{aligned} \tag{62}$$

with two arbitrary integers s, t.

It is easy to check that vectors $\boldsymbol{k}_1$, $\boldsymbol{k}_2$, $\boldsymbol{k}_3$, $\boldsymbol{k}_4$ belong to the same class Cl_1, with weights

$$p_1 = s^2+t^2+st,\ \ p_2 = s^2+t^2-st,\ \ p_3 = p_4 = s^2+t^2,$$

and obviously $p_1 + p_2 = p_3 + p_4,\ \forall s,t \in \mathbb{Z}$.

Parametrization (62) corresponds to the tridents oriented along the X-axis with its vectors $\boldsymbol{k}_1$ and $\boldsymbol{k}_2$ and, therefore, they are called *axial* tridents [63].

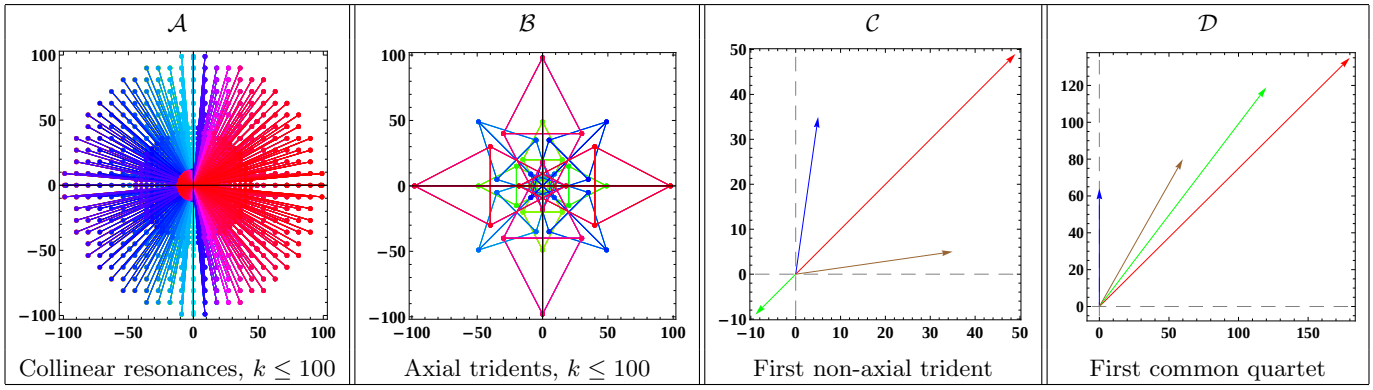

FIG. 22: Color online. Structure of scale quartets of the surface gravity waves.

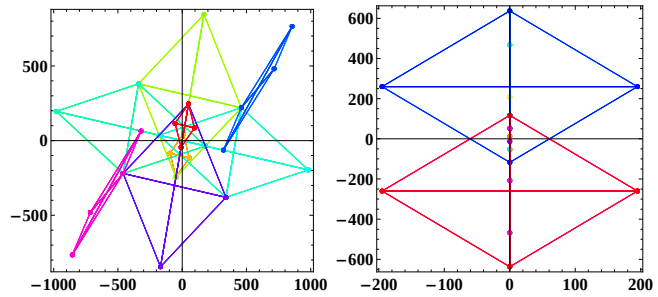

FIG. 23: Shortest cluster formed by six tridents and two common quartets (upper panel); shortest cluster formed by four collinear and two non-collinear quartets (lower panel)

b. Non-axial tridents. In the spectral domain N parameters s, t are bounded by $\sqrt{\mathcal{N}}$. Therefore the total number of such tridents can be estimated as $\mathcal{N}$. For $\mathcal{N} = 100$ this estimation is very close to the actual number 96 of such tridents [85]. However for $\mathcal{N} = 1000$ this estimation is much smaller then the total number 14.848 of the tridents in this domain. The reason is that there also exist *non-axial* tridents, for instance, the quartet $\{\{49, 49\}, \{-9, -9\}, \{5, 35\}, \{35, 5\}\}$, shown in Fig. 22$\mathcal{C}$. As it was mentioned in [74, 85], all the non-axial tridents can be obtained from the axial ones, (62), via a rotation by angles with rational values of cosine combined with respective re-scaling (to obtain an integer-valued solution out of rational-valued ones).

c. Common quartets. Not all non-collinear scale resonances are tridents. Examples of quartets of common type, without any special symmetries or relationships between wave vectors, are given below:

$$\{180, 135\}, \quad \{0, 64\} \quad , \quad \{120, 119\}, \quad \{60, 80\}\,; \quad \text{(63a)}$$
$$\{990, 180\}, \{128, 256\}, \quad \{718, 236\}, \quad \{400, 200\}\,. \quad \text{(63b)}$$

The first common quartet (63a) (shown in Fig. 22$\mathcal{D}$) lies in the spectral domain $k \leq 225$. The total number of common quartets for $\mathcal{N} = 1000$ is 1856 and is much smaller then the total number 14848 of tridents in the same domain.

First of them can be found in the spectral domain $k \leq 225$. This means, for example, that if one is interested only in the large-scale quartets, say, quartets with $k \leq 100$, the complete set of 1728 scale-quartets includes 1632 collinear quartets (dynamically not relevant) and 96 tridents (described by analytical formulas (62)).

4. Mixed cascade

An important characteristic of resonance clustering is *wavevector multiplicity* [56], which describes how many times a mode (with given wavevector) participates in different non-trivial quartets. It turned out that only 9% of all modes belonging to non-collinear quartets (664 from overall amount 7384) have multiplicity > 1, i.e. they are parts of at least two quartets. Cluster shown in Fig.11 is formed by four common quartets that involves six modes with multiplicity 2 and one mode with multiplicity 4. There are also clusters formed by different types of scale-resonances, for instance, clusters containing tridents and common quartets (shortest one is shown in Fig. 23, upper panel) or collinear and non-collinear quartets; shortest example is shown in Fig. 23, lower panel.

Clearly large clusters may involve both angle and scale quartets. Simple example of such *mixed cluster* is shown in Fig. 24$\mathcal{D}$. The energy cascade mechanism in a big mixed cluster is presented schematically in Fig. 24$\mathcal{E}$ where the quadrangles S_1 and S_2 denote scale-quartets so that 4-tuples $(V_{1,1}, ..., V_{1,4})$ and $(V_{2,1}, ..., V_{2,4})$ represent scale-quartets and squares $A_1, ...A_i, .., A_n$ represent angle–quartets.

If a mode takes a part simultaneously in angle- and scale-resonances, corresponding nodes of S_1, S_2 and A_j are connected by (red) dashed arrows so that $V_{1,1} = V_{n,2}$ and $V_{n,1} = V_{2,3}$. Examples of such mixed clusters are many, one is given below:

$$S_1 = [(-64, -16), (784, 196)\,; \ (144, 36), (576, 144)]\,;$$
$$A_n = [(-64, -16), \quad (4, 16)\,; \quad (-64, 16), \quad (4, -16)]\,,$$

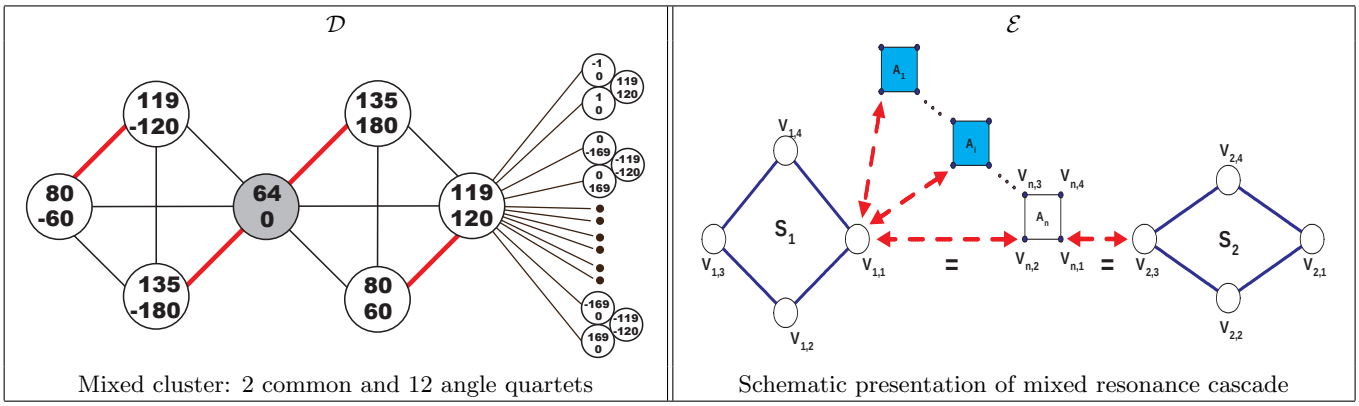

Mixed cluster: 2 common and 12 angle quartets

Schematic presentation of mixed resonance cascade

FIG. 24: Color online. Examples of cluster structures. Wavenumbers m, n are shown in the circles as upper and lower numbers. In Panel $\mathcal{D}$ wave (64,0) participates in common quartets, where 1-pairs are connected by (red) thick lines, while 2-pairs are connected by (black) thin lines. Wave (119,120) takes part in 1 scale-resonance and in 12 angle-quartets.

with $V_{1,1} = V_{n,2} = (-64, -16)$, and

$$S_2 = [(-49, -196),\, (4, 16)\,;\; (-36, -144),\, (-9, -36)]\,,$$

which is further on connected with the angle-quartets

$$A_{\tilde{n}} = [(-49, -196),\, (784, 196)\,;\; (-49, 196),\, (784, -196)]\,,$$

(not shown in Fig. 24$\mathcal{E}$) *via* a wavevector $(-49, -196)$.

Notice that wave multiplicity in the angle quartets is huge. Indeed, four modes with

$$\begin{aligned} \boldsymbol{k}_1 &= (m, n)\,, \qquad \boldsymbol{k}_2 = (m', -n)\,, \\ \boldsymbol{k}_3 &= (m, -n)\,, \quad \boldsymbol{k}_4 = (m', n)\,, \end{aligned} \tag{64}$$

obviously satisfy Eqs. (58) with any m_1, m_2 and n_1. This example shows, that any mode [say, $\boldsymbol{k} = (m, n)$] participate in infinite one-parametrical set of resonance quartets (in this example, with any m'). This means that that 1) multiplicity can be as large as $\sim \mathcal{N}$, and 2) the angle-quartets play an important role in the overall dynamics of the wave field, participating in mixed clusters, and connecting different scale clusters. Important conclusion to be made here is follows. *Kinematically* mixed cascade in infinite spectral domain always forms an infinite cluster, in finite domain the size of it is defined by the boundary of the domain. *Dynamical* considerations allow to conclude that depending on the range of frequencies and the size of nonlinearity, mixed energy cascade may terminate at a smaller wavenumbers. A possible mechanism is appearing of quasi-resonances taking over the energy flux from the exact resonances. This option will be discussed in more details below in Sec. V.

As we discussed in Sec. II B 2 excitation of only one mode or 2-pair of modes in a quartet does not yield energy transfer into other modes in the quartet. The first nontrivial possibility to do this is to excite a 1-pair (say modes ω_1 and ω_2). Then in case of positiveness of the instability increment ν_{12}, Eq. (39e), one has energy flux to the second 1-pair (with frequencies ω_3 and ω_4 in our case). For an angle quartet (**??**) it means that one has to excite two modes with the wave vector lengthes k and k' in order to excite two other modes with different direction of the wave-vectors $\boldsymbol{k}_3$, $\boldsymbol{k}_4$ but with the same lengthes k and k'. This means that angle quartets can redistribute energy among the initial wavenumbers, in both the direction $\boldsymbol{k}/k$ and the scale k. The efficiency of such an evolution depend on the magnitudes and signs of the interaction coefficients, and on the initial energy distribution. To the best of our knowledge, this process was not yet studied for any specific system with 4-wave resonances.

One can assume that long free evolution of these systems will lead to the a thermodynamically equilibrium state of the wave modes, with Rayleigh-Jeans distribution determined by the initial values of the motion integrals (the energy and the waveaction in the this case). Surely, such a thermalization could happen only among the resonant wavenumbers, and many wavenumbers which are initially excited but not in resonance would not evolve at all. Such an absence of the evolution was called "frozen turbulence" in [101] where the capillary waves were studied for which there are no exact resonances.

To illustrate this mixed angle-scale energy transport one may think about a full of energy man, driving a car in Manhattan, NY city, from South to the North via Ave. of the Americas and 6$^{\text{th}}$ avenue. This avenue is blocked by the South end of the Central Park. A way out is to turn left to a street (oriented in the orthogonal West-East direction), e.g. to W. 57-th street, to drive and then to turn right to the North direction a again, e.g. via Amsterdam avenue. Unfortunately, Columbus av. ?? is blocked by the Morningside park. Here the man can turn right to the (West-East) 110-th street toward the North end of the Central park, were he can again turn left taking one of the avenues toward the North of Manhattan. In such a way he reaches Harlem, where he may happily dissipate his energy.

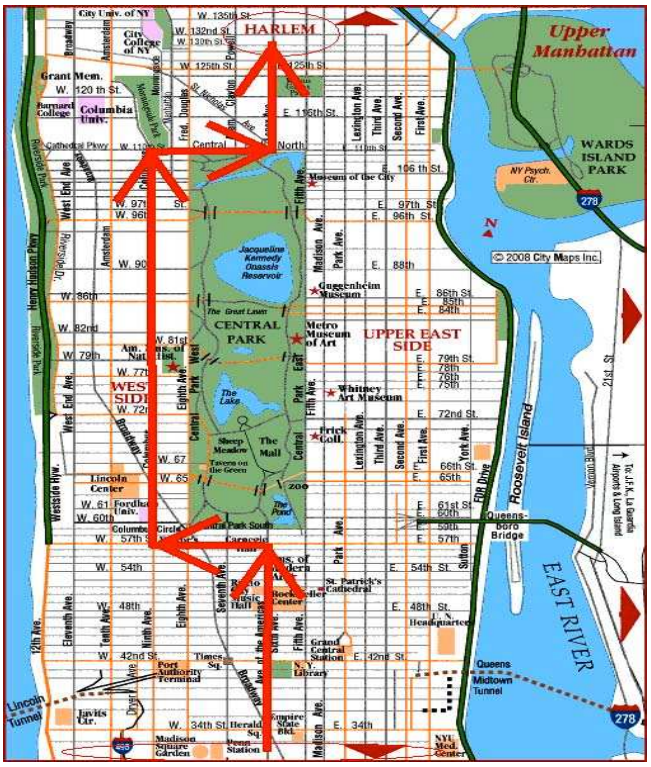

FIG. 25: Considering South-North avenue direction as the scale direction and West-East streets direction as the angle direction one finds analogy between driving in Manhattan and mixed scale-angle energy cascade: the red marked way from the Sough to the North includes parts, where one should take West-East directions to be able to continue to drive North.

D. Quasi-resonances

Quasi-resonances were studied in [11, 21, 74, 100, 101, 109**?**] and in this section we will briefly describe the findings of these papers. Let us consider equations

$$|\omega(\boldsymbol{k}_1) \pm \omega(\boldsymbol{k}_2) \pm ... \pm \omega(\boldsymbol{k}_s)| = \Omega\,, \qquad (65a)$$

$$\boldsymbol{k}_1 \pm \boldsymbol{k}_2 \pm ... \pm \boldsymbol{k}_s = 0\,. \qquad (65b)$$

with $s = 3$ and 4. Here Ω is called *finite resonance width*. In the case $\Omega = 0$, solutions of (65b) are called *exact resonances*. Otherwise, i.e. if $\Omega > 0$, equations (65b) describe *quasi-resonances*.

From the physical point of view, resonance width is caused by finite nonlinearity, in which case the nonlinear interaction is effective is only if $\Omega \leq \Gamma_k$. The resonance broadening can also be caused by linear dissipation or by a weak inhomogeneity on the background medium (density gradient, shear flow etc.), imperfection of boundaries and time-dependent external conditions.

Intuitively, it is rather obvious that for a finite set of modes there must exist a minimal Ω for which the quasi-resonances exist. Following [51], we will call it the *local low boundary*. The local low boundary of Ω is often surprisingly small even for rather small sets of modes, as it was first noticed in [100]. Even more surprising is the fact that the minimal Ω sometimes does not tend to zero and remains finite even when the set of modes tends to infinity. The minimal Ω for which the quasi-resonances exist for an infinite set will be further called the *global low boundary* [51]. Accurate lower bounds were studied in [51] analytically and in [109**?**] numerically. Whether or not the global low boundary exists, depends on the form of dispersion function and the number of resonantly interacting waves. The local low boundary exists always as we show below.

1. *Global low boundary*

Let us demonstrate the notion of the global low boundary with example of gravity water waves. Corresponding dispersion function $\omega = (m^2 + n^2)^{1/4}$ transforms a couple of integers $m, n \in \mathbb{Z}$ into an algebraic number q of a special form,

$$\omega : \mathbb{Z} \times \mathbb{Z} \to \mathbb{Q}(q).$$

Here q is an algebraic number of degree 4 and the field $\mathbb{Q}(q)$ denotes corresponding algebraic expansion of $\mathbb{Q}$. Thus, (65a) defines a a linear combination of different ω_i over the field of rational numbers $\mathbb{Q}$. To estimate the magnitude of this linear combination, one can use the generalization of the Thue-Siegel-Roth theorem [5, 102, 103] which is formulated below for the reader's convenience.

Theorem *If the algebraic numbers $\alpha_1, \alpha_2, ..., \alpha_s$ are linearly independent with 1 over $\mathbb{Q}$, then for any $\varepsilon > 0$ we have*

$$|t_1\alpha_1 + t_2\alpha_2 + ... + t_s\alpha_s - t| > ct^{-s-\varepsilon}$$

for all $t, t_1, t_2, ..., t_s \in \mathbb{Z}$ with $t = \max_i |t_i|$. (The non-zero constant c has to be constructed for every specific set of algebraic numbers separately.)

This is a fundamental result of the theory of diophantine approximations to algebraic numbers. Simply speaking, the Theorem states that a given algebraic number may not have too many rational number approximations, that are "very good". Now, for an algebraic number $\alpha = (m^2 + n^2)^{1/4}$ and four-term combination, i.e. $s = 4$, this statement means in particular that

$$|\omega_1 \pm \omega_2 \pm \omega_3 \pm \omega_4| > 1$$

if at least one of ω_i is *not a rational number*.

The use of q-class decomposition allows to distinguish two types of integer solutions of (58) accordingly:

Type I: all wavevectors belong to the same class Cl_q

$$\omega_i = p_i q^{1/4},\ \forall i = 1, 2, 3, 4\,, \quad \text{or} \qquad (66a)$$

Type II: all wavevectors belong to two classes Cl_{q_1} and Cl_{q_2}

$$\omega_1 = \omega_3 = p_1 q_1^{1/4},\ \omega_2 = \omega_4 = p_2 q_2^{1/4}\ \ q_1 \neq\ q_2. \quad (66b)$$

It follows that resonance width Ω necessary to start quasi-resonances *is bounded from below*, $\Omega > 1$, for all wavevectors but those of the form I) with $q = 1$. In particularly, computations in the spectral domain $m, n \leq 1000$ among about $6 \cdot 10^8$ exact resonances there are only 136 exact resonances for which this theorem does not work and which should be studied separately. The class Cl_1 is always special because a (generally) irrational dispersion function takes *rational* values on all the wavevectors belonging to this class.

2. Local low boundary

In the case of a rational dispersion function, the non-zero global low boundary obviously does not exist. Indeed, let us regard dispersion function for atmospheric planetary waves in the following form: $\omega \sim m/[n(n+1)]$. Then

$$\begin{aligned} |\omega_1 \pm \omega_2 \pm \omega_3| \ &\leq\ \frac{1}{n_1 n_2 n_3 (n_1+1)(n_2+1)(n_3+1)} \\ &\leq\ \frac{1}{[\max_j (n_j+1)]^6}\,, \qquad (67) \\ \text{and} \qquad &\frac{1}{[\max_j (n_j+1)]^6} \to 0 \ \text{ if } \ n_j \to \infty \end{aligned}$$

On the other hand, a local low boundary always exists which is defined by the spectral domain

$$D = \{(m,n) : 0 < |m|, |n| \leq T < \infty\}$$

under consideration. Indeed, let us define $\Omega_T = \min_p \Omega_p$, where

$$\Omega_p = |\omega(\vec{k}_1^p) \pm \omega(\vec{k}_2^p) \pm ... \pm \omega(\vec{k}_4^p)|, \quad \vec{k}_j^p = (m_j^p, n_j^p) \in D,$$

for $\forall j = 1, 2, 3, 4$, and

$$\omega(\vec{k}_1^p) \pm \omega(\vec{k}_2^p) \pm ... \pm \omega(\vec{k}_4^p) \neq 0 \quad \forall p,$$

where index p runs over all wavevectors in D, i.e. $p \leq 4T^2$. So defined Ω_p obviously is a non-zero number as a minimum of finite number of non-zero numbers and Ω_T is minimal resonance width which allows discrete quasi-resonances to start (in chosen domain D). In particularly, the local low boundary for (67) in the spectral domain $T < \infty$ will be just $1/(T+1)]^6$.

A very interesting effect can be observed when a dispersion function "degenerates" not into rational but into *integer-valued function*. Indeed, for resonances of gravity water waves from the class Cl_1 we get

$$\Delta\omega = |\omega_1 \pm \omega_2 \pm \omega_3 \pm \omega_4| = |p_1 \pm p_2 \pm p_3 \pm p_4|$$

where all p_j are integers, i.e. $\omega \geq 1$ for all quasi-resonances, as a modulus of a linear combination of integers. In this case, we see that what should be only local low boundary turned into global boundary, independent on the spectral domain. The same reasoning holds for three-waves capillary waves with dispersion function $\omega = (m^2+n^2)^{3/4}$, that is there exists global low boundary for quasi-resonances in this case, too, and this is 1.

The difference between rational and integer-valued functions are due to the fundamental difference between $\mathbb{Q}$ and $\mathbb{Z}$: rational numbers are everywhere dense while the minimal distance between two integers is fixed.

Clearly, any interpretation of numerical results has to take into account interplay between the time step of the numerical scheme dt, Ω_T and Γ. Indeed, any chosen $dt > 2\pi/\Omega_T$ will allow some number of quasi-resonances. Similarly, the quasi-resonances appear if $\Gamma > \Omega_T$. Thus, the finite time-step effect is similar to the one of the finite nonlinearity. Importance of interplay between Γ and Ω_T is taken into account in the dynamical "sandpile" model of water-wave turbulence where switching between different regimes of spectrum evolution is defined by condition $\Gamma = \Omega_T$. This model will be presented in the Section V.

E. Kinematic energy cascades

Above we considered a "static" picture where quasi-resonances were found in the whole set of modes (finite or infinite) simultaneously. However, in turbulence the energy is usually put initially into a limited set of scales (e.g. low wavenumbers) and it is later spread in the k-space via a cascade process. To model such a process, the following kinematic cascade model was suggested in [21].

(i) Let us put some energy into a small collection of initial modes. We denote this initial collection of excited modes by S_0 (e.g. in within a circle or a ring at small k's which corresponds to forcing at large scales).

(ii) We now examine which modes can interact at the given level of nonlinear broadening Γ. Let us define a new set S_1 as the union of all k's satisfying the quasi-resonance conditions Eq. (65a) and Eq. (65b) for all $\Omega < \Gamma$ with $s-1$ wavenumbers in S_0 and the remaining wavenumber outside of S_0. Provided that Γ is large enough, the set S_1 will be greater than S_0.

(ii) We can now iterate this procedure to generate a series of cascade generations S_0, $S_1, ...$, S_N which will mark the sets of active modes as the system evolves.

This model is purely kinematic: it allows to find the "cascade tree" but it does not say anything about how energy might be exchanged dynamically among the active modes along the branches of this "tree". We shall see however that the kinematics alone allows one to make some interesting observations.

Let us consider the example of the gravity waves on deep water [74]. Fig. 26 shows quasi-resonant generations of modes on space 128×128, where initially (gener-

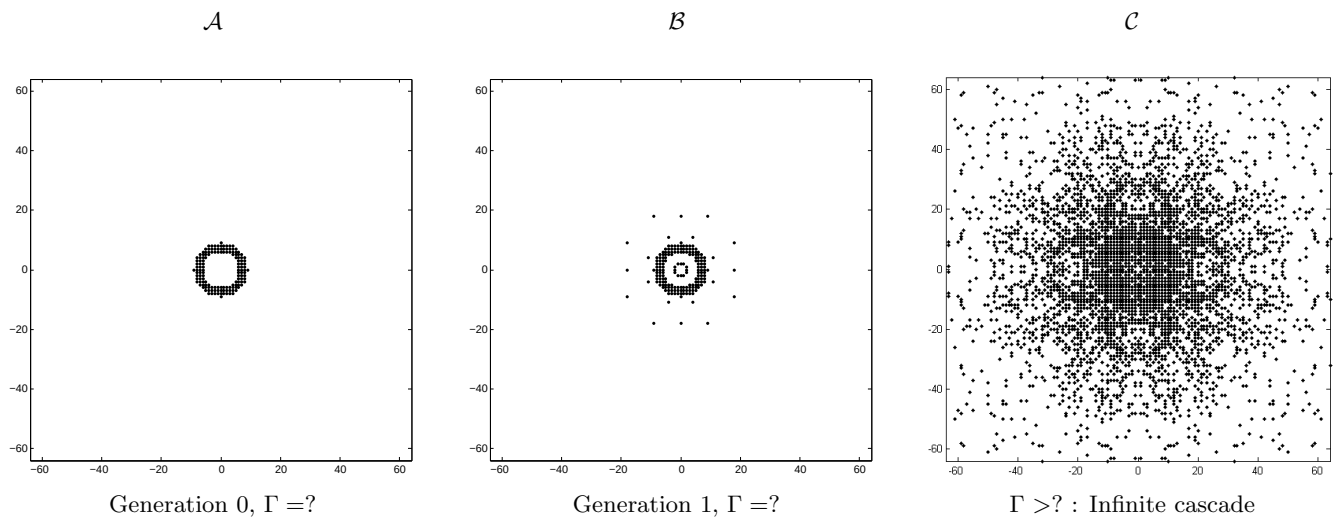

FIG. 26: Kinematic cascade of the gravity water waves. Development of the quasi-resonant generations starting with modes in the ring $6 \le |k| \le 9$ (from [74])

ation 0) only modes in the ring $6 < |k| < 9$ were present (as it is usually done in direct numerical simulations of the gravity wave system). With broadening of the resonant manifold smaller than the critical $\Gamma_{\rm crit} = 1.4 \times 10^{-5}$, a finite number of modes outside the initial region get excited due to exact resonances (generation 2) but there will be no quasi-resonances to carry energy to outer regions in further generations. If the broadening is larger than $\Gamma_{\rm crit}$, the energy cascades infinitely. Note that because of the fractal snowflake structure seen in Fig. 26, the active modes are rather sparse in the front of the cascade propagating to higher k, with pronounced anisotropic and intermittent character.

Similar picture of intermittent cascades was also observed for the capillary wave system [21]. However, because there is no exact resonances for this system, the generation 1 appears only if Γ is greater than some minimal value $\Gamma_{\rm crit1}$ (which is the local low boundary for the set S_0). Further, there exists a second critical value $\Gamma_{crit2} > \Gamma_{\rm crit1}$: the number of generations is finite for $\Gamma_{crit2} > \Gamma > \Gamma_{\rm crit1}$ and the cascade process dies out not reaching infinite k's, whereas for $\Gamma > \Gamma_{\rm crit2}$ the number of generations is infinite and the cascade propagates to arbitrarily high k's. Note that this later property makes the capillary wave system different from the gravity waves for which the cascade always spread through the wavenumber space infinitely provided $\Gamma > \Gamma_{\rm crit}$.

Another example where the (three-wave) quasi-resonances and the kinematic energy cascades were studied recently is the system of inertial waves in rotating 3D fluid volumes [11]. This system is anisotropic and the study of the kinematic cascades allows to find differences between the 2D modes, with wavevectors perpendicular to the rotation axis, and the 3D modes. First of all, frequency of the 2D modes is equal to zero, i.e. they are non-wave modes which correspond to strongly nonlinear hydrodynamical eddies. However, as far as the evolution of the 3D modes is concerned, the resonances and quasi-resonances, with both the 3D and 2D modes, are more important than non-resonant k-triads

what is it - k-triad?

. It appears that the "catalytic" interactions which involve triads including simultaneously 2D and 3D wavevectors dominate over the triads which involve 3D wavevectors only. Note that any catalytic triad contains one 2D vector and two 3D wavevectors whose projections on the rotation axis is the same. Thus, the energy cascade to large k's leaves the parallel wavenumber component unchanged, which at large time leads to very anisotropic state with x-space structures parallel to the rotation axis (Taylor columns).

F. Physical and numerical implications

• q-class decomposition is analytical method which allows to get some important information about dynamics of the resonance system without solving corresponding equations of motion and even before the complete resonance set is constructed. Indeed, let us regard oceanic planetary waves with dispersion function $\omega(m,n) \sim 1/\sqrt{m^2+n^2}$. Mode $(2,4)$ to the $q = 5$ class because $\sqrt{2^2+4^2} = \sqrt{20} = 2\sqrt{5}$ and possibly (not necessary) can interact with the mode $(1,2)$ belonging obviously to the same class. In fact these two modes form a solution of Eq. (51a) with the third mode $(4,2)$. These three modes form the resonant triad $\omega(2,4) + \omega(4,2) = \omega(1,2)$ and thus can effectively exchange the energy. On the other hand, say, $(1,8)$-mode belongs to the class with $q = 65$ and therefore can not interact resonantly with any of

wavevectors belonging to the class with $q = 5$. This mode takes part in resonant interactions only with the modes of its own class, for instance: $\omega(2,16) + \omega(14,8) = \omega(1,8)$.

Moreover, for some dispersion laws it can happen that there are no resonant triads in any q-class. This is the case for the capillary waves in a rectangular periodic domain. In this case dispersion function has the form $\omega(m,n) = (m^2+n^2)^{3/4} = \sqrt[4]{(m^2+n^2)^3}$. Correspondingly any frequency can be presented as $p^3 q^{1/4}$ with some integer p and with q having no prime multiples of degree ≥ 4. As all three frequencies must belong to the same q-class, (51a) is transformed into

$$p_1^3 + p_2^3 = p_3^3\,, \quad \forall i = 1,2,3. \tag{68}$$

with natural $p_i \in \mathbb{N}$. Eq.(68) is particular case of Last Fermat Theorem, (54), and therefore has no integer solutions. All this is important to know while planing laboratory experiments.

• q-class decomposition provides the most efficient known algorithm for fast computing of the complete resonance sets. Its program implementation can be found in [54], Appendix 2, and it allows to compute resonance sets in the domains of order 10^3 in a few seconds for 3-wave systems and in a few minutes for 4-wave systems (for solver benchmarks see [54], Fig.7.1). Notice that, for instance, direct search (without applying q-class decomposition) for solutions in the domains of order of 10^2 in 4-wave system takes more that 72 hours on similar computer.

• Having constructed a resonance solution set for a given dispersion function, we can further to study the structure of resonance clusters. The very fact that resonance clustering do exist has been discovered this way [44]. Graphical representation of a cluster in the form of NR-diagram is a powerful tool for describing general dynamical characteristics of the clusters, without solving dynamical systems (size of the clusters, PP-reduction, angle- and scale-resonances, mixed cascade, etc.). For instance, using any Galerkin-type numerical model, in spectral domain $m, n \leq 50$ we have 5000 real variables (real and imaginary parts of the modes' amplitudes). This yields system of 5000 connected nonlinear ODEs to be solved. However, looking at Fig.6 we conclude immediately that in fact we need to solve only a small number *independent* systems of ODEs, and the largest of them consists of only 12 complex or 24 real equations. This procedure of cutting off equations for non-interacting modes is called *clipping method* [45] allowing to essentially simplify the study - both analytical and numerical - of dynamical behavior of nonlinear resonant systems. Clipping was also used in [47] for planing relevant laboratory experiments. As it was shown in numerical simulations in [44], all other (non-resonant) modes just keep initial magnitudes of amplitudes. The theory underlying this fact has been worked out by Poincare [99] and is applicable for arbitrary wave systems with small enough amplitudes (for more discussion see [54], Chapter 1).

• Turbulence of capillary waves, $\omega^2 \sim k^3$, was studied in [101] in the frame of simplified dynamical equations for the potential flow of an ideal incompressible fluid. Coexistence of KZ energy spectra and a set of discrete waves with constant amplitudes was clearly demonstrated. As it follows from (68) exact resonances do not exist in this case. Similar numerical simulations [**?**] with gravity waves on the surface of deep ideal incompressible fluid, $\omega \sim \sqrt{k}$, show again coexistence of KZ energy spectra and a set of discrete waves. But in this case waves amplitudes are not constant any more, discrete modes do exchange their energy and in fact play major role in the energy transfer due to the fact that equation

$$k_1^{1/2} + k_2^{1/2} = k_3^{1/2} + k_4^{1/2}$$

has many non-trivial integer solutions as it was shown in Section **??**.

• Some recurrent patterns, found in different atmospheric data sets (rawindsonde time series of zonal wind, atmospheric angular momentum, atmospheric pressure, etc.), can be attributed to some resonance clusters of spherical planetary waves. These large-scale quasi-periodic patterns appear repeatedly at fixed geographic locations, have periods 10-100 days and are called intra-seasonal oscillations in the Earth atmosphere. In [60] it is shown that a possible explanation of the intra-seasonal oscillations can be done in terms of a few specific, resonantly interacting triads of planetary waves, isolated from the system of all the rest planetary waves.

IV. DISCRETE WAVE TURBULENCE

We have developed the *kinematic* description which deals with finding the resonant modes and finding how these modes are linked to form clusters. Now we move to considering the *dynamical* and *turbulent* properties, i.e. finding how the energy is exchanged among the resonant modes and how it marches along a cluster. This could be compared with studying a large protein molecule, where one first finds the molecule structure, i.e. how the constituent atoms are linked and geometrically positioned, which is followed by studying how such structure leads to a particular function in a biological environment.

The goal of this Section is to create a background and to present some preliminary description of dynamical and statistical behavior of clusters consisting of finite number of resonant triads or quartets. The weak nonlinearity parameter allows us to account only processes with the smallest amount of interacting waves: three-wave interactions (resonant triads), if they are allowed by the resonance conditions, or four-wave interactions (resonant quartets). In some very specific systems (for example, for Kelvin waves, propagating along vortex lines in superfluids [**?**]) when these resonances are irrelevant, one should account for high order primary clusters (sextets in our example).

Thus, one might conclude that the smallness of the nonlinearity simplifies the description, allowing to neglect numerous non-resonance waves and even quasi-resonant waves, if the nonlinearity parameter is very small. However, in any waves system which includes *only* exact resonances, one can change variables from the wave amplitudes a_j to "slow" amplitudes A_j, Eq. (23b), after which the wave frequencies ω_j disappear from the equations of motion: see, e.g. Eqs. (23a) and (47) for triads and Eqs. (31) and Eqs. (48) for quartets. Thus, paradoxically it may sound, the weak nonlinearity parameter drops out of the game when the wave amplitudes are very small, and the resulting equations, which describe dynamics of resonant clusters, are strongly nonlinear. This complicates tremendously analytical description of the problem.

Another important parameter in systems of finite size L is its ratio to the characteristic wave length λ. When the L/λ is of the order of unity the dynamics of waves can be very well described by low-dimensional chaotic models of the type studied intensively in recent decades, see e.g. [60, 61], etc. For larger (but not infinite) ratios L/λ we are dealing with discrete weak-wave turbulence: chaotic behavior of clusters. In this Section we consider the nonlinear dynamics of weakly interacting waves when the parameter L/λ is neither of order unity nor very large. This regime of parameters cannot be described either by kinetic equations or as low-dimensional chaos; it calls for new approaches and novel concepts, as partially demonstrated in this review.

Clearly, wave systems, consisting of finite number of primary resonant clusters, represent nice finite dimensional systems for numerical simulations which would be an interesting subject for future studies. The questions to be addressed in these studied could include, in particular, how transition from deterministic to chaotic dynamics occurs, and whether the chaotic dynamics represent a thermodynamical state, e.g. with equipartition of the energy and other integrals of motion over the modes, maximum entropy principle, etc. Note that even for systems with very large degrees of freedom the thermalization property is not obvious *a priori* because it is not clear if the ergodicity and mixing are exhibited by these systems. One could recall here the example of the 2D hydrodynamic turbulence in a periodic box, for which it was shown by the way of numerical experiment that mixing occurs for a class of initial conditions but it does not occur for other initial conditions [**?**]. Another interesting question is how the energy is propagated from large to small scales and over the angles within a cluster, and what is the role of the scale and the angle resonances in it.

In this Section we will overview discrete turbulence in systems with three-wave resonances, mainly following [78].

A. Analytical results

Three-wave Hamiltonian (6b) for any cluster of connected resonant triads after change of variables (23b) and (24b) takes the form [78]:

$$\mathcal{H}_{N\Delta} = \sum_{j=1}^{N} \mathcal{H}_{j\Delta}\,,\ \mathcal{H}_{j\Delta} = 2Z_j\,\mathrm{Im}\left\{B^*_{1|j}B^*_{2|j}B_{3|j}\right\},\ (69)$$

where $\mathcal{H}_{j\Delta}$ is the Hamiltonian of isolated j-triad with Z_j being its (positive) interaction coefficient. To connect triads one has just to equate the amplitudes of the common modes in the cluster.

Canonical equation of motion for amplitude $B_{i|j}$ of $i = 1, 2, 3$-mode in the j-triad has standard form (2), namely:

$$i\frac{dB_{i|j}}{dt} = \frac{\partial \mathcal{H}}{\partial B^*_{i|j}}\ . \qquad (70)$$

1. Double-triad clusters

For PP-butterfly, shown in Fig. 18$\mathcal{B}$, the common mode is passive in both triads, say

$$B_{1|a} = B_{1|b} \qquad \text{PP-butterfly}\ . \qquad (71a)$$

In PA-butterfly, Fig. 18$\mathcal{C}$, the common mode is passive in a-triad and active in the second, b-triad:

$$B_{1|a} = B_{3|b} \qquad \text{PA-butterfly}\,; \qquad (71b)$$

while for an AA-butterfly, Fig. 18$\mathcal{D}$, the common mode is active in both triads:

$$B_{3|a} = B_{3|b} \qquad \text{AA-butterfly}\ . \qquad (71c)$$

Hamiltonian (69) for butterflies, consisting from a- and b-triad with wave amplitudes $B_{j|a}$, $B_{j|b}$, $j = 1, 2, 3$, connected *via* one common mode and for kites, connected via two common modes, has the form

$$\mathcal{H}_{2\Delta} = 2\mathrm{Im}\left\{Z_a B^*_{1|a}B^*_{2|a}B_{3|a} + Z_b B^*_{1|b}B^*_{2|b}B_{3|b}\right\}\ . \ (72)$$

a. PP-, PA-, and AA-butterflies. Hamiltonian equation of motions for PP-butterfly, Fig. 18$\mathcal{B}$, follows from Eq. (70), if one equates in the Hamiltonian (72) common passive modes: $B_{1|a} = B_{1|b}$ [61]:

$$\begin{cases} \dot B_{1|a} = Z_a B^*_{2|a}B_{3|a} + Z_b B^*_{2|b}B_{3|b},\ , \\ \dot B_{2|a} = Z_a B^*_{1|a}B_{3|a}\,, \quad \dot B_{2|b} = Z_b B^*_{1|a}B_{3|b}\,, \\ \dot B_{3|a} = -Z_a B_{1|a}B_{2|a}\,,\ \dot B_{3|b} = -Z_b B_{1|a}B_{2|b}\ . \end{cases} \qquad (73a)$$

For PA-butterfly, Fig. 18$\mathcal{C}$, equating $B_{1|a} = B_{3|b}$, one gets from Eqs. (70) and (72):

$$\begin{cases} \dot B_{1|b} = Z_b B^*_{2|b}B_{3|b}\,, \quad \dot B_{3|a} = -Z_a B_{3|b}B_{2|a}\,, \\ \dot B_{2|b} = Z_b B^*_{1|b}B_{3|b}\,, \quad \dot B_{2|a} = Z_a B^*_{3|b}B_{3|a}\,, \\ \dot B_{3|b} = -Z_b B_{1|b}B_{2|b} + Z_a B^*_{2|a}B_{3|a}\,, \end{cases} \qquad (73b)$$

Similarly, for AA-butterfly, Fig. 18$\mathcal{D}$, taking $B_{3|a} = B_{3|b}$ one gets from Eqs. (70) and (72):

$$\begin{cases} \dot{B}_{1|a} = Z_a B^*_{2|a} B_{3|a}\,, \;\; \dot{B}_{1|b} = +Z_b B^*_{2|b} B_{3|a}\,, \\ \dot{B}_{2|a} = Z_a B^*_{1|a} B_{3|a}\,, \quad \dot{B}_{2|b} = Z_b B^*_{1|b} B_{3|a}\,, \\ \dot{B}_{3|a} = -Z_a B_{1|a} B_{2|a} - Z_b B_{1|b} B_{2|b}\;. \end{cases} \tag{73c}$$

In addition to the Hamiltonian (72) we have three more invariants of the Manley-Rowe type for each butterfly. For the PP-, PA- and AA-butterflies they respectively are [61]

$$\begin{aligned} I_{2,3|a} &= |B_{2|a}|^2 + |B_{3|a}|^2\,, \quad I_{2,3|b} = |B_{2|b}|^2 + |B_{3|b}|^2\,, \\ I_{|a,b} &= |B_{1|a}|^2 + |B_{3|a}|^2 + |B_{3|b}|^2\;, \text{ PP;} \qquad (74a) \\ I_{1,2|b} &= |B_{1|b}|^2 - |B_{2|b}|^2\,, \quad I_{2,3|a} = |B_{2|a}|^2 + |B_{3|a}|^2\,, \\ I_{|a,b} &= |B_{1|b}|^2 + |B_{3|b}|^2 + |B_{3|a}|^2\;, \text{ PA;} \qquad (74b) \\ I_{1,2|a} &= |B_{1|a}|^2 - |B_{2|a}|^2\,, \quad I_{1,2|b} = |B_{1|b}|^2 - |B_{2|b}|^2\,, \\ I_{|a,b} &= |B_{1|a}|^2 + |B_{1|b}|^2 + |B_{3|a}|^2\;, \quad \text{AA.} \qquad (74c) \end{aligned}$$

The first two invariants for the *PP*-butterfly, $I_{2,3|a}$ and $I_{2,3|b}$, do not involve the common mode $B_{1|a} = B_{1|b}$, and are similar to the invariant I_{23}, Eq. (27), for an isolated triad. Obviously, *PP*-butterfly is PP-reducible into two isolated triads. In other words, if initially only one of two triads a or b is excited, the second one is unable to absorb the energy during the nonlinear evolution.

For PP-butterfly, when at $t = 0$ the b-triad is excited much more than the a-triad the smallness of the positively defined invariant $I_{2,3|a}$, Eq. (74b), prevents the a-triad from absorbing energy from b-triad during the time evolution. The situation is different when the a-triad is initially excited and $I_{2,3|a} \gg I_{1,2|b}$. In this case the initial energy of a-triad can be easily shared with b-triad. Under this type of the initial conditions the a- and b-triad were referred in [78] to as "leading" and "driven" triads respectively.

Similar analysis of the invariants (74c) for the AA-butterfly shows that energy, initially held in one of the triads will be shared between both triads dynamically.

The conclusion that was drawn in Refs [61, 78] from these examples is general: any triad which is connected to an arbitrary cluster of any size whatsoever where the connection occurs *via* its passive mode cannot absorb the energy from the cluster, if initially the triad is not excited. In contrast, a triad connected to a cluster of any given size *via* an active mode can freely adsorb energy from the cluster during the nonlinear evolution.

2. *Triple-triad clusters*

Hamiltonian (69) of triple-triad clusters includes three terms with $j = a\,, b\,,$ and c:

$$\begin{aligned} \mathcal{H}_{3\Delta} \;=\; & 2\mathrm{Im}\big\{ Z_a B^*_{1|a} B^*_{2|a} B_{3|a} + Z_b B^*_{1|b} B^*_{2|b} B_{3|b} \\ & + Z_c B^*_{1|c} B^*_{2|c} B_{3|c} \big\}\;, \end{aligned} \tag{75}$$

To connect triads one has again to equate here amplitudes of common modes.

Equation of motions for triple-stars, with one common mode in three triads, follow from Eqs. (70) and (75) and read

AAA-stars with $\quad B_{3|a} = B_{3|b} = B_{3|c}$:

$$\begin{cases} \dot{B}_{1|a} = Z_a B_{2|a} B_{3|a}\,, \quad \dot{B}_{2|a} = Z_a B_{1|a} B_{3|a}\,, \\ \dot{B}_{1|b} = Z_b B_{2|b} B_{3|a}\,, \quad \dot{B}_{2|b} = Z_a B_{1|b} B_{3|a}\,, \\ \dot{B}_{1|c} = Z_c B_{2|c} B_{3|a}\,, \quad \dot{B}_{2|c} = Z_c B_{1|c} B_{3|a}\,, \\ \dot{B}_{3|a} = -Z_a B_{1|a} B_{2|a} - Z_b B_{1|b} B_{2|b} - Z_c B_{1|c} B_{2|c}\;; \end{cases} \tag{76a}$$

AAP-stars with $\quad B_{3|a} = B_{3|b} = B_{1|c}$:

$$\begin{cases} \dot{B}_{1|a} = Z_a B_{2|a} B_{3|a}\,, \quad \dot{B}_{2|a} = Z_a B_{1|a} B_{3|a}\,, \\ \dot{B}_{1|b} = Z_b B_{2|b} B_{3|a}\,, \quad \dot{B}_{2|b} = Z_a B_{1|b} B_{3|a}\,, \\ \dot{B}_{3|c} = -Z_c B_{3|a} B_{2|c}\,, \quad \dot{B}_{2|c} = Z_c B_{3|a} B_{3|c}\,, \\ \dot{B}_{3|a} = -Z_a B_{1|a} B_{2|a} - Z_b B_{1|b} B_{2|b} + Z_c B_{2|c} B_{3|c}\;. \end{cases} \tag{76b}$$

PPA-stars with: $\quad B_{1|a} = B_{1|b} = B_{3|c}\,,$

$$\begin{cases} \dot{B}_{3|a} = -Z_a B_{1|a} B_{2|a}\,, \quad \dot{B}_{2|a} = Z_a B_{1|a} B_{3|a}\,, \\ \dot{B}_{3|b} = -Z_b B_{1|a} B_{2|b}\,, \quad \dot{B}_{2|b} = Z_a B_{1|a} B_{3|b}\,, \\ \dot{B}_{1|c} = Z_c B^*_{2|c} B_{1|a}\,, \quad \dot{B}_{2|c} = Z_c B_{1|a} B_{1|c}\,, \\ \dot{B}_{1|a} = Z_a B^*_{2|a} B_{3|a} + Z_b B^*_{2|b} B_{3|b} - Z_c B_{1|c} B_{2|c}\;. \end{cases} \tag{76c}$$

PPP-star with: $\quad B_{1|a} = B_{1|b} = B_{1|c}\,,\,,$

$$\begin{cases} \dot{B}_{3|a} = -Z_a B_{1|a} B_{2|a}\,, \quad \dot{B}_{2|a} = Z_a B_{1|a} B_{3|a}\,, \\ \dot{B}_{3|b} = -Z_b B_{1|a} B_{2|b}\,, \quad \dot{B}_{2|b} = Z_a B_{1|a} B_{3|b}\,, \\ \dot{B}_{3|c} = -Z_c B_{1|a} B_{2|c}\,, \quad \dot{B}_{2|c} = Z_c B_{1|a} B_{3|c}\,, \\ \dot{B}_{1|a} = Z_a B^*_{2|a} B_{3|a} + Z_b B^*_{2|b} B_{3|b} + Z_c B_{2|c} B_{3|c}\;. \end{cases} \tag{76d}$$

In addition to Hamiltonian, all triple-star clusters have four invariants of the Manley-Rowe type, three of them does not involve the common mode. For example, for

$$\begin{cases} \text{PPA-star:} \qquad I_{1,2|a} = |B_{1|a}|^2 - |B_{2|a}|^2\,, \\ I_{2,3|b} = |B_{2|b}|^2 + |B_{3|b}|^2\,, \quad I_{2,3|c} = |B_{2|c}|^2 + |B_{3|c}|^2\,, \\ I_{|a,b,c} = |B_{1|a}|^2 + |B_{3|a}|^2 + |B_{3|b}|^2 + |B_{3|c}|^2\;. \end{cases} \tag{77}$$

Integrals $I_{2,3|b}$ and $I_{2,3|c}$ prevent b- and c-triads (connected via the P-mode) from adopting energy of initially excited a-triad. In cases when b- and/or c-triad are initially exited, a-triad can freely share their energy via connecting A-mode.

Similarly one finds (see [78]) equations and integral of motions for triple chains, triangles and more complicated clusters. For example, for PA-PA chain with $B_{1|a} = B_{3|b}$ and $B_{1|b} = B_{3|c}$

$$\begin{cases} \dot{B}_{1|a} = Z_a B^*_{2|a} B_{3|a} - Z_b B_{1|b} B_{2|b}\,, \\ \dot{B}_{2|a} = Z_a B^*_{1|a} B_{3|a}\,, \quad \dot{B}_{3|a} = -Z_a B_{1|a} B_{2|a}\,, \\ \dot{B}_{2|b} = Z_b B^*_{1|b} B_{3|b}\,, \\ \dot{B}_{1|b} = Z_b B^*_{2|b} B_{3|b} - Z_a B_{1|c} B_{2|c}\,, \\ \dot{B}_{1|c} = Z_c B^*_{2|c} B_{1|b}\,, \quad \dot{B}_{2|c} = Z_c B^*_{1|c} B_{1|b}\;. \end{cases} \tag{78a}$$

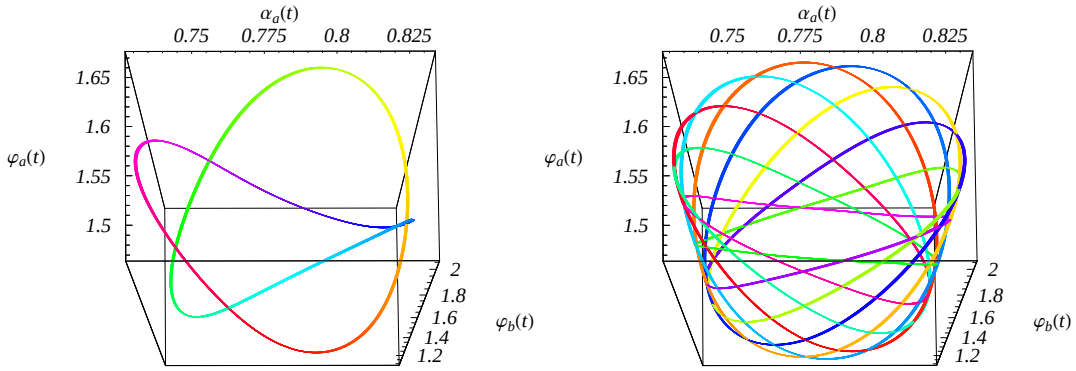

FIG. 27: Color online. To facilitate tracking the motion along the trajectory, the later is colored with the color hue being a linear function of time t, varying from 0 to 1 as t runs through one period. **Left panel**: $Z_a = 8/100, Z_b = 12/100, I_{ab} \approx 2.2088$. **Right panel**: $Z_a = 9/100, Z_b = 11/100, I_{ab} \approx 2.1846$.

$$\begin{cases} I_{|a,b} = |B_{1|a}|^2 - |B_{2|a}|^2 + |B_{2|b}|^2 \,, \\ I_{|b,c} = |B_{1|b}|^2 - |B_{2|b}|^2 + |B_{2|c}|^2 \,, \\ I_{2,3|a} = |B_{2|a}|^2 + |B_{3|a}|^2 \,, \\ I_{1,2|c} = |B_{1|c}|^2 - |B_{2|c}|^2 \,. \end{cases} \tag{78b}$$

3. *Structure of the effective phase space*

As one sees from the Hamiltonian (69) that equation of motion for any N-triad cluster involve $3N$ real amplitudes $C_j \equiv |B_j|$ and N triad phases (26), which we denote here as

$$\varphi_j \equiv \varphi_{1|j} + \varphi_{2|j} - \varphi_{3|j} \,. \tag{79}$$

For butterflies ($N = 2$) with one common mode and three independent Manley-Rowe integrals (74) only two independent amplitudes left. In this way the dimensionality of the effective phase space of butterflies can be reduced to $2\,N = 2$. Notice, that re-normalization $C_j \Rightarrow \lambda_j C_j$, leads only to the re-normalization of the time-scale. Therefore the form of the trajectories in the phase space depends only on the ratios of amplitudes. Therefore phase trajectories of butterflies can be presented in three dimensional space, φ_a, φ_b and one ratio of two independent amplitudes. As an example, we presented in Fig. 27 (taken from [**?**]) dynamics of a generic PP-butterfly in coordinates φ_a, φ_b and $\alpha_a = \arctan(C_{3a}/C_{2a})$. As it is shown in [**?**] in some special cases, e.g., a) real amplitudes, i.e. $\varphi_a = \varphi_b = 0$; b) complex amplitudes, $\mathcal{H}_{2\Delta} = 0$; c) b) complex amplitudes, $Z_a = Z_b$; etc. equations of motion for butterflies are explicitly integrable.

Obviously, N-triad clusters with n-connections have $(2N - n)$ Manley-Rowes' integrals. According to this rule isolated triads ($N = 1$, $n = 0$) have two Manley-Rowes'[see Eqs. (27)], butterflies ($N = 2$, $n = 1$) have three Manley-Rowes', triple-stars and triple-chains ($N = 3$, $n = 2$) have four Manley-Rowes', Eqs. (77) and (78b) respectively. Special 6-triad cluster, caterpillar, studied in [78], has 5 connections and seven independent Manley-Rowes', etc. General N-triad clusters have $4N$ variables, $3N$ amplitudes and N triad phases. In this clusters n connections and $(2N-n)$ Manley-Rowes integrals reduce the dimensionality of the effective phase space down to $4N - n - (2N - n) = 2N$, which is the same as dimensionality of the effective phase space of isolated N triads.

B. Numerical results

In this Section we overview results of [78] concerning the energy flux through resonant triads in the regime of finite-dimensional wave turbulence. In the first Subsubsec. IV B 1 we consider free evolution of the smallest clusters – butterflies – from asymmetrical initial conditions, in which only one triad is excited to high amplitudes, exceeding by orders of magnitudes the initial amplitudes in the other triad. The questions are how the energy flux from the energetic "leading" triad depends on the type of connection, on the ratios of the interaction coefficients etc. Subsubsection IV B 2 overviews the free evolution of the triple-triad clusters: stars and chains from initial conditions in which only the leading a-triad is substantially excited, the levels of excitation of the two other triads are much smaller. *All these examples serves as building blocks of bigger clusters and the knowledge about the energy flux through them allows to qualitatively predict efficiency of the energy transfer through bigger clusters.*

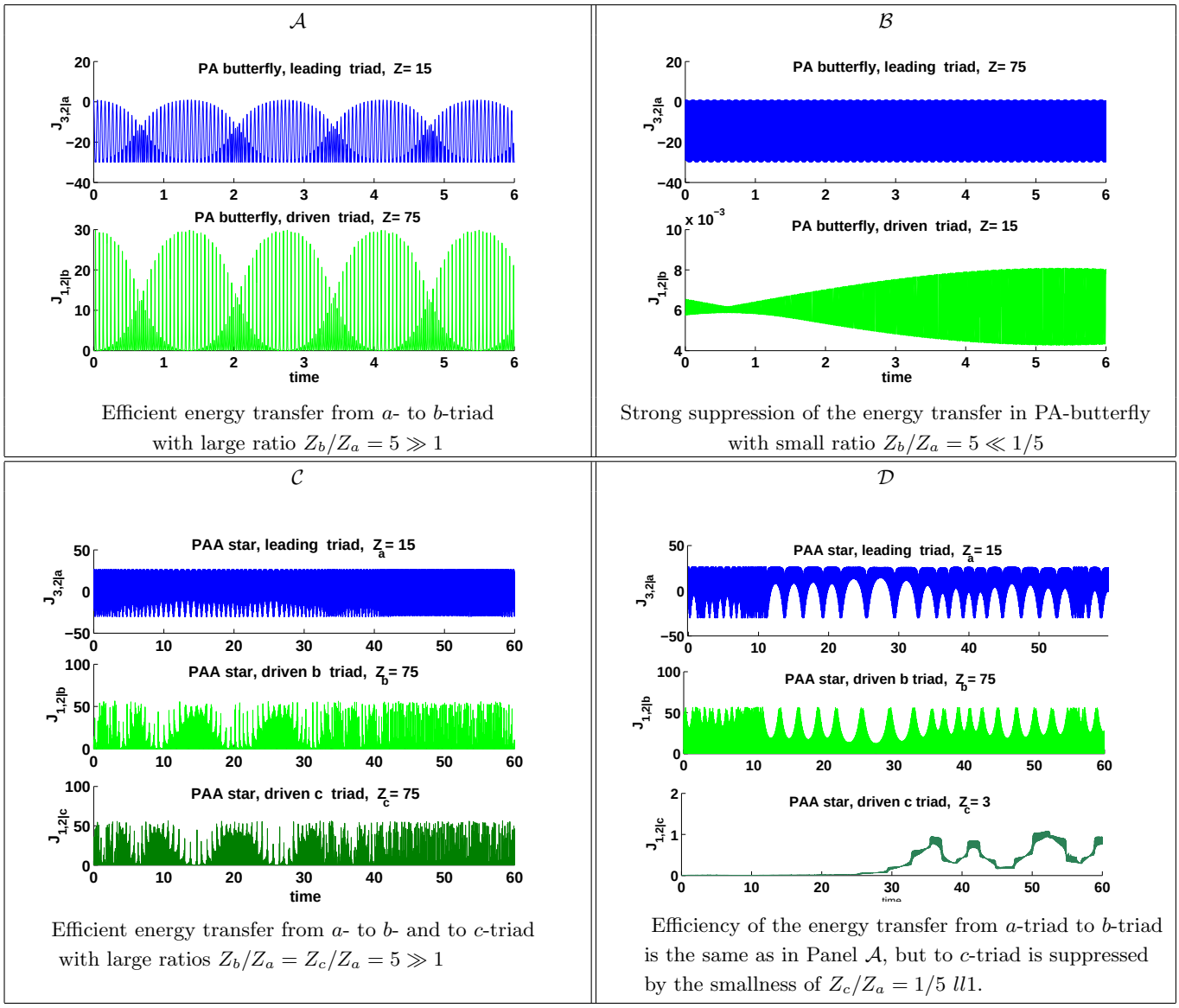

FIG. 28: Color online. Time evolution of PA-butterfly and PAA-star from "efficient" initial conditions with different interaction coefficients (taken from [78]).

1. *Energy transfer in butterflies*

The simplest topology that allows consideration of the energy flux between resonant triads is the double-triad clusters: *butterflies* that is discussed in this Subsubsection. We begin with discussion of the effect of initial conditions.

a. Effect of initial conditions. It was shown in [78] that details of the time evolution in butterflies and efficiency of the energy transfer from the leading triad to the driven triad are very sensitive to the initial conditions. The reason is very simple: initial conditions determine the values of the dynamical invariants, Menley-Rowes integrals, that may restrict the amplitude of common mode though which energy can penetrate from the leading to the driven triad.

To demonstrate this, we consider for concreteness PA-butterfly and estimate the amplitude of common mode, neglecting the excitation of the driven triad. In this case invariants (74b) can be written as:

$$I_{1,3a} = C_{1a}^2 + C_{3a}^2,\ I_{1,2a} = C_{1a}^2 - C_{2a}^2. \qquad (80)$$

At initial moment of time the amplitude $C_{1a} \ll C_{2a},\ C_{3a}$. Therefore $I_{1,3a} \simeq C_{3a}(t=0)^2 \equiv [C_{3a}^{(0)}]^2$ and $I_{3,2a} = [C_{3a}^{(0)}]^2 - [C_{2a}^{(0)}]^2$. Thus the first of Eqs. (80) gives

$$C_{1a}^2 = C_{3b}^2 \le [C_{3a}^{(0)}]^2\,, \qquad (81)$$

while the second one leads to the trivial restriction $C_{1a}^2 \ge -[C_{3a}^{(0)}]^2$, that is satisfied automatically. The conclusion

is that the efficiency of the energy transfer is determined by the initial magnitudes of the individual A-mode: the larger value of $C_{3a}^{(0)}$, the more energy can be transferred to the driven b-triad. If, in contrary, all initial energy is localized in the passive free mode $C_{2a}^{(0)}$, then nothing appears in the b-triad. These conclusions were illustrated by numerics in [78]. Similar analysis was done for AA-butterfly with the conclusion that in the most efficient initial conditions two free P-modes in the leading triad should be exited equally [78].

Another conclusion is that the efficiency of the energy transfer is practically independent of the initial amplitudes in the driven triad provided that they are not identically equal zero [78]. The reason is simple: due to the decay instability, amplitudes in the driven triad initially grow exponentially in time, see Eq. (29). Therefore on the values of these amplitudes depend (logarithmically) only expectation time.

b. Effect of the ratio of the interaction coefficients. Interestingly enough, the ratio of the interaction coefficients in the leading and driven triads, Z_a/Z_b essentially effects on the energy transfer: see in Fig. 28 $\mathcal{A}$ and $\mathcal{B}$ (taken from [78]) time evolution of two objects, orthogonal to Manley-Rowe integrals in the corresponding triads:

$$J_{2,3|a} \equiv |B_{2|a}|^2 - |B_{3|a}|^2\,, \quad J_{1,2|b} \equiv |B_{1|a}|^2 + |B_{2|b}|^2\,. \tag{82}$$

In both cases we took efficient for the energy transfer initial conditions. As a result one sees in Fig. 28 $\mathcal{A}$ that energy freely penetrate from a- to b-triad, while in Fig. 28 $\mathcal{B}$ this energy transfer is strongly suppressed. The difference between these two cases is that in Panel $\mathcal{A}$ the ratio $Z_b/Z_a = 5$ is large, while in Panel $\mathcal{B}$ this ratio is small.

An explanation of the suppression of the energy flux, from $a-$ to b-triad by smallness of the ratio Z_b/Z_a is given in [78]. The reason is that the common mode $B_3(t)$ experiences fast oscillations with (almost) zero mean and with frequency Ω_a, that can be estimated as $Z_a B_a$, where $B_a \equiv \sqrt{J_{1,2|a}}$ is a characteristic value of mode magnitudes in $a-$triad. As one can see from the equations of motion (73) for butterflies, the mean energy flux from the leading, $a-$, to the driven b-triad (with A-connection), $\varepsilon_{a\to b}$, can be written as

$$\varepsilon_{a\to b} = 2Z_b \mathrm{Re}\big[B_{1|b}B_{2|b}B^*_{3|b}\big] \propto \cos\phi_b\,, \tag{83}$$

where $\varphi_b = \varphi_{1|b} + \varphi_{2|b} - \varphi_{3|b}$ is the triad phase, introduces by Eq. (26). Fast oscillations of $B_a(t)$, equivalent to fast growth of $\varphi_{3|b}(t)$ with the speed $d\varphi_{3|a}(t)/dt = d\varphi_{3|b}(t)/dt \approx \Omega_a(t)$, lead to self-averaging of $\cos\varphi_b$ almost to zero, if phases $\varphi_{1|b}$ and $\varphi_{2|b}$ cannot react fast enough to variations of $\varphi_{3|b}(t)$. This is a qualitative explanation of the observed fact that the energy flux from $a-$ to $b-$triad is strongly suppressed if $Z_a \gg Z_b$ and is observable (but still suppressed) if $Z_a \lesssim Z_b$. One can hope that the $a-b$ energy flux can be significant if $B_{3|a}(t)$ has a nonzero mean and therefore $\langle\varphi_{3|b}(t)\rangle$ also does not vanish. But this is impossible under the initial conditions of interest: we do not want to put initially energy to $b-$triad, taking large value of $B_{3|a}(t) = B_{3|b}(t)$ at time zero. Therefore at $t = 0$ $|B_{3|a}| \ll |B_{1|a}|, |B_{2|a}|$. If so, according to the equation of motion, the time derivative $\dot{B}_{3|a} = -Z_a B_{1|a}B_{2|a}$ is large enough to allow $B_{3|a}$ to cross quickly zero and to reach significant value with different sign. Having in mind periodical character of evolution of isolated triad it practically means that $\langle B_{3|a}\rangle \ll \sqrt{\langle|B_{3|a}|^2\rangle}$.

2. Energy junction in triple-triad clusters

Energy junction in the triple-triad clusters, i.e. energy flux from the leading a-triad to two driven b- and c-triads was discussed in details in [78]. Here we only illustrate briefly, how connection of A-mode of an additional c-triad to the common mode in the PA-butterfly effect on the energy flux. After this connection PA-butterfly becomes PAA-star. We took PA-butterfly with $Z_a = 15$, $Z_b = 75$ (with the time evolution shown in Fig. 28 $\mathcal{A}$) and connected c-triad with $Z_c = 75$ (and, consequently $Z_c/Z_a = 5$) and with $Z_c = 3$ (and, consequently $Z_c/Z_a = 1/5$). In the first case the characteristic values of the triad excitations, shown in Fig. 28 $\mathcal{C}$ is very similar to that in Fig. 28 $\mathcal{C}$. Another words, additional connected c-triad does not change much the mean energy excitation of b-triad. However if the interaction coefficient in the connected c-triad is small, like in in Fig. 28 $\mathcal{D}$, the energy excitation of this triad is suppressed, as expected from the discussion in Par. IV B 1 b.

Additional fact, important for future studies, is that the time evolution in stars, shown in Fig. 28 $\mathcal{C}$ and $\mathcal{D}$ is much less regular that that in triads, Fig. 28 $\mathcal{A}$ and $\mathcal{B}$. To see this even more straightforwardly, one can compare typical phase trajectories of butterflies, presented in Fig. 27, with three-parametrical representation of phase trajectories of PAA-stars, shown in Fig. 29.

3. Universality of statistics in N-chains

In this Section we consider results of numerical simulations [78], for the stationary energy distributions of resonant waves and energy exchange between triads in the long-chain clusters in the regime of finite-dimensional wave turbulence with constant energy flux and during free evolution. The studied clusters consist of N triads and is constructed by connecting the first P-mode of $(n-1)$'s triad, $B_{1|n-1}$, with the A-mode of the next, n's triad, $B_{3|n}$. To mimic scale invariance of the cluster, the interaction coefficients Z_n were chosen in geometric progression, $Z_n = \lambda Z_{n-1} = Z_1\lambda^{n-1}$. The chain is forced by an independent freely evolving triad. The linear dissipation with the damping frequency γ was added to the equations of two P-modes of the last triad, $B_{1|N}$ and $B_{2|N}$.

It was shown [78] that initial conditions do not effect the stationary statistics in the cluster. This is expected,

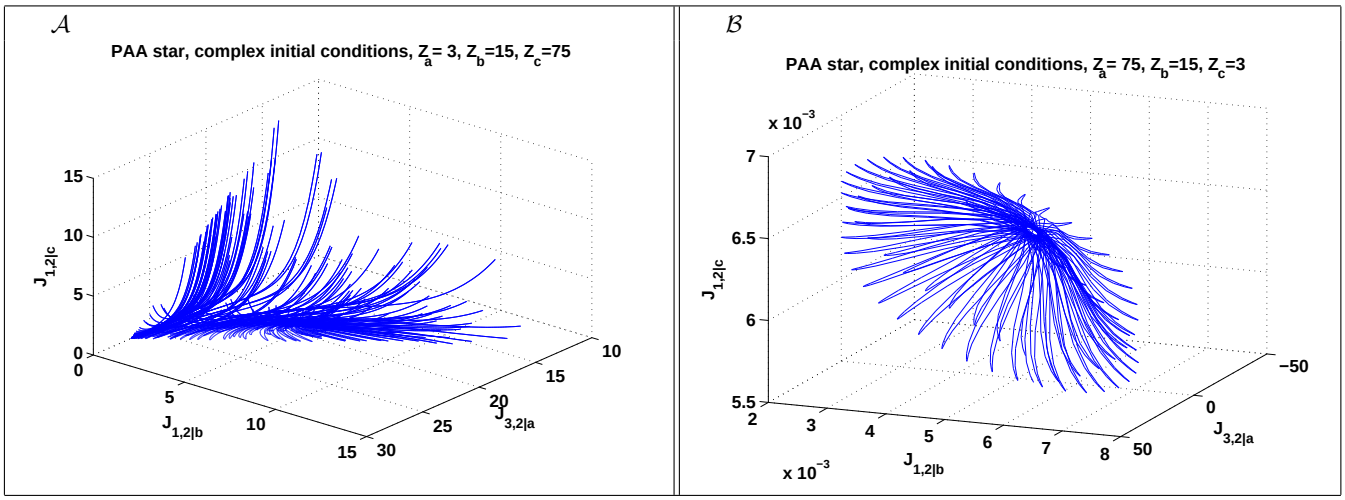

FIG. 29: Color online. Three dimensional parametric representation of trajectories of PAA-star with $Z_a = 3$, $Z_b = 15$, $Z_c = 75$, panel $\mathcal{A}$ and with $Z_a = 3$, $Z_b = 15$, $Z_c = 75$, panels $\mathcal{B}$ from complex initial conditions. Taken from [78].

because in the presence of the energy pumping and damping numerous integrals of motion (for isolated systems) do not conserve any more.

What is unexpected and much less trivial is that in the wide range of cluster parameters λ, N and γ the energy distribution in the clusters is (almost) independent on these parameters, i.e. universal. These facts are demonstrated in Fig. 30, taken from [78], were logarithm of the amplitude square of "free" modes $\langle|B_{2|n}|^2\rangle$ and "connected" modes $\langle|B_{3|n}|^2\rangle = \langle|B_{1|n-1}|^2\rangle$ are shown as function of n in the chains with different number of triads and for the set of the frequency scaling parameter λ. Panel $\mathcal{A}$ shows energy distributions for the chains consisting of $N = 16$ triads and with different $\lambda = 1,\ \sqrt{2},\ 2$ and $\lambda = 2\sqrt{2}$, while in Panel $\mathcal{B}$ scaling parameter is fixed $\lambda = \sqrt{2}$ but the chain length is varying: $N = 12,\ 16,\ 20$ and $N = 24$. In both Panels the dissipation parameter γ is fixed, while in Panel $\mathcal{C}$ γ is varying but $\lambda = \sqrt{2}$ and $N = 16$ are fixed.

First, one sees in Panel $\mathcal{A}$ that the lines for different λ are quite close, quickly converging for larger λ. One conclude that the distributions of $\langle|B_{2|n}|^2\rangle$ and $\langle|B_{3|n}|^2\rangle$ are almost λ-independent at least for $\lambda \geq 2$.

Second, one sees in Panel $\mathcal{B}$ that the lines for different N practically coincide. The conclusion is that the distributions of $\langle|B_{2|n}|^2\rangle$ and $\langle|B_{3|n}|^2\rangle$ are N-independent in the limit of large N.

Third, Panel $\mathcal{C}$ shows collapse of the energy distributions for various, but small values of γ. One can ask, what happens if one increases further the damping parameter? It was shown [78] that increasing γ drastically suppresses individual amplitudes in the last triad. Its ability to absorb the energy flux from the previous triad diminishes to the stage at which it can not anymore serve as an energy sink. This leads to accumulation of the energy in the N-1'th triad and later in N-2nd triad etc, thus creating a "bottleneck effect". The reason for this effect is presented in [78].

4. *Forced- vs free-evolution of N-chains*

One more surprise, found in [78], is that in the conditions of the energy-flux equilibrium in the scale-invariant situations (in our case, $Z_n \propto \lambda^n$) one did not observe the expected power-like behavior, when $\langle|B_{j|n}|^2\rangle \propto \lambda^{n\,\zeta}$. Moreover, the ratio $\langle|B_{2|n}|^2\rangle/\langle|B_{3|n}|^2\rangle$ depends on n and the connected modes $\langle|B_{3|n}|^2\rangle$ weakly depend on n, as one expects in the thermodynamic equilibrium, after a long free evolution.

That is why it is reasonable to compare forced distributions of $\langle|B_{2|n}|^2\rangle$ and $\langle|B_{3|n}|^2\rangle$ with the distributions of $\langle|B_{2|n}|^2\rangle$ and $\langle|B_{3|n}|^2\rangle$ after long free evolutions (without forcing and damping) in the same cluster, This is done in Fig. 30 $\mathcal{D}$. Solid (blue) lines show energy distributions for forced case, while dashed (red) lines correspond to the free evolution with initial conditions that resulted after long-time forced evolutions. As one sees these distributions practicably coincide. In other words, the distributions with constant energy flux and the distributions with zero energy flux are almost identical. The reason for this [78] is enormous fluctuations of the energy flux between triad $\varepsilon_n(t)$ that exceed its mean value in many orders of magnitude. This means that there is a strong energy exchange between triads in the cluster, that essentially exceeds minor mean flux. Therefore one can switch off the mean energy flux without almost any effect on the cluster statistics. The conjecture made in [78] is that this general statement is valid for all kind on clusters, consisting of connected triads. The only difference between forced and free long-time evolution of the clusters is the restriction, that follows from the conservations laws, that are satisfied exactly in free evolutions

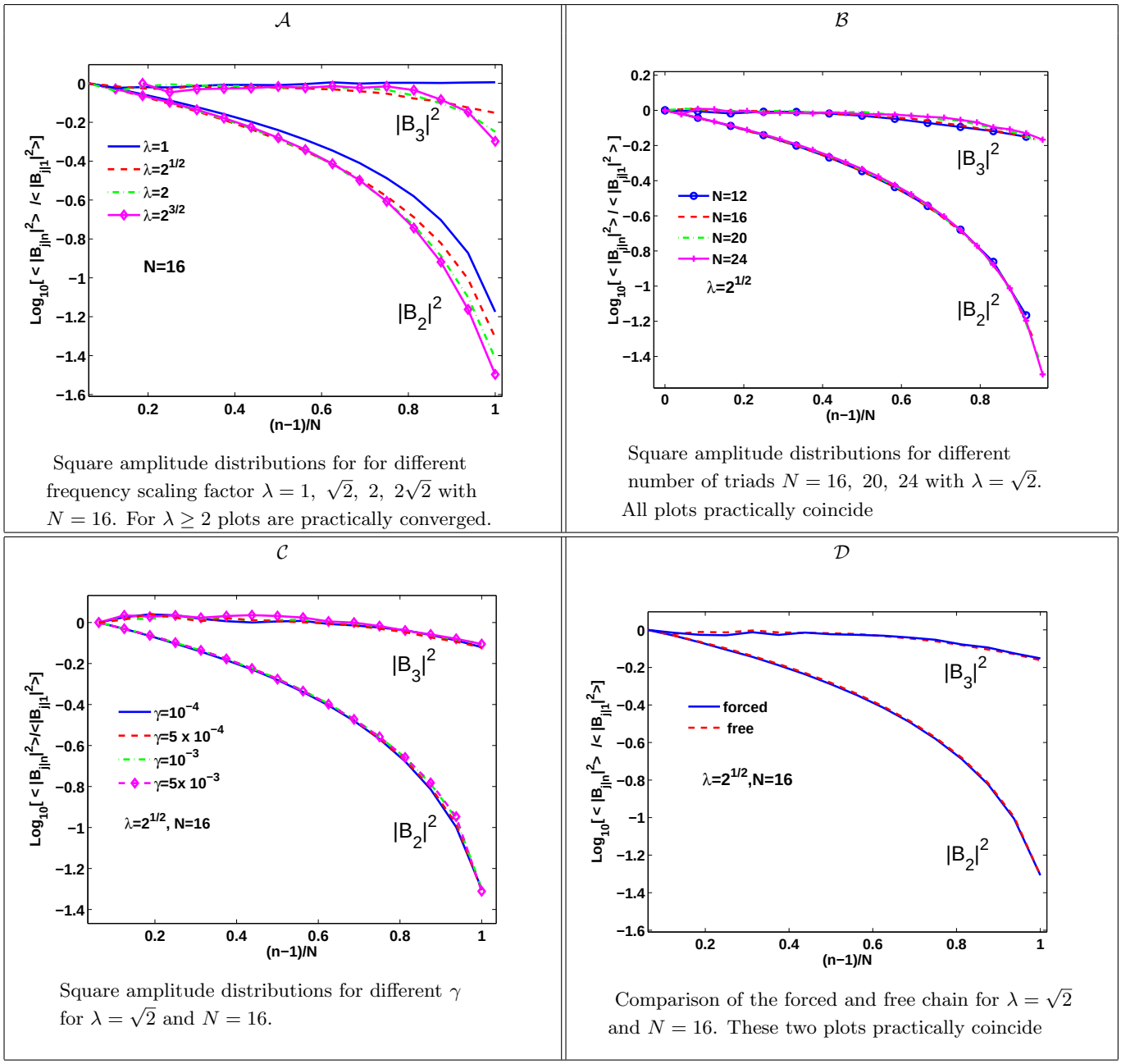

Square amplitude distributions for for different frequency scaling factor $\lambda = 1,\ \sqrt{2},\ 2,\ 2\sqrt{2}$ with $N = 16$. For $\lambda \geq 2$ plots are practically converged.

Square amplitude distributions for different number of triads $N = 16,\ 20,\ 24$ with $\lambda = \sqrt{2}$. All plots practically coincide

Square amplitude distributions for different γ for $\lambda = \sqrt{2}$ and $N = 16$.

Comparison of the forced and free chain for $\lambda = \sqrt{2}$ and $N = 16$. These two plots practically coincide

FIG. 30: Comparison of the plots of $\ln \langle |B_{j|n}|^2 \rangle$ vs $n/(N-1)$ for different λ, panel $\mathcal{A}$, for different N, panel $\mathcal{B}$ and for different γ, panel $\mathcal{C}$. Panel $\mathcal{D}$ compares distributions for the free and forced evolutions.

and approximately in the forced case.

V. SAND-PILE MODEL

As we explained in Sec. II D *mesoscopic wave turbulence* is the regime of weak wave turbulence, intermediate between finite-dimensional wave turbulence of finite-size clusters of connected triads or quartets with exact resonance and kinetic wave turbulence, in which infinitely many quasi-resonances lead to the closeness of the system statistics to the Gaussian one and guarantee applicability of the statistical description in the framework wave kinetic equation.

Physically, co-existence of the two layers of laminated turbulence can also be associated with the transitional regime where the conditions for both continuous and discrete WT are violated, see equation (44). In the other words, in this regime neither the discrete low-dimensional model nor the continuous kinetic equation when taken

separately can fully describe the system. Instead, the discrete and the continuous processes coexist: either simultaneously in some k-range, or they sporadically alternate in time for the entire range of scales or, more realistically, there will me a mixture of both kinds of behavior.

In the first case, we appeal to fundamental nonuniformity of the nonlinear behavior in the k-space and we can imagine a system where WT is purely discrete at low k's, purely continuous at large k's, and laminated at a buffer range of intermediate k's (with gradual change from predominantly discrete at lower-k side and predominantly continuous at the high-k end of the buffer range). One has to also keep in mind that some resonant clusters are nonlocal in the k-space and they can "inject" discrete behavior into a k-range with dominant continuous interactions by connecting it with the low-k discrete range.

In the second case, the same set of k-modes can alternate in time from the discrete layer to the continuous one and vice versa. This can happen via a sandpile scenario which was suggested in [85] and which we already mentioned above. Let us now consider this process in more detail and extend that analysis of [85] by elaborating the role of the discrete and the continuous regimes in forming the wave spectra at different stages of the sandpile cycle.

Let us consider a wave system which has no waves initially and which is forced at low k's with a very weak forcing at $t > 0$. At early time the waves are weak and the nonlinear resonance broadening $\Gamma \sim \Gamma_{\text{D}}$ is so low that condition (22) is satisfied. Then only a very limited number of modes which are in exact resonance with the forcing scales, and those connected to the forcing scales through exact resonant clusters, will be excited. It is natural to expect that energy will propagate through scales via such sparse clusters rather inefficiently and not fast enough to take the energy away from the forcing scales. This will lead to an energy accumulation at and near the forcing scales, which in turn will lead to bigger Γ and an increasing number of quasi-resonances with corresponding acceleration in the energy transfer rate. At some sufficiently high amplitudes the energy cascade will find its way to the small dissipation scales, perhaps via still rather depleted and anisotropic set of quasi-resonant modes, as was suggested above in the kinematic cascade model, see Fig. 26. At the same time, the evolution becomes more random and the energy cascade is likely to experience sporadic on-off fluctuations because the resonance broadening Γ (assumed constant in the kinematic cascade model) is amplitude dependent and therefore itself time dependent and random. This energy cascade resembles more a set of sandpile avalanches rather than a steady flow in the scale space.

In paper [85] an example of the water gravity waves was considered and a spectrum was derived for the system in the sandpile regime. For this, the most crude estimate was made which ignores that the set of the cascade carrying modes may be depleted, and which assumes that the sandpile avalanche is triggered when the energy accumulates to a critical level when the resonant broadening Γ becomes of the order of the frequency spacing in the discrete k-space, $\Gamma \sim v_k \delta_k$. This condition means that the modes change from the discrete layer to the continuous one. It was also assumed in [85] that the evolution is predominantly random in this case, so that Γ is determined by the characteristic timescale of the wave kinetic equation, i.e. $\Gamma = \Gamma_k$ with Γ_k given by (41). This estimate gave for the 1D energy spectrum $E_\omega \sim \omega^{-6}$ which is significantly steeper than the KZ spectrum of the water gravity waves $E_\omega \sim \omega^{-4}$ (the latter is caller Zakharov-Filonenko spectrum in this context [119]). Spectrum $E_\omega \sim \omega^{-6}$ was indeed observed for smaller levels of forcing in laboratory experiments reported in [23].

On the other hand, the assumption about the purely random character of evolution in the sandpile is clearly oversimplified. It would mean that the we are much closer to the left side of the range (44) than to the right one. The true nonlinear dynamics may be a mixture of the deterministic and the kinetic evolutions, with the precise proportion of deterministic vs random determined by the forcing strength. Let us assume for a moment that the forcing is so weak that the deterministic behavior win, which means that we are closer to the right side of the range (44). Then the condition $\Gamma \sim \Gamma_{\text{D}} \sim v_k \delta_k$ will give us the critical spectrum $E_\omega \sim \omega^{-7}$. Thus in general the spectra for the sandpile states must have exponents somewhere in between -7 to -6. In fact, spectra steeper than -6 were indeed observed in laboratory experiments of [23] at very low forcings, but most of this data was excluded from the presentation in (44) because the scaling ranges were not well developed for such low amplitudes, resulting in large slope uncertainties and the error bars.

VI. DISCUSSION

**** (this part will be improved)****

Having in mind the extremely rich variability of the structure of concrete finite clusters of resonance triads and the various important aspects of the cluster dynamics and statistics it is clear that preliminary results, presented above, open more questions than answers. Following [78] we will mention some of them:

– What might be the peculiarities of free evolutions of finite clusters from other initial conditions, more general than those review here, especially for particular clusters which may be important in some applications?

– How energy goes through more complicated junctions, than triple stars, studied in this paper, such as stars with four and five and more triads, etc.?

– How integrability of clusters (with special choice of the ratios of interaction coefficients and/or initial conditions or closeness to the integrable cases affect the energy transfer and the statistics of the mode amplitudes?

– What is the dimensionality of the cluster trajectories, how does it depends on the details of the initial

conditions and/or the ratios of interaction coefficients for various cluster structure?

– How different-mode, different-time correlation functions depend on the mode position in a cluster and on the time difference between them?

– What is the values of the flatness (ratio of the forth-order correlation functions to the square of the second-order ones) and how does it depend on the cluster structure, initial conditions, etc.?

– To what extent can the statistics of the amplitudes of individual modes be considered close to Gaussian at least for very large (but finite) clusters?

– How does this closeness (if it exists) depend on the mode position in a cluster and on initial conditions?

– If this closeness exists (we believe that it does), how can one formulate appropriate closures that will lead to an analytical statistical description of the finite cluster behavior?

A few of the most important questions, at least from the theoretical viewpoint, are:

– What is the principal difference between finite size cluster behavior for three-wave resonances, discussed here, and that for four-wave resonance systems?

– How mode statistics and possible applicability of the closure procedures changes, if one accounts for small damping of the mode energy and external random noise, that can mimic interaction of a cluster with the "rest of the world"?

– How all the features of a cluster behavior (both for those studied and those left open) get modified if one accounts for quasi-resonances that can become crucially important with increasing the level of the modes excitation?

– How to describe the statistical behavior of finite-size dynamical systems (in the case of three- and four-wave interactions) with further increases in the system size or in the level of system excitation? How this behavior approaches (step by step, probably via an intermediate kind of behavior) the limit of infinite system with quasi-Gaussian statistics, that can be successfully described with the help of wave-kinetic equations?

*****

Acknowledgements. Authors are very grateful to Oleksii Rudenko for useful and stimulating discussions. E.K. acknowledges the support of the Austrian Science Foundation (FWF) under project P20164-N18 "Discrete resonances in nonlinear wave systems". V.L. and S.N. acknowledge the support of the Transnational Access Programme at RISC-Linz, funded by European Commission Framework 6 Programme for Integrated Infrastructures Initiatives under the project SCIEnce (Contract No. 026133).

APPENDIX A: KINETIC WAVE TURBULENCE

Classical Wave Turbulence theory provides a statistical description of weakly nonlinear waves with random phases. As discussed above, theory of wave turbulence is valid in a range of wave-field strengths such that

$$1 > \frac{\Gamma_{\text{D}}}{\omega_k} > \frac{1}{\sqrt{kL}}, \tag{A1}$$

where Γ_{D} is given by (21a) or (21b) for the three- or four-wave processes respectively.

The most popular statistical object in the theory of wave turbulence is the waveaction spectrum, although theory of wave turbulence has been recently extended to description of higher moments and probability density functions (PDF) in [17–19]. This allowed to deal with non-gaussian wave fields, as well as to study validity of the underlying statistical assumptions such as *e.g.* random phases. We will now briefly describe these results.

Let us represent the complex amplitudes as $a_k = \sqrt{J_k}\psi_k$ with wave intensity $J_k \in \mathbb{R}^+$ (positive real number) and phase factor $\psi_k \in \mathbb{S}^1$ (complex number of length 1). Let us define the M-mode joint PDF $\mathcal{P}^{(M)}$ so that the probability for the wave intensities of the selected M modes, J_k, to be in the range $(s_k, s_k + ds_k)$ and for their phase factors ψ_k to be on the unit-circle segment between ξ_k and $\xi_k + d\xi_k$ is $\mathcal{P}^{(M)} \prod_{k=1}^{M} ds_k\, |d\xi_k|$. (Therefore $\mathcal{P}^{(M)}$ is a function of $2M + 1$ variables: M amplitudes, M phases and time).

Notion of random phases refers to the cases where all factor ψ_k are statistically independent and uniformly distributed on $\mathbb{S}^1$, i.e.

$$\mathcal{P}^{(M)} = \frac{1}{(2\pi)^M}\, \mathcal{P}_a^{(M)} \tag{A2}$$

for any $M \le N$, where N is the total number of dynamically active modes. Here $\mathcal{P}_a^{(M)}$ is the joint PDF of the amplitudes only. WTT considers wavefields with random phases at some initial time and with intensities satisfying condition (A1). This leads to the following equation for the joint PDF for the three-wave case,

$$\dot{\mathcal{P}}^{(N)} = 16\pi \int |V_{23}^1|^2 \delta(\omega_1 - \omega_2 - \omega_3)\delta(\boldsymbol{k}_1 - \boldsymbol{k}_2 - \boldsymbol{k}_3) \left[\frac{\delta}{\delta s}\right]_3 \left(s_1 s_2 s_3 \left[\frac{\delta}{\delta s}\right]_3 \mathcal{P}^{(N)}\right) d\boldsymbol{k}_1 d\boldsymbol{k}_2 d\boldsymbol{k}_3, \tag{A3}$$

where $\left[\frac{\delta}{\delta s}\right]_3 = \frac{\delta}{\delta s_1} - \frac{\delta}{\delta s_2} - \frac{\delta}{\delta s_3}$. This equation was first derived for a specific example of waves in anharmonic crystals by Peierls [96] and for general three-wave systems in [17, 19, 38]. It was also extended to the four wave systems in [18], in which case we have

$$\dot{\mathcal{P}}^{(N)} = \pi \int |T_{34}^{12}|^2 \delta(\omega_1 + \omega_2 - \omega_3 - \omega_4)\delta(\boldsymbol{k}_1 + \boldsymbol{k}_2 - \boldsymbol{k}_3 - \boldsymbol{k}_4) \left[\frac{\delta}{\delta s}\right]_4 \left(s_1 s_2 s_3 s_4 \left[\frac{\delta}{\delta s}\right]_4 \mathcal{P}^{(N)}\right) d\boldsymbol{k}_1 d\boldsymbol{k}_2 d\boldsymbol{k}_3 d\boldsymbol{k}_4, \tag{A4}$$

where $\left[\frac{\delta}{\delta s}\right]_4 = \frac{\delta}{\delta s_1} + \frac{\delta}{\delta s_2} - \frac{\delta}{\delta s_3} - \frac{\delta}{\delta s_4}$ (and similar equations can be written for resonant processes of any finite order).

Note that the phase variables are not involved in these equations. Therefore, the random phase assumption is consistent with these equations, namely the system which has random phases initially will remain random-phased over the typical nonlinear time (i.e. its PDF will remain independent of ξ's). Thus, equations for the joint PDF's (A3) and (A4) allow an *a posteriori* justification of the random phase assumption underlying their derivations.

However, as we already mentioned, the most frequently considered object in the theory of wave turbulence is the spectrum which is defined as

$$n_k = \left(\frac{2\pi}{L}\right)^d \langle J_k \rangle, \tag{A5}$$

where d is the dimension of the space and the angular brackets mean the ensemble averaging over the wave statistics. The spectrum is a one-mode statistical object, and it is the first in the series of one-mode moments,

$$M_k^{(p)} = \left(\frac{2\pi}{L}\right)^{pd} \langle J_k^p \rangle, \tag{A6}$$

all of which can be expressed in terms of the one-mode PDF as

$$M_k^{(p)} = \left(\frac{2\pi}{L}\right)^{pd} \int_0^\infty s_k^p \mathcal{P}^{(1)}(s_k)\, ds_k. \tag{A7}$$

Note that for deriving closures for the one-mode objects the random phase property is insufficient and one has to assume additionally that the amplitudes J_k are also statistically independent of each other at different k's. Statistical independent of the amplitude can also be justified based on the equations for the joint PDF's (A3) and (A4), although this issue is more subtle than the phase randomness because variables s_k do not separate (A3) and (A4) and, therefore any product factorization of the joint PDF in terms of the one-mode PDF's would not generally be preserved by the nonlinear evolution. However, this situation seems to be typical for many systems, *e.g.* for the relation between the multiparticle and one-particle distribution functions described by the Louisville and Boltzmann equations respectively. In these situations, a sufficient for the closures property is that the *low-order* PDF's, $\mathcal{P}^{(M)}$ with $M \ll N$, can be product factorized. It is easy to see from (A3) and (A4) that it is the case for the weakly nonlinear wave systems, i.e. that factorization

$$\mathcal{P}^{(M)} = \prod_{k=1}^{M} \mathcal{P}_k^{(1)} + O(M/N) \tag{A8}$$

survives over the characteristic nonlinear time.

Contrary to popular belief, the distribution of wavefields in the theory of wave turbulence does not need to be Gaussian or close to Gaussian, and one can consider evolution of the one-mode PDF's $\mathcal{P}^{(1)}$ that correspond to strongly non-gaussian fields (Gaussian fields would mean $\mathcal{P}^{(1)} \sim e^{-s/\langle J \rangle}$). Integrating the joint PDF equations (A3) or (A4) we get

$$\frac{\partial \mathcal{P}_k^{(1)}}{\partial t} + \frac{\partial F_k}{\partial s_k} = 0, \tag{A9}$$

with F is a probability flux in the s-space,

$$F_k = -s_k(\gamma_k \mathcal{P}_k^{(1)} + \eta_k \frac{\delta \mathcal{P}_k^{(1)}}{\delta s_k}). \tag{A10}$$

where for the three-wave case we have:

$$\eta_k = 4\pi \int \left(|V_{12}^k|^2 \delta(\omega_k - \omega_1 - \omega_2)\delta(\boldsymbol{k} - \boldsymbol{k}_1 - \boldsymbol{k}_2) + 2|V_{k1}^2|^2 \delta(\omega_2 - \omega_k - \omega_1)\delta(\boldsymbol{k}_2 - \boldsymbol{k} - \boldsymbol{k}_1)\right) n_1 n_2\, d\boldsymbol{k}_1 d\boldsymbol{k}_2, \tag{A11}$$

$$\gamma_k = 8\pi \int \left(|V_{12}^k|^2 \delta(\omega_k - \omega_1 - \omega_2)\delta(\boldsymbol{k} - \boldsymbol{k}_1 - \boldsymbol{k}_2)\, n_1 + |V_{k1}^2|^2 \Delta_{k1}^2 \delta(\omega_2 - \omega_k - \omega_1)\delta(\boldsymbol{k}_2 - \boldsymbol{k} - \boldsymbol{k}_1)(n_1 - n_2)\right) d\boldsymbol{k}_1 d\boldsymbol{k}_2. \tag{A12}$$

and for the four-wave case:

$$\eta_k = 4\pi \int |T_{23}^{k1}|^2 \delta(\omega_k + \omega_1 - \omega_2 - \omega_3)\delta(\boldsymbol{k} + \boldsymbol{k}_1 - \boldsymbol{k}_2 - \boldsymbol{k}_3)\, n_1 n_2 n_3\, d\boldsymbol{k}_1 d\boldsymbol{k}_2 d\boldsymbol{k}_3, \tag{A13}$$

$$\gamma_k = 4\pi \int |T_{23}^{k1}|^2 \delta(\omega_k + \omega_1 - \omega_2 - \omega_3)\delta(\boldsymbol{k} + \boldsymbol{k}_1 - \boldsymbol{k}_2 - \boldsymbol{k}_3) \Big[n_1(n_2 + n_3) - n_2 n_3\Big]\, d\boldsymbol{k}_1 d\boldsymbol{k}_2 d\boldsymbol{k}_3. \tag{A14}$$

Equation (A9) has an obvious exponential solution which corresponds to a zero flux F:

$$\mathcal{P}_k^{(1)} = \frac{1}{\langle J_k \rangle}\, e^{-s_k/\langle J_k \rangle}$$

which corresponds to Gaussian statistics of the wave field a_k. However, there are also solutions corresponding to F =const$\neq$ 0 which for $s_k \gg \langle J_k \rangle$ has a power-law asymptotic [17, 18],

$$\mathcal{P}_k^{(1)} = -\frac{F}{\gamma_k s_k}.$$

These solution corresponds to enhanced probability (with respect to gaussian) of strong waves which is called intemittency of WT. Here, the constant flux in the amplitude space F can be associated with a wavebreaking process the exact form of which depends on the physical system. For example, for the gravity water surface waves the wavebreaking process takes form of whitecapping, and for the focusing NLS system the wavebreaking is represented by filamentation/collapsing events. Obviously, this power-law tail of the PDF cannot extend to infinity because the integral of the PDF must converge. Thus, there exists a cutoff which can also be associated with the wave breaking, which can simply be understood that the probability of waves with amplitude greater than some critical value must be zero. Such critical value roughly corresponds to the amplitude for which

the nonlinear term becomes of the order of the nonlinear one so that the WT description breaks.

Multiplying equation (A9) by s_k^p and integrating over s_k, we have the following equation for the moments $M_j^{(p)} = \langle A_j^{2p} \rangle$:

$$\frac{d}{dt} M_k^{(p)} = -p\gamma_k M_k^{(p)} + p^2 \eta_k M_k^{(p-1)}. \qquad \text{(A15)}$$

which, for $p = 1$ gives the kinetic equation for the wave-action spectrum,

$$\frac{d}{dt} n_k = -\gamma_k n_k + \eta_k. \qquad \text{(A16)}$$

Substituting into this equation expressions for γ_k and η_k, we obtain more familiar forms of the kinetic equations:

$$\begin{aligned} \frac{d}{dt} n_k = \; & 4\pi \int |V_{12}^k|^2 \delta(\omega_k - \omega_1 - \omega_2) \delta(\boldsymbol{k} - \boldsymbol{k}_1 - \boldsymbol{k}_2) \\ & (n_1 n_2 - n_1 n_k - n_2 n_k)\, d\boldsymbol{k}_1 d\boldsymbol{k}_2 + \\ & 8\pi \int |V_{k1}^2|^2 \delta(\omega_2 - \omega_k - \omega_1) \delta(\boldsymbol{k}_2 - \boldsymbol{k} - \boldsymbol{k}_1) \\ & (n_1 n_2 - n_1 n_k + n_2 n_k)\, d\boldsymbol{k}_1 d\boldsymbol{k}_2, \qquad \text{(A17)} \end{aligned}$$

and for the four-wave case

$$\begin{aligned} \frac{d}{dt} n_k = \; & 4\pi \int |T_{23}^{k1}|^2 \delta(\omega_k + \omega_1 - \omega_2 - \omega_3) \delta(\boldsymbol{k} + \boldsymbol{k}_1 - \boldsymbol{k}_2 - \boldsymbol{k}_3) \\ & n_k n_1 n_2 n_3 \left(\tfrac{1}{n_k} + \tfrac{1}{n_1} - \tfrac{1}{n_2} - \tfrac{1}{n_3} \right) d\boldsymbol{k}_1 d\boldsymbol{k}_2 d\boldsymbol{k}_3. \qquad \text{(A18)} \end{aligned}$$

Based on (A17) and (A18) (or (A9) or (A15)) one can obtain the estimate for the nonlinear frequency broadening in the WT regime, i.e. inverse characteristic time of the nonlinear evolution (41). This leads to the WT applicability condition (A1).

Classical statistical approach allows to obtain some interesting and physically relevant solutions, such as Kolmogorov-Zakharov (KZ) spectra corresponding to the energy and waveaction cascades through scales. Such solutions can be obtained analytically using so-called Zakharov transformation, as well as from the scalings of the frequency and the interaction coefficients based on the dimensional analysis. Discussion of these issues is beyond the scope of our review, and the interested reader is referred for details to book [122]. Here, it suffices to say that in most systems there exists a shortcut way to obtain KZ spectra. It works for the systems with only one relevant dimensional parameter, for example the gravity constant g for the water surface gravity waves, surface tension constant σ for the capillary waves, speed of sound c_s for acoustic turbulence, quantum of circulation κ for Kelvin waves on quantized vortex lines, etc. In this case the 1D energy spectrum $E_k \sim k^\nu$ can be immediately obtained from the physical dimension of this constant which gives for the direct cascade [21]:

$$\nu = 2\alpha + d - 6 + \frac{5 - 3\alpha - d}{N - 1}, \qquad \text{(A19)}$$

where α is the power of the dispersion relation $\omega \sim k^\alpha$ (which is uniquely determined by the above dimensional constant), d is the dimension of the system and N is the number of waves involved in the resonance interaction. For example, for the water surface gravity waves we have $E_k \sim k^{-5/2}$, for the capillary waves $E_k \sim k^{-7/4}$ (both of these spectra are called Zakharov-Filonenko spectra [119**?**]), for acoustic turbulence $E_k \sim k^{-3/2}$ (Zakharov-Sagdeev spectrum [71]), for Kelvin waves on quantized vortex lines $E_k \sim k^{-7/5}$ (Kozik-Svistunov spectrum [70]). Similar approach one can use for finding the inverse cascade spectra, e.g. for the water surface gravity waves or Kelvin waves [21].

[1] Anderson, P.W., and H. Suhl, 1955. Phys. Rev. **100**: 1788.
[2] Annenkov, S., and V. Shrira, 2006. Phys. Rev. Lett. **96**: 204501.
[3] Annenkov, S., and V. Shrira, 2009. Phys. Rev. Lett. **102**: 024502.
[4] Arnold, V.I., 1963. Russian Math. Surveys **18**, 9.
[5] Baker A., 1990. *Transcendental Number Theory* (Cambridge University Press).
[6] Balk, A.M., and S.V. Nazarenko, 1990. Sov. Phys.-JETP **70** : 1031.
[7] Benjamin, T.B., and J.E. Fair, 1967. Fluid Mech. **27**: 417.
[8] Berman, G.P., and F.M. Israilev, 2005. Chaos **15** (1): 015104.
[9] Besikovitch, A.S., 1940. Proc. London Math. Society **15** (1): 3.
[10] Bigg, G.R., 2003. *Ocean-atmosphere interaction* (Cambridge University Press)
[11] Bourouiba, L., 2008. Phys. Rev. E **78**: 056309.
[12] Braznikov, M., G. Kolmakov, A. Levchenko and L. Mezhov-Deglin, 2002. EPL **58**: 510.
[13] Bustamante, M.D., and E. Kartashova, 2009. EPL **85**: 14004.
[14] Bustamante, M.D., and E. Kartashova, 2009. EPL **85**: 34002.
[15] Bustamante, M.D., and E. Kartashova, 2009. In preparation.
[16] Caillol, P. ,and V. Zeitlin, 2000. Dyn. Atm. Oceans, **32**: 81.
[17] Choi, Y., Y. Lvov and S.V. Nazarenko, 2004. Phys. Lett. A **332** (3-4): 230.
[18] Choi, Y., Y. Lvov, S.V. Nazarenko and B. Pokorni, 2004. Phys. Lett. A **339** (3-5): 361.
[19] Choi, Y., Y. Lvov and S.V. Nazarenko, 2005. Physica D **201**: 121
[20] Choi, Y., Y. Lvov and S.V. Nazarenko, 2004. Rec. Devel. Fluid Dyn. **5**: 225.

[21] Connaughton, C., S.V. Nazarenko and A. Pushkarev, 2001. Phys. Rev E **63**: 046306.

[22] Constantin, A., and E. Kartashova, 2009. EPL, **86**: 29001.

[] A. Constantin, E. Kartashova and E. Wahlén. E-print: arXiv:1001.1497v1.

[23] Denissenko, P., S. Lukaschuk and S. Nazarenko, 2007. Phys. Rev. Lett. **99**: 014501.

[24] Dyachenko, A.I., Y.V. Lvov and V.E. Zakharov, 1995. Physica D **87** (1-4): 233.

[25] Dyachenko, A., A.C. Newell, A. Pushkarev and V.E. Zakharov, 1992. Physica D **57** (1-2): 96.

[26] Eguíluz, V.M., M.T. Levinsen and P. Alstrom, 2002. EPL **58**: 517.

[27] Falcon, E., C. Laroche and S. Fauve, 2007. Phys. Rev. Lett. **98**: 094503.

[28] Fournier, J.-D., U. Frisch and H.A. Rose, 1978. Physics A: Math. and Gen. **11**(1): 187.

[29] Galeev, A.A., and R.Z. Sagdeev, 1973. In *Reviews of Plasma Physics* **6**, Ed. M A Leontovich (New York: Consultants Bureau).

[30] Galtier, S., 2003. Phys. Rev. E **68**: 015301.

[31] Galtier, S., S.V. Nazarenko, A.C. Newell and A. Pouquet, 2000. J. Plasma Phys. **63**: 447.

[32] Grant, H.L., R.W. Stuart and A. Moilliet, 1961. Fluid Mech. **12**: 241.

[33] Hasselmann, K., 1967. Fluid Mech. **30**: 737.

[34] Goldreich P., 2001, Astrophys. Space Sci., **278**(1-2): 17.

[35] Goldreich, P. and S. Sridhar, 1995, Astrophys. J. **438**: 763.

[36] Janssen, P., 2004, *Ocean-atmosphere interaction* (Cambridge University Press)

[37] Iroshnikov; R.S., 1963, Astron. Zh. **40**: 742 (English trans.: 1964, Sov. Astron. **7**, 566).

[38] Jakobsen, P. and A. Newell, 2004. J. Stat. Mech. L10002.

[39] Falgarone, E., and T. Passot (Eds), 2003. *Turbulence and Magnetic Fields in Astrophysics* (Lecture Notes in Physics, Springer)

[40] Kalmykov, V.A., 1998. *in Nonlinear Waves and Weak Turbulence*, edited by V.E. Zakharov (Springer-Verlag), p.83.

[41] Kartashova, E.A., 1990. Physica D **46** (1): 43.

[42] Kartashova, E.A., 1991. Physica D **54** (1-2): 125.

[43] Kartashova, E.A., 1991. *in Procedings of the International Nonlinear Water Waves Workshop*, edited by Pelegrin (University of Bristol, Bristol, UK), p.43.

[44] Kartashova, E.A., 1994a. Phys. Rev. Lett. **72**: 2013.

[45] Kartashova, E.A., 1994b. Theor. Math. Phys. **99**: 675.

[46] Kartashova, E.A., 1994c. *in Current Topics in Astrophysical and Fusion Plasma*, edited by Heyn M.F., Kernbichler W., and Biernat K. (Verlag fuer die Technische Universitaet Graz, Graz, Austria), p.179

[47] Kartashova, E.A., 1995. *in Advanced series in nonlinear dynamics 7*, edited by Mielke A., Kirchgaessner K. (World Scientific), p. 282.

[48] Kartashova, E.A., 1998. *in Nonlinear Waves and Weak Turbulence*, edited by V.E. Zakharov (Springer-Verlag), p.95.

[49] Kartashova, E.A., 2006a. JETP Letters **83** (7): 341.

[50] Kartashova, E., 2006b. Low Temp. Phys. **145** (1-4): 286.

[51] Kartashova, E., 2007: Phys. Rev. Lett. **98** (21): 214502.

[52] Kartashova, E., 2009. DCDS Series B **12** (3): 607.

[53] Kartashova, E., 2009. EPL **87**, 44001.

[54] Kartashova, E., 2009. *Nonlinear Resonance Analysis* (Cambridge University Press, to appear)

[55] Kartashova, E., and A. Kartashov, 2006. Int. J. Mod. Phys. C **17**(11): 1579.

[56] Kartashova, E., and A. Kartashov, 2007. Comm. Comp. Phys. **2** (4): 783.

[57] Kartashova, E., and A. Kartashov, 2007. Physics A: Stat. Mech. Appl. **380**: 66.

[58] Kartashova, E., and A. Kartashov, 2009. In preparation.

[59] Kartashova, E., and F. Leyvraz, 2009. In preparation.

[60] Kartashova, E., and V.S. L'vov, 2007. Phys. Rev. Lett. **98** (19): 198501.

[61] Kartashova, E. and V.S. L'vov, 2008. EPL **83**: 50012.

[62] Kartashova, E., and G. Mayrhofer, 2007. Physica A: Stat. Mech. Appl. **385**: 527.

[63] Kartashova, E., S. Nazarenko and O. Rudenko, 2008a. Phys. Rev. E **78**: 016304.

[64] Kartashova, E.A., L.I. Piterbarg and G.M. Reznik, 1990, Oceanology **29**: 405.

[65] Kartashova, E., C. Raab, Ch. Feurer, G. Mayrhofer and W. Schreiner, 2008b. *in Extreme Ocean Waves*, edited by E. Pelinovsky and Ch. Harif (Springer), 97.

[66] Kartashova, E.A., and G.M. Reznik, 1992. Oceanology **31**: 385.

[67] Kolmakov, G., A. Levchenko, M. Braznikov, L. Mezhov-Deglin, A. Slichenko and P. McClintock, 2004. Phys. Rev. Lett. **93**: 74501.

[68] Kolmogorov, A.N., 1954. Dokl. Akad. Nauk SSSR **98**: 527. English translation in: *LNP 93*, 51 (Springer, 1979).

[69] Korotkevich A.O., 2008. E-print: http://arxiv.org/abs/0805.0445

[70] Kozik, E.V., and B.V. Svistunov, 2004. Phys. Rev. Lett. **92**: 035301.

[71] Zakharov, V.E., and R.Z. Sagdeev, 1970. Sov. Phys. - Dokl. **15**: 439.

[72] Krasitskii, V.P., 1994. J. Fluid Mech. **272**: 1.

[73] Lvov, Y.V., 1997. Phys. Lett. A **230**: 38.

[74] Lvov, Y.V., S. Nazarenko and B. Pokorni, 2006. Physica D **218** (1): 24.

[75] Lvov, Y.V., and E.G. Tabak, 2001. Phys. Rev. Lett. **87**: 169501.

[76] L'vov, V.S., 1994. *Wave Turbulence under parametric excitation* (Series in Nonlinear Dynamics, Springer).

[77] L'vov, V.S., S.V. Nazarenko and O. Rudenko, 2007. Phys. Rev. B **76**: 024520.

[78] L'vov, V.S., A. Pomyalov, I. Procaccia and O. Rudenko, 2009. Phys. Rev. E, submitted.

[79] Longuet-Higgins, M.S., and A.E. Gill, 1967. Proc. R. Soc. London, Ser. A **299** (1456): 120.

[80] Manley, J.M., and H. E. Rowe, 1956. Proc. IRE **44**: 904 (1956).

[81] Matijasevich, Yu.V., 1993. *Hilbert's Tenth Problem* (MIT Press, Cambridge, MA)

[82] Monin, A.S., and L.I. Piterbarg, 1987. Dokl. Akad. Nauk SSSR **295**: 816.

[83] Moser, J., 1962. Nachr. Akad. Wiss. Goett., Math. Phys. Kl., 1.

[84] Musher, S.L., A.M. Rubenchik and V.E. Zakharov, 1985. Phys. Rep. **129**: 285.

[85] Nazarenko, S., 2006. J. Stat. Mech. LO2002.

[86] Nazarenko, S., 2006. JETP Lets., **84**: 700.

[87] Nazarenko, S., 2007. New J. Phys. **9**: 307.

[88] Lvov, Y., and S.V. Nazarenko, 2004. Phys. Rev. E **69**: 1539.

[89] Nazarenko, S.V., Y. Choi and Y. Lvov, 2005. Physica D **201**: 121.

[90] Lvov, Y.V., S. Nazarenko and B. Pokorni, 2006. Physica D **218**: 24.

[91] Newell, A.C., and V.E. Zakharov, 2008. Phys. Lett. A **372**: 4230

[92] Ng, C.S., and A. Bhattacharjee, 1996. Astrophys. J. **465**: 845.

[93] https://www.risc.uni-linz.ac.at/people/schreine/DiscreteWaveTurbulence/

[94] Oraevsky, V.N., and R.Z. Sagdeev, 1962. Zh. Tekh. Fiz. **32**: 1291; [Sov. Phys. Tech. Phys. **7**: 955 (1963)].

[95] Pedlosky, J., 1987. *Geophysical Fluid Dynamics.* (Springer).

[96] Peierls, R., 1929. Annalen Physik **3** (8): 1055.

[97] Phillips, O.M., 1967. Proc. R. Soc. London, Ser. A **299** (1456): 105.

[98] Piterbarg, L.I., 1998. *in Nonlinear Waves and Weak Turbulence*, edited by V.E. Zakharov (Springer-Verlag), p.131.

[99] Poincaré, H., 1951. *Oeuvres* (Paris)

[100] Pushkarev, A.N., 1999. Eur. J. Mech. - B/Fluids **18** (3): 345.

[101] Pushkarev, A.N., and V.E. Zakharov, 2000. Physica D **135** (1-2): 98.

[102] Ridout, D., 1958. Mathematika **5**: 40.

[103] Roth, K.F., 1955. Mathematika **2**, 1.

[104] Rudenko, O. and E. Kartashova, 2008. The Wolfram Demonstrations Project,http://demonstrations.wolfram.com/NonlinearWaveResonances

[105] Silberman, I., 1954. Meteorology **11**: 27.

[106] Shemer, L., and M. Stiassnie, 1985. *in The ocean surface.*, edited by Y. Toba, H. Mitsuyasu and F.D. Reidel (Dodrecht, Holland) p.51.

[107] Stiassnie, M., and L. Shemer, 2005. Wave motion **41**: 307.

[108] Tanaka, M., 2001. Fluid Mech. **444**: 199.

[109] Tanaka, M., 2007. J. Phys. Oceanogr. **37**: 1022.

[110] Tanaka, M., and N. Yokoyama, 2004. Fluid Dyn. Research **34**, 216.

[111] Vedenov, A.A., 1967. In *Reviews of plasma physics* (ed. M. A. Leontovich). New York, Consultants Bureau **3**, 229.

[112] Verheest, F., 1988. Phys. A: Math. Gen. **21**: L545.

[113] Verheest, F., 1988. J. Math. Phys. **29**: 2197.

[114] Vinen, W. F., and J. J. Niemela, 2002. Low Temp. Phys. **128**: 167.

[115] Vinen, W. F., M. Tsubota and A. Mitani, 2003. Phys. Rev. Lett. **91**: 135301.

[116] Whitham, G.B., 1999. *Linear and Nonlinear Waves* (Wiley Series in Pure and Applied Mathematics).

[117] Whittaker, E.T., and G.N. Watson, 1990. *A Course in Modern Analysis* (Cambridge University Press).

[118] Zakharov, V., 1999. Eur. J. Mech. B **18** (3): 327.

[119] V. E. Zakharov and N. N. Filonenko, 1967, J. Appl. Mech. Tech. Phys. **4**: 506.

[120] Zakharov, V.E., P. Guyenne, A.N. Pushkarev and F. Dias, 2001. Physica D **152-153**, 573.

[121] Zakharov, V.E., A.O. Korotkevich, A.N. Pushkarev and A.I. Dyachenko, 2005. JETP Lett. **82** (8): 491.

[122] Zakharov, V.E., V.S. L'vov and G. Falkovich, 1992. *Kolmogorov Spectra of Turbulence* (Series in Nonlinear Dynamics, Springer).

[123] Zakharov, V.E., and L.I. Piterbarg, 1987. Sov. Phys. Doklady **32**: 560.

[124] Zakharov, V.E., and L.I. Piterbarg, 1988. Phys. Lett. A **126** (8-9): 497.

[125] Zaslavskii, G.M., and R.Z. Sagdeev, 1967. Sov. Phys. JETP **25**: 718.